



# This is to certify that the

## thesis entitled

# Development of a Microwave Part-Shaped Cavity for Liquid Composite Molding

presented by

Trent Alan Shidaker

has been accepted towards fulfillment of the requirements for

M.S. degree in Chemical Engineering

Major professor

Date July 8 , 1996

MSU is an Affirmative Action/Equal Opportunity Institution

**O**-7639



PLACE IN RETURN BOX to remove this checkout from your record. TO AVOID FINES return on or before date due.

DATE DUE	DATE DUE	DATE DUE

MSU is An Affirmative Action/Equal Opportunity Institution cyclecidatedus.pm3-p.1

# DEVELOPMENT OF A MICROWAVE PART-SHAPED CAVITY FOR LIQUID COMPOSITE MOLDING

Ву

Trent Alan Shidaker

# **A THESIS**

Submitted to
Michigan State University
in partial fulfillment of the requirements
for the degree of

**MASTER OF SCIENCE** 

Department of Chemical Engineering

### **ABSTRACT**

# DEVELOPMENT OF A MICROWAVE PART-SHAPED CAVITY FOR RESIN TRANSFER MOLDING

By

#### Trent Alan Shidaker

A microwave part-shaped applicator was designed to be competitive with conventional liquid composite molding processes. This thesis presents the developmental work for this apparatus. Specifically, the electromagnetic behavior, including modes of propagation, electric field distribution, and cutoff frequencies, in the part-shaped applicator system is determined theoretically using Maxwell's equations. Microwave heating patterns, using fully cured glass-reinforced polyester plates, are experimentally characterized in the part-shaped applicator for comparison to theory. Three glass-reinforced diglycidyl ether of bisphenol A epoxy composites with a diaminodiphenyl sulfone curative are processed in the part-shaped cavity by microwave heating, conventional heating, and hybrid heating where both microwave and conduction heating are employed. Hybrid heating provided superior heating uniformity. Because of the penetrating nature of microwave energy, the time required to attain the cure temperature in the composite center was reduced by more than 85% using microwave and hybrid heating methods.

# **DEDICATION**

To God, through Whom all things are possible (Matthew 19:26), and to the loving and supportive women in my life:

my mother, Sandra, and my wife, Layne.

## **ACKNOWLEDGMENTS**

I would like to express my sincere appreciation to my advisor Dr. Martin Hawley for providing the numerous learning experiences to make this thesis a valuable endeavor for me. Grateful acknowledgment is also due to the committee members, Drs. Jes

Asmussen, Jr. and Lawrence Drzal, for their interest in this work. Sincere appreciation is extended to Scott Hebner, Ann Glenn, Yunchang Qiu, Michael Muczinski, and Dr.

Yong-Joon Lee for their friendship and valuable research assistance that they so willingly provided. I would like to thank Rick Delgado, Dr. Valerie Adebite, Dr. K.M. Chen and Dr. Jianghua Wei for providing many beneficial insights through our discussions. The professional services of Terry Casey, Brian Rook, Michael Rich, and Barry Tigner are highly acknowledged. A special appreciation is extended to my wife, Layne, for her love, encouragement, and support throughout the duration of my program. This research was made possible by the financial support of the National Science Foundation State/Industry/University Co-operative Research Center on Low-Cost, High Speed Polymer Composites Processing at Michigan State University.

# **TABLE OF CONTENTS**

List of Tables	viii	
List of Figuresix		
Chapter One: Introduction	1	
1.1. Research Description and Scope	1	
1.2. Microwave Processing of Materials	3	
1.2.1. Rationale	5	
1.2.2. Applications	12	
1.2.2.1. Polymer Processing	12	
1.2.2.2. Composite Processing	16	
1.2.3. Microwave Processing Systems	19	
1.3. Resin Transfer Molding	23	
1.3.1. Process Cycle	24	
1.3.2. Polymer Matrices	27	
1.3.3. Fiber System	28	
Chapter Two: Theory	30	
2.1. Maxwell's Equations	30	

2.2. Wave Propagation	32
2.2.1. Rectangular Waveguide	33
2.2.2. Rectangular Resonant Cavity	37
2.3. Microwave Energy Absorption Mechanisms	39
2.4. Penetration Depth	42
Chapter Three: Experimental	46
3.1. Experimental System	46
3.1.1. Part-Shaped Cavity	46
3.1.2. External Applicators	49
3.1.3. Experimental Setup and Microwave Circuitry	51
3.1.4. Thermometry System	54
3.1.5. Process Material	55
3.2. Cavity Characterization Methods	57
3.3. Glass Fiber-Reinforced DGEBA/DDS Processing	58
3.4. Mechanical Strength Tests	60
Chapter Four: Results and Discussion	63
4.1. Cavity Characterization Results	63
4.1.1. Temperature Profiles and Heating Patterns	63
4.1.2. Aperture Effects	72
4.2. Theoretical Calculations	79
4.2.1. Electromagnetic Modes in the External Applicators	79

4.2.2. Electromagnetic Modes in the Cavity83	
4.3. Processing of Glass-Reinforced DGEBA/DDS90	
4.3.1. Complex Permittivity90	
4.3.2. Curing Results91	
4.4. Mechanical Strength Tests	
Chapter Five: Conclusions	
5.1. Part-Shaped Cavity Processing Capabilities and Limitations	
5.2. Project Status	
Chapter Six: Recommendations	
Appendix A: Vector Wave Equation Development	
Appendix B: Solution to Vector Wave Equations	
Appendix C: Power Penetration Depth Calculation	
Appendix D: Cutoff Frequency 120	
Appendix E: Guided Wavelength 121	
Appendix F: Unsteady-State Energy Balance Development	
Appendix G: FORTRAN Code for the Heat Transfer Model	
List of Deferences	

# LIST OF TABLES

Table 1.1.	Comparison of Conventional to Microwave Thermoset Processing.	6
Table 1.2.	Microwave Characteristics and Effects.	7
Table 1.3.	Examples of Components Manufactured by RTM.	25
Table 4.1.	Thermal Paper Images for Various Aperture Widths.	78
Table 4.2.	Heat Transfer Model Parameters for Conventional, Microwave, and Hybrid Heating.	99
<i>Table 4.3.</i>	Modulus of Elasticity Data for E-glass-Reinforced DGEBA/DDS	106

# **LIST OF FIGURES**

Figure 1.1.	The Electromagnetic Spectrum and Microwave Frequencies for Heating.	4
Figure 1.2.	Generalized Thermoset Processing Window.	9
Figure 1.3.	Typical Microwave System Circuitry	21
Figure 1.4.	RTM Processing Cycle	26
Figure 2.1.	Instantaneous Vector E-field Plots for the TE <sub>01</sub> Mode in a Rectangular Waveguide	35
Figure 2.2.	Cutoff Frequency Versus Dielectric Constant for a Dielectric-Filled Waveguide with a Cross-Section of 3.8 cm x 8.7 cm	36
Figure 2.3.	Vector Plots of E-field for the TE <sub>011</sub> Mode in a Rectangular Resonant Cavity.	38
Figure 2.4.	Mode Chart for a Rectangular Resonant Cavity with a Cross-Section of 6.4 cm x 7.6 cm.	40
Figure 2.5.	Power Penetration Depth for the TE <sub>01</sub> Mode in a 4.2 cm by 8.9 cm Dielectric-Filled Waveguide.	44
Figure 3.1.	Drawing of the Part-Shaped Cavity.	47
Figure 3.2.	Cross-Section of the External Applicator.	50
Figure 3.3.	Microwave Circuitry and Cavity Configurations for Standing Wave Operation.	52
Figure 3.4.	Microwave Circuitry and Pumping Configuration for Traveling Wave Operation.	53

Figure 3.5.	Chemical Structure of Diglycidyl Ether of Bisphenol A and Diaminodiphenyl Sulfone	56
Figure 3.6.	Fiber Mat Orientation and Sample Locations for Curing	<i>c</i> 1
	Experiments in Part-Shaped Cavity	61
Figure 4.1.	Glass-Reinforced Polyester Temperature Profiles for Heating	
	Runs With One External Applicator at Port A and an Aperture Width of 4.19 cm.	64
Figure 4.2.	Glass-Reinforced Polyester Temperature Profiles for Heating	
	Runs With One External Applicator at Port C and an Aperture	
	Width of 4.19 cm.	65
Figure 4.3.	Glass-Reinforced Polyester Temperature Profiles for Heating	
<b>9</b>	Runs With One External Applicator at Port D and an Aperture	
	Width of 4.06 cm.	66
Figure 4.4.	Thermal Paper Images for Polyester Plates in the Part-Shaped	
	Cavity: Standing Wave Operation	68
Ti 4 2		
rigure 4.5.	Glass-Reinforced Polyester Temperature Profiles for Heating Runs With an Active External Applicator at Port A and Non-	
	Active External Applicators at Ports B and C With an Aperture	
	Width of 3.61 cm.	69
Figure 4.6.	Glass-Reinforced Polyester Temperature Profiles for Heating	
	Runs With an Active External Applicator at Port C and Non-	
	Active External Applicators at Ports A and B With an Aperture	
	Width of 3.61 cm.	70
Figure 4.7.	Thermal Paper Images for Polyester Plates in the Part-Shaped	
	Cavity: Traveling Wave Operation	71
Figure 4.8	Investigated Aperture Characteristics	73
	Air doingailed 1 sportatio Cimination	
Figure 4.9.	Initial Temperature Profile as a Function of Aperture Width at	
	Port A.	75
Figure 4.10.	Initial Temperature Profile as a Function of Aperture Width at	
•	Port C.	76
Figure 4 11	Initial Temperature Profile as a Function of Aperture Width at	
riguie 4.11.	Port D	77

Figure 4.12.	. Theoretical Mode Chart for a 6.4 cm x 7.6 cm Rectangular Cavity.	
Figure 4.13.	Theoretical Vector Plots of E-field for the TE <sub>011</sub> Mode and the Aperture Configuration.	82
Figure 4.14.	Cutoff Frequency in the Cavity as a Function of the Process  Material Dielectric Constant	84
Figure 4.15.	Theoretical E-field Strength Plots and Thermal Paper Image for the Mid-Plane (i.e., $y = 0.5$ b) of a 4.2 cm x 8.9 cm Waveguide Filled With Dielectric Material ( $\epsilon^{*} = 4.30$ -j0.049)	86
Figure 4.16.	X-Y Vector Plots for the TE <sub>10</sub> , TM <sub>11</sub> , and TE <sub>01</sub> Modes	87
Figure 4.17.	Theoretical Temperature Profiles at Various Times for a Constant Microwave Power Input of 0.115 W/cm³ in an Infinite Slab of Polymer Between Brass Boundaries.	<b>8</b> 9
Figure 4.18.	Complex Permittivity of Uncured DGEBA/DDS at 25°C as a Function of Fiber Content.	93
Figure 4.19.	Temperature Profiles for Conventional Curing of E-glass-Reinforced DGEBA/DDS in the Part-Shaped Cavity.	94
Figure 4.20.	Temperature Profiles for Microwave Curing of E-glass-Reinforced DGEBA/DDS in the Part-Shaped Cavity.	95
Figure 4.21.	Temperature Profiles for Hybrid Curing of E-glass-Reinforced DGEBA/DDS in the Part-Shaped Cavity	96
Figure 4.22.	Average Center-to-Wall Temperature Gradient for Microwave, Conventional, and Hybrid Curing of E-glass-Reinforced DGEBA/DDS in the Part-Shaped Cavity	97
Figure 4.23.	Theoretical Temperature Profiles at Various Times for Conventionally Heating an Infinite Slab of Polymer Between Brass Boundaries.	100
Figure 4.24.	Theoretical Temperature Profiles at Various Times for a Constant Microwave Power Input of 2.0 W/cm <sup>3</sup> in an Infinite Slab of Polymer Between Brass Boundaries.	102

Figure 4.25.	Theoretical Temperature Profiles at Various Times for Hybrid Heating With a Constant Microwave Power Input of 2.0 W/cm <sup>3</sup>		
	in an Infinite Slab of Polymer Between Brass Boundaries	103	
Figure 4.26.	Load-Deflection Data With Initial Slope for Sample 7H (Hybrid Cured E-glass-Reinforced DGEBA/DDS).	104	
Figure F.1.	Boundary Conditions of the One-Dimensional Heat Transfer Model	125	

#### CHAPTER ONE

#### INTRODUCTION

# 1.1. Research Description and Scope

Increasing demand for composites and polymers in the automotive, aerospace, construction, and sporting goods industries has invited efficient and novel techniques for processing polymeric materials. Most conventional closed mold processing techniques using thermosets rely on conduction heating from the hot mold surfaces to induce the crosslinking. Large temperature gradients inherently develop in resins and composite systems with thick cross-sections or with low thermal conductivities. Residual thermal stresses, anisotropic degrees of cure, resin degradation, and part warpage may originate from these large temperature gradients, diminishing the mechanical properties of the processed part. Additionally, production of thick cross-section parts with low thermal conductivities requires longer cycle times due to low heat transfer rates.

Virtues of microwave heating make microwave processing a viable candidate as an alternative to many conventional polymer and composite processes. However, despite the demonstrated advantages of microwave curing on the laboratory scale, microwave processing has not fully developed in industry. A major factor restraining industrial use of microwave processing is the lack of suitable tooling.

Composites have been cured using a microwave resonant cavity. Molds are fabricated with low loss materials to the desired part geometry, charged with process material, and placed in a cylindrical resonant cavity. This technology has demonstrated

potential for processing composites in an atmospheric pressure environment. However, the low loss mold materials, such as Teflon, quartz, or polyethylene, typically do not possess the mechanical properties to maintain integrity for any cyclic process using pressure. In order to be competitive with liquid composite molding processes requiring pressure such as resin transfer molding (RTM) and structural reaction injection molding (SRIM), a microwave part-shaped cavity was designed. In this design, a metallic cavity serves as the mold for the processed part and as the microwave applicator. This novel approach allows pressure during processing and eliminates the need for fabricating a microwave transparent mold.

In this research, the electromagnetic behavior of the part-shaped applicator system is characterized theoretically using Maxwell's equations. As part of this development, key scale-up issues such as modes of propagation, penetration depths, electric field (E-field) distribution, and cutoff frequencies are determined. The microwave heating patterns, using fully cured glass-reinforced polyester plates, are experimentally characterized in the part-shaped applicator for comparison to theory and for determining a heating scheme for maximum heating uniformity during a cure cycle. This research also includes the development of the part-shaped applicator into a laboratory RTM unit including a pumping system, an external heating system for hybrid heating, and a microwave multiplexing system. Three epoxy parts are cured in the part-shaped cavity by microwave heating, conventional heating, and hybrid heating where both microwave and conduction heating are employed.

## 1.2. Microwave Processing of Materials

Microwaves are oscillating electromagnetic waves with a frequency roughly between 300 MHz and 300 GHz, as shown in Figure 1.1, which correspond to characteristic wavelengths of 1 m to 1 mm, respectively. Since the end of World War II, microwave energy has been utilized extensively in both communication and non-communication applications<sup>1</sup>. The primary non-communication applications are in medicine and heating. Typically, those frequencies designated by International Telecommunication Union for industrial, scientific, and medical (ISM) applications are used for heating. The ISM frequencies are specific to each nation<sup>2</sup>. Two commonly used ISM frequencies, regulated by the Federal Communications Commission, for microwave heating in the United States are 915 MHz and 2.45 GHz. Non-ISM frequencies may also be used for heating purposes; however, leakage must be controlled to avoid interference with frequencies designated for other purposes such as communications<sup>3</sup>.

Microwave processing of polymeric materials became of interest in the late 1960s, followed by a lull and then a renewed interest in the mid-1980s<sup>4</sup>. A major research area today is in the development of microwave processing of high-performance polymeric composite materials<sup>5-9</sup>. Numerous advantages over conventional polymer processing have been demonstrated. The following section expounds on select virtues of microwave processing of polymers and composites.

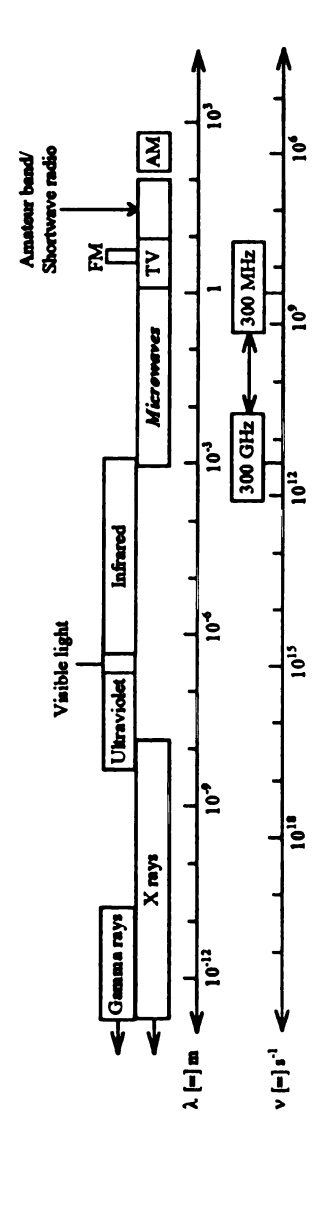


Figure 1.1. The Electromagnetic Spectrum and Microwave Frequencies for Heating.

### 1.2.1. Rationale

As shown in Table 1.1, the fundamental differences in heat transfer result in distinctions between conventional and microwave processing. Compared to the conductive heating techniques employed by most conventional composite and polymer processes, microwaves offer many advantages due to the electromagnetic interaction with the process material. The advantages of microwave processing are typically divided into two categories: microwave characteristics and microwave effects. The former encompasses all virtues of microwave processing that are predictable based on electromagnetic and/or heat transfer theory. Benefits of microwave processing that can not be explained using traditional theories are classified as microwave effects. Naturally, many emerging theories on microwave effects create a controversial research area.

Table 1.2<sup>16-13</sup> presents a summary of microwave characteristics and effects.

Attaining the desired processing temperature in the center of thick cross-section parts is often a limiting factor in polymer and composite processing. Due to the penetration of microwave radiation into the process material, heating occurs throughout the material volume for relative low loss systems. In fact, microwave applicators typically provide preferential heating in the center of the part which results in a temperature gradient that is the inverse of that for conventional processing.

By implementing the proper microwave generator and applicator, heating for most polymer systems is very rapid and efficient. In contrast, conduction heating, as

Table 1.1. Comparison of Conventional to Microwave Thermoset Processing.

	Conventional Processing	Microwave Processing
Temperature gradient	highest temperature near mold walls - lowest temperature at part center	inverse of conventional temperature gradient
Heat transfer to the part center	limited by the thermal diffusivity	direct energy input due to penetrating nature of electromagnetic radiation
Rate of energy input	directly proportional to the temperature difference between the tooling or surroundings and the part surface	directly proportional to the square of the E-field and the effective dielectric loss of the process material
Control of energy input	limited by controllability of the tooling or surrounding temperature	instantaneous control

Table 1.2. Microwave Characteristics and Effects 10-13.

Characteristic/Effect	Advantage	
Penetrating radiation (Characteristic)	Volumetric heating	
	Rapid and efficient heating	
	On/off controllability	
Controllable E-fields (Characteristic)	Ability to process low-loss materials	
	Ability to process parts of complex geometry	
Differential coupling (Characteristic)	Self-limiting heating of thermosets	
	Improved matrix/carbon fiber interfacial strength	
Reaction rate enhancement (Effect)	Potential cycle time reduction	
Improved physical properties (Effect)	Potential improvement in part performance	

employed by most conventional processes, occurs across a surface and heat transfer from the surface to the center of the polymer system is slow due to relatively small thermal diffusivities. Heat transfer to process material in conventional molds is proportional to the temperature difference between the material and the mold. The mold temperature and, hence, the heat transfer rate are limited by polymer degradation temperature. Figure 1.2 illustrates a qualitative processing window for thermoset processing. The characteristic microwave penetration offers potential on an industrial scale to shift the processing time closer to t<sub>1</sub> and, therefore, reduce cycle time and production cost.

Microwave penetration also aids in the controllability of heating. Conversion of electromagnetic energy to thermal energy is instantaneous; therefore, microwave heating offers on-off controllability of energy input into the process material. An intrinsic time lag is often associated with the control of conventional tooling due to the mold material heat capacity.

Electromagnetic fields can be tailored to provide very high localized field strengths. This is beneficial for processing low-loss materials (i.e., materials with low microwave power absorption) and irregularly shaped materials. Fellows and Hawley<sup>14, 15</sup> exploit this concept in the processing of V-shaped composites in a single-mode cavity using a technique called mode-switching. Using only one mode in a single-mode cavity during a curing cycle often results in localized heating. By switching modes, one can generate field patterns with varying intensities and spacial locations. To maximize heating uniformity, Fellows identified complementary modes and switched between these modes by mechanically adjusting the cavity length. Qiu et al. <sup>16-18</sup> demonstrated the same

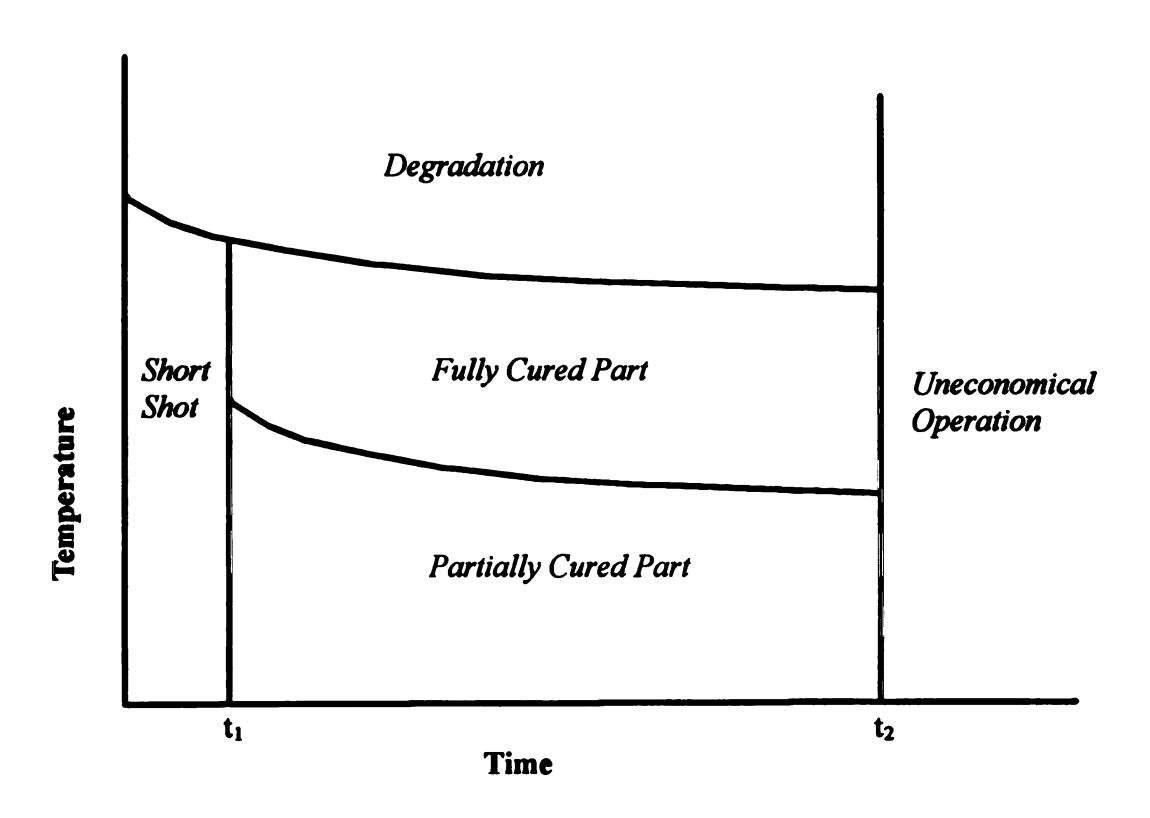


Figure 1.2. Generalized Thermoset Processing Window.

concept in a single-mode cavity with a fixed cavity length by switching modes electronically. This technique is termed variable frequency processing, where the several frequencies are selected alternatively to excite modes in an intelligent switching sequence. In general, variable frequency processing offers a more robust and efficient processing method than mechanical mode switching.

The dielectric loss is one of the physical parameters that determines the microwave power absorption in a material. When a mixture of components with different dielectric losses is electromagnetically heated, the various components exhibit differential coupling. In some polymer processing cases, this phenomenon has been demonstrated to improve mechanical properties. For instance, Agrawal and Drzal<sup>19</sup> cured carbon fiber-reinforced epoxy specimens using microwave radiation; these samples showed as much as a 70% increase fiber-matrix adhesion. This observation could possibly be attributed to an improved epoxy network structure at the fiber-matrix interface due to the relatively high energy absorption of the carbon fibers.

Wei<sup>26</sup> investigated the effects of microwaves on the crosslinking of two stoichiometric epoxy mixtures: diglycidyl ether of bisphenol A (DGEBA) with a high loss curing agent, diaminodiphenyl sulfone (DDS), and DGEBA with a low loss curing agent, meta phenylene diamine (*m*-PDA). Wei reported an enhanced reaction rate for the microwave cure as compared to the thermal cure at the same temperature. Additionally, the T<sub>g</sub> analysis indicated that similar glass transition temperatures for microwave and thermally cured samples were obtained at low conversion. However, at larger conversions, higher T<sub>g</sub>'s were observed for the microwave cured samples. Again, improved network structure may be

responsible for the increased T<sub>g</sub> in microwave cured epoxies at high extents. This enhancement is much more significant in the DDS cured DGEBA than in the m-PDA cured DGEBA, possibly due to the fact that DDS has a much higher dipole moment than m-PDA.

For thermosets, microwaves offer self-limiting heating during processing. Cross-linked materials are relatively less susceptible to microwave heating due to the decrease in dipolar mobility and, hence, dielectric properties with extent of reaction. During polymerization, the concentration and magnitude of dipoles can decrease, further causing diminished dielectric properties. Therefore, the microwave energy will concentrate intrinsically on the unreacted resin. This is another illustration of differential coupling.

As discussed above, the microwave characteristics, including radiation penetration, controllable E-fields, and differential coupling, lead to advantages of microwave processing over conventional processing. Some of the controversial microwave effects include enhanced polymerization rates, greater T<sub>B</sub> and improved mechanical properties include. These enhancements may be due to one or more phenomena on the molecular level, including enhanced segmental vibration, preferential alignment of dipolar segments, and creation of "energetic species". One theory attributes the reaction rate enhancement to a non-equilibrated temperature effect where high loss species, such as DDS, experience a higher local temperature than the bulk<sup>22</sup>. Further studies are required to clarify and quantify these microwave effects.

## 1.2.2. Applications

Microwave heating is a relatively new technology. Significant developments in the use of microwaves for heating purposes did not commence until after World War II. In 1951, the first microwave generator became commercially available for restaurant use, followed by the infusion of the domestic microwave ovens in the 1960s<sup>23</sup>. To date, microwave processing has been well established in the food, rubber, textile and lumber industries.

Commercial applications of microwave processing of polymers have been limited to a few successful operations, including vulcanization of rubber 12,24-26, production of polyvinylchloride belts<sup>27</sup>, production of urethane foam<sup>27</sup>, and curing plywood adhesives 11. Some experts speculate that possible users of microwave processing have been turned away because of the lack of knowledge of the details and limitations of equipment and processes 28, the lack of suitable tooling 3, and conservatism 29. In the past decade, there has been a concentrated effort in exploring and developing microwave processing techniques for polymers and composites. The following two sections highlight specific research findings in the use of microwave processing of polymers and composites on the laboratory scale.

## 1.2.2.1. Polymer Processing

Microwaves have been utilized in the processing of both thermosets and thermoplastics in various capacities. With thermoplastic processing, microwaves have been used as an energy source for such operations as drying<sup>30</sup>, polymerization<sup>11</sup>, melting<sup>31</sup>, and

foaming<sup>31</sup>. For the processing of thermosets, microwave energy has been used primarily to promote crosslinking.

In general, the physical processes occurring during the conversion of electromagnetic energy to thermal energy for thermoplastics are different than those for thermosets. Chen<sup>32-34</sup> et al. performed a thorough investigation of the factors influencing microwave absorptivity of several amorphous and semicrystalline thermoplastics. Inflections in the microwave heating rates as a function of temperature or frequency are attributed to molecular relaxations.

Microwave calorimetric studies revealed a critical temperature, T<sub>e</sub>, above which rapid volumetric heating is feasible. T<sub>e</sub> is typically between the T<sub>g</sub> and the melt temperature, T<sub>m</sub>. Since most T<sub>g</sub>s are above room temperature, microwave heating of thermoplastics from room temperature is challenging. To overcome the low microwave absorptivity at room temperature, the temperature of the thermoplastic can be raised to T<sub>e</sub> by employing conventional heating or relatively lossy molds to absorb microwave radiation at lower temperatures.

George et al.<sup>30</sup> presented results of heating tests conducted on polyvinyl chloride (PVC), polycarbonate (PC), polypropylene (PP), and acrylonitrile butadiene-styrene polymer (ABS) pellets. These polymers were dried using a tray dryer at 104°C and, for comparison, a microwave oven with an air sweep above the oven bottom. The penetrating nature of microwaves results in internal heating of the water bound in the plastics, thus water is forced out from the pellet center. Conversely, conventional heating relies on heat transfer to the center of the pellets and water diffusion from the center to the surface of the pellets. As a result, the microwave oven dried the polymers

4 to 16 times more rapidly, depending on the hygroscopic nature of the polymers. The tensile strength and impact resistance were slightly improved for the microwave drying cases possibly due to less thermal degradation at the shorter drying times.

Several investigations have been performed on microwave curing of thermosets, including epoxies<sup>7-9,19-21,35,36</sup>, polyesters<sup>6,36,38</sup>, polyimides<sup>39-41</sup>, and polyurethanes<sup>36,42,43</sup>. For microwave curing, epoxies are the most widely studied thermosets.

During the early stages of cure, the dielectric properties of thermosets typically increase to a maximum followed by a decrease to a constant value. To commence crosslinking, the resin is usually heated to a cure temperature. During this stage, the viscosity of the thermoset decreases, corresponding to an increase in molecular mobility. The dipolar groups of the resin are less restricted to rotate with the oscillating E-field, so the microwave absorptivity increases. Two molecular phenomena that affect the polarizability occur during crosslinking are changes in the types and concentration of polar groups and the formation of a three-dimensional network. For example, curing an epoxy with an amine curative involves a decrease in epoxide dipoles, a change of amine dipoles from primary to secondary and tertiary, and the creation of hydroxyl dipoles. As the crosslinking density increases, the polarizability greatly decreases causing diminished dielectric properties of the cured thermoset. Research in modeling dielectric properties has become an increasingly intensified area 44.51. The dielectric behavior of a thermosetting system can give indications of mechanisms of microwave - molecular interaction for systems that exhibit microwave effects (i.e., enhanced reaction rates) and provide a means of in situ monitoring of the cure process.

Reports in the literature on comparative kinetic studies between conventionally and microwave cured samples vary dramatically 52-60, ranging from no statistical deviation to a 40-fold increase in reaction kinetics for microwave cured samples. The inconsistent results could be attributed to the lack of a standardized testing procedure. Mijovic and Wijaya<sup>52</sup> initially claimed a decrease in reaction kinetics for microwave curing of digylcidyl ether of bisphenol A (DGEBA) and diaminodiphenyl sulfone (DDS) and later<sup>53</sup> argued that the difference was statistically insignificant. Mijovic also observed a broad two-step glass transition in some of the microwave cured DSC thermographs for the DGEBA/DDS samples. Two-step glass transitions were not observed with thermal cures, possibly indicating a different reaction mechanism and network structure between microwave and thermally cured epoxies. Mijovic studied DGEBA with a 4,4'methylenedianiline (MDA) curative and found no apparent change in reaction kinetics with the processing method. However, DeLong et al. 60 discovered a slightly enhanced DGEBA/MDA reaction rate under the influence of an electromagnetic field. Further kinetic studies are necessary to elucidate the apparent effect of reaction rate enhancement.

Many investigators have demonstrated that controlling the microwave pulse frequency can be an important process variable. For instance, Beldjoudi and Gourdenne<sup>61</sup> reported that a DGEBA/DDM system reached the gel point in 19.0 minutes using a 1000 Hz pulse frequency with a pulse length of 0.25 ms and an average power of 40W. Gelation occurred in 23.8 minutes for the continuously radiated epoxy at 40W. A more rapid gel time is actually a phenomenological effect due to an enhanced heating rate for the case

with pulsed energy due to what Beldjoudi explains as a double relaxation. That is, the microwave source provides the dipolar orientation, and the lower frequency pulses excite molecular segmental relaxations.

Jow et al. 62 cured DGEBA/DDS samples utilizing conventional heating and continuous and pulsed microwave radiation. More rapid heating and higher temperatures were realized with pulsed microwave heating. Additionally, pulse heating provided superior temperature control.

Lewis et al. 55 conducted an experimental investigation on the crosslinking of DGEBA epoxy resin with 4,4'- or 3,3'-diaminodiphenyl sulfone using microwave radiation. Results show that the mechanical properties of the microwave-crosslinked resin were similar to those of the thermally crosslinked system. But microwave radiation significantly accelerated the crosslinking. The degree of acceleration in the rate of crosslinking depended on both power and sample size.

## 1.2.2.2. Composite Processing

Polymer composites have found numerous applications as structures and components in the automotive, aerospace, recreational, construction, and appliance industries. Some of the benefits of composites include the high strength property-to-weight ratio, low specific gravity, and ability to integrate components. The selection of metal versus composites, however, is often driven by the composite unit cost. Since long processing times can contribute significantly to the unit cost, the potentially enhanced reaction kinetics and faster cycle times make microwave processing an

attractive alternative to the conventional processes such as autoclaving, RTM, and SRIM.

Lee and Springer<sup>63</sup> performed one of the earlier investigations of composite curing experiments. A low-loss press, constructed of polypropylene and glass-reinforced Teflon, provided pressure during the cure of Fiberite S2/9134B glass epoxy and Hercules AS/3501-6 graphite epoxy specimens. The press apparatus and lay-up composite were placed in a domestic multimode 2.45 GHz microwave oven with controllable power up to 700 watts. The effect of polarization angle on both unidirectional and multidirectional laminates on the temperature distribution and curability was investigated. Lee discovered that the glass-reinforced epoxy samples could be cured effectively for any ply orientation and polarization angle. However, effective curing was only realized for the unidirectional graphite-reinforced epoxy samples and a polarization angle of 90°; multidirectional laminates could not be sufficiently cured. Poor heating of the graphite-reinforced epoxy laminates can be attributed to electromagnetic reflection at the sample surface due to the large electrical conductivity of the graphite fibers.

By using a single-mode cavity, Wei et al. <sup>64</sup> demonstrated curability of 72-ply crossply and unidirectional graphite-reinforced epoxy samples (Hercules AS4/3501-6) in a single-mode cavity. The single-mode cavity offers selectivity of the resonant electromagnetic modes and, hence, control of the heating profiles. In commercial multimode ovens, the heating patterns are uncontrollable, often resulting in anisotropic

cure. This could explain the ineffective cure of crossply samples reported by Lee and Springer in the multimode oven.

Power dissipation in a fully cured carbon fiber-reinforced epoxy disk was studied in a cylindrical single-mode cavity by Fritz and Asmussen<sup>65</sup>. Since carbon fibers are conductive, a significant microwave power attenuation, or a skin effect, occurs from the disk surface. By studying temperature profiles, Fritz calculated a penetration depth of approximately 1 cm for a 2.45 GHz microwave source. The penetration depth is the distance through which the microwave power density is reduced to 1/e of the surface power density. Because of the skin effect, microwave heating of composites with conductive fibers is often achieved by thermal conduction from the surface layer.

Since composites are often implemented in structural applications, the effect of microwave processing on the composite mechanical properties is of interest to many investigators. Wei et al. 66 studied the failure modes of graphite fiber-reinforced epoxy composites (Hercules AS4/3501-6) using SEM analysis. The photomicrographs revealed that microwave processed samples failed in a matrix failure mode.

Conventionally cured samples failed in a combination of interfacial and matrix failure modes. This suggests an enhanced graphite fiber/epoxy bonding for the microwave processed composites.

Agrawal and Drzal<sup>19</sup> studied the mechanical property characteristics of epoxy composites. Single fiber properties were investigated by curing DGEBA with a metaphenylene diamine (m-PDA) curative with a single carbon, glass, or aramid (kevlar) fiber in a dogbone cavity. For each fiber type, samples were cured using microwave and

and photomicrographs reveal that the fiber-matrix adhesion for the graphite composites was enhanced. The interfacial shear strength for the microwave cured samples was 70% greater than that for conventionally cured samples. Failure occurred in the matrix for microwave cured specimens; however, conventionally cured specimens failed at the interface. The tensile test for the aramid and glass fiber samples revealed that the interfacial shear strength for the conventionally cured samples is 15% greater than that for the microwave cured samples. This could possibly be attributed to an incomplete network structure around the glass and aramid fibers for the microwave cured samples.

By using a lap shear compression test with E-glass panels, Boey and Yue<sup>67</sup> demonstrated that microwave cured samples could have a greater shear strength than conventionally cured samples. In fact, a 100% increase in shear strength was realized for microwave cured samples that were exposed to 500 W for 15 minutes. From this work, however, one can not conclude that microwave processing of glass-reinforced epoxy results in improved shear strength relative to conventionally cured samples in all cases. Several power ratings and radiation times were investigated for microwave cured samples, while no indication was given that the time and temperature for the conventional cure cycle was optimized to yield the best shear strength. This paper does illustrate the importance of engineering a proper microwave power cycle. The physical properties are highly dependent on the processing cycle.

## 1.2.3. Microwave Processing Systems

The microwave circuitry is the system through which microwaves are directed to the applicator. Figure 1.3 illustrates a typical cavity configuration. Arrangement and type of the circuitry components may vary depending on the particular process needs. For example, high power applications (i.e., approximately > 500W) typically use waveguides instead of coaxial transmission lines. Waveguides have very little loss compared to coaxial lines.

Of the commercially available microwave sources, magnetrons, klystrons, traveling wave tubes (TWT), and gyrotrons, magnetrons are the most commonly used generators. Magnetrons offer high power outputs, efficient operation, frequency stability, and relatively low cost<sup>68</sup>. The desired heating rate of the process material must be considered when the proper generator power requirements in polymer processing are engineered. Typically, during the cure of thermosetting polymers, the resin experiences two network transformations: gelation and vitrification. Gelation refers to the process of converting a thermosetting resin to a crosslinked network with an infinite weight-average degree of polymerization. Vitrification refers to the transformation of the liquid or gel to a glassy state. For maximum physical strength, complete gelation should occur before vitrification. Using excessive microwave powers can cause vitrification before complete gelation to produce a gelled rubber or a charred polymer. Boey and Lee<sup>69</sup> discovered that using an 800 W power source for curing a 10-mm thick glass-reinforced DGEBA/DDS composite resulted in thermal degradation of the sample. This case study illustrates the importance of implementing process control and selecting the proper generator power.

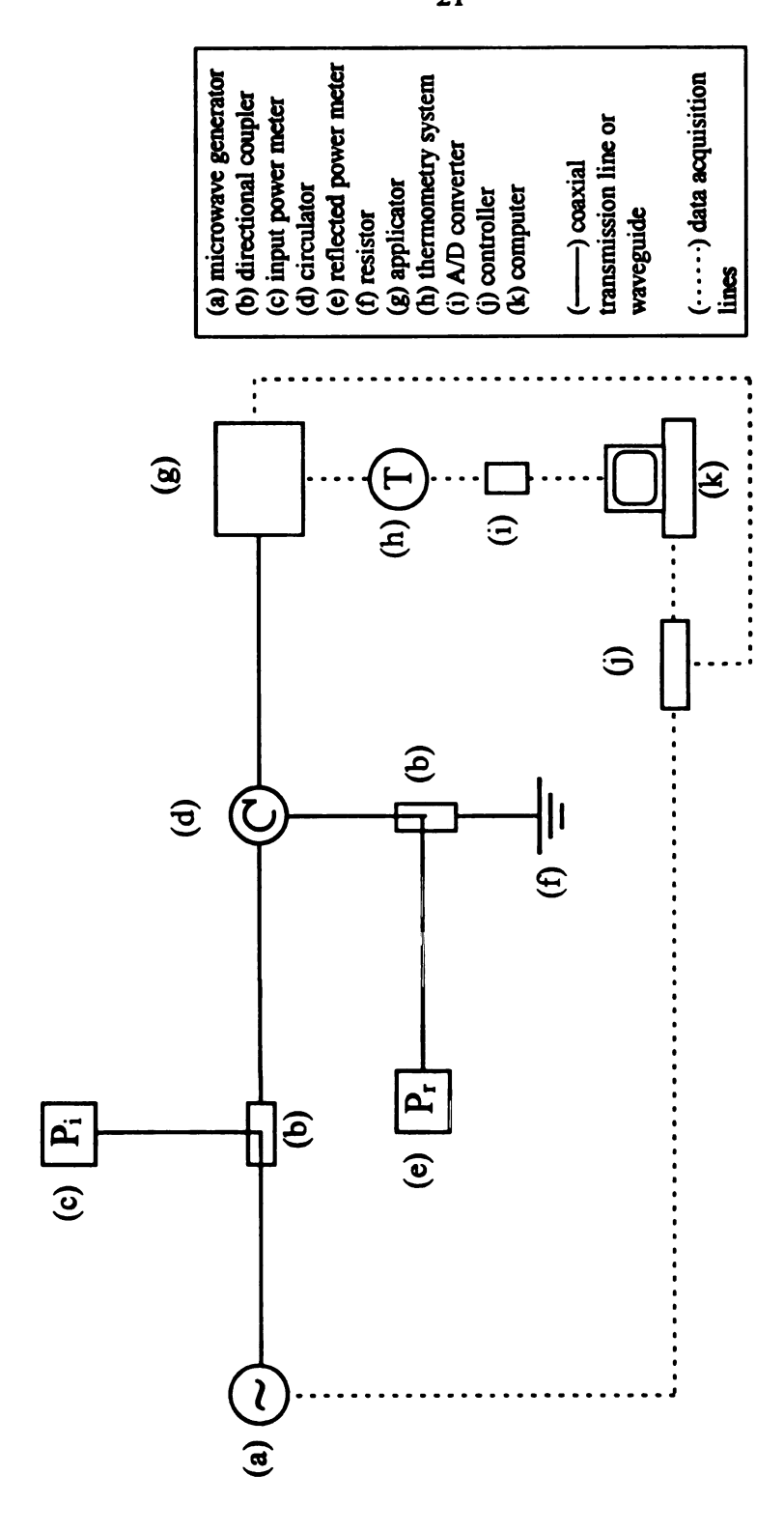


Figure 1.3. Typical Microwave System Circuitry.

Successful commercialization of microwave processes requires process control and automation to provide an attractive "user-friendly" system. Issues of process control and automation of microwave systems have been investigated experimentally. Compared to a manually operated system, an automated system can improve the overall process efficiency, reduce sample temperature gradients, minimize temperature excursions due to reaction exotherms, and eliminate the need for an experienced operator.

The microwave applicator is the apparatus through which microwaves are applied to the process material. Of the four basic types of applicators (i.e., multimode, traveling wave, single-mode, and specialized), the multimode applicator is the most common. However, the multimode oven is, ironically, the most empirical of the four types. A multimode oven is, generally, a parallelopipedic box or cube in which several modes are excited over a small frequency band. One of the major challenges with processing with a multimode oven is heating uniformity due to uneven distributions of electromagnetic energy in the cavity. Several techniques have been investigated to improve heating uniformity. For example, Kashyap and Wyslouzil<sup>71</sup> address two methods that improved the energy distributions: multislot waveguide feed with a stirrer system and frequency sweeping. With the stirrer system, the multi-slot waveguide feed essentially transports the microwave incident energy to select locations inside the cavity. Frequency sweeping alters the mode types that are excited in the cavity, and, therefore, redistributes the energy.

Traveling wave applicators are chiefly used for continuous processing of high loss material; low loss materials require an excessively long waveguide or slow processing speed to absorb the necessary energy<sup>72</sup>. Waveguides are hollow circular or rectangular pipes

through which electromagnetic energy is transmitted. For continuous processing of materials, slots for the feed and exit are cut in the waveguides at locations of low E-field to minimize energy leakage. Theoretically, the microwave radiation in traveling wave applicators propagates in one direction only. The energy that is not absorbed by the process material is directed to a matched load.

Relative to multimode and traveling wave applicators, the efficiency and field strength of single-mode applicators are greater. In principle, the single-mode applicator is a cavity in which an incident wave in superposition with reflected waves creates a standing wave at a resonant frequency. The well-defined distribution of electric and magnetic field vectors is termed a mode. Controllability of these modes is attained by adjusting the cavity volume or the microwave frequency. Because of the high E-field capability, single-mode cavities are ideal for the processing of low loss materials.

Applicators that cannot be purely classified as multimode, traveling wave, or single-mode are categorized as specialized applicator. Specialized applicators are often hybrids of two applicators. For instance, the part-shaped cavity is a specialized applicator in that both resonance and traveling wave conditions exist during processing. Details on the overall equipment and components are given in Chapter 3.

# 1.3. Resin Transfer Molding

Resin transfer molding (RTM) is regarded by some as being the "leading technology to provide large primary structures in the future" and "perhaps the only composites fabrication technique that is simultaneously gaining rapid acceptance in both

the aerospace and automotive industries"<sup>74</sup>. RTM technology has been in existence for over half a century and, more recently, has demonstrated the capability of producing structural composites as well as class A surfaces for cosmetic applications. Chrysler corporation is demonstrating this capability by manufacturing the limited-edition Dodge Viper. Over half of the Viper exterior, including the hood, front fenders, rear quarter panels, decklid, and roof supports, is manufactured using RTM<sup>75</sup>. In another case study, the General Motors Corporation produces a glass reinforced-epoxy composite leaf spring for the Corvette using RTM. Several other industries manufacture composite components using the RTM technology, as outlined in Table 1.3<sup>(76)</sup>.

#### 1.3.1. Process Cycle

The development of RTM began in the 1940s as a one-pot process called the *Marco* process<sup>77</sup>. This technique involved mixing a thermosetting resin and a catalyst before injecting the resin system into a mold cavity filled with randomly-oriented fiberglass. At room temperature, the final composite would then cure.

Today the RTM process concept is the same; however, the processing details have evolved to meet the specific needs of the RTM industry. Figure 1.4<sup>(78)</sup> illustrates the various steps, in essence, involved with RTM. Initially, the mold is prepared by removing foreign particles and preparing the seals, sprue, and vents. If necessary, various coatings are applied to the mold walls. For instance, a mold release agent can be utilized to assist in part removal. A gel-coat could also be applied to improve the surface quality of the molded part by minimizing reinforcement read-through. The gel-coat may

Table 1.3. Examples of Components Manufactured by RTM<sup>76</sup>.

Industry	Component
Aerospace	airplane wing ribs
	cockpit hatch cover
	fuselage frame
	radar housing
	wing flaps
Automotive	body panel
	cross member
	decklid
	fender
	hood
	leaf spring
	rear quarter panel
	transmission housing
Recreational	boat hull
	canoe paddle
	golf clubs
	ice hockey stick
	ski poles
	snowmobile body
	trailer
Construction	bathtub
	safety helmet
	seating
	septic tank
	water tank
Appliance	computer housing
	fan blade
	television antenna

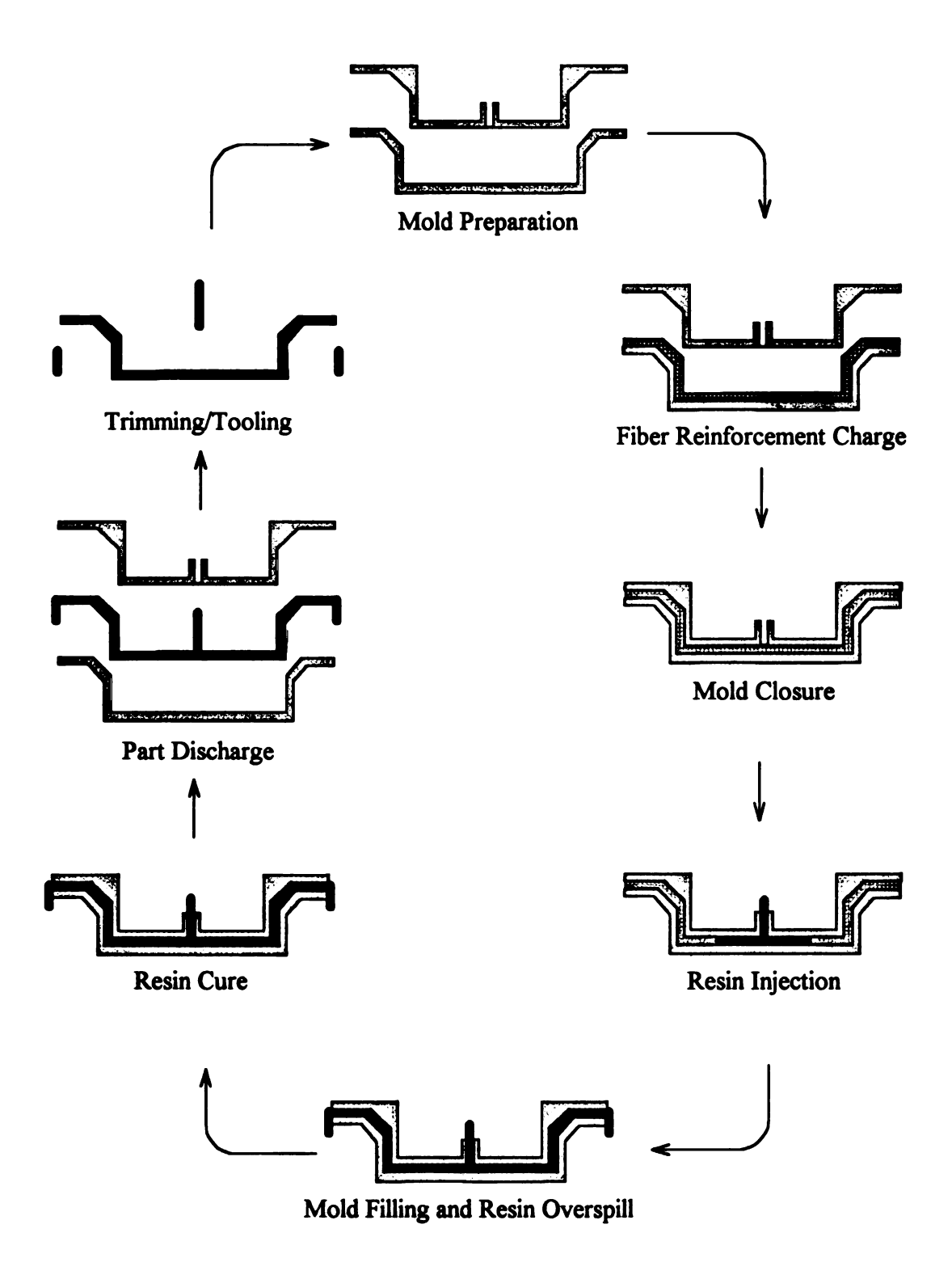


Figure 1.4. RTM Processing Cycle<sup>78</sup>.

also protect the part surface from weathering. Next, a continuous, strand mat, woven roving, or cloth reinforcement system is placed on the mold surface. The fibers may or may not be preshaped. The mold is closed, and a thermosetting resin is injected into the mold cavity through a sprue that is typically centrally located. The resin displaces the air in the fiber reinforcement and fills the mold to the air vents. The final composite is either cured at room temperature or at elevated temperatures, depending on the selected resin system. Upon reaching the desired conversion, the composite is removed from the mold and trimmed, if necessary.

Because of the low thermal conductivities of most thermosets and fiber reinforcements, large temperature gradients can develop in parts with a thick cross-section. Additionally, the curing stage could be excessive due to inadequate temperatures in the composite center. Considering these issues, the penetrating characteristic of microwave processing offers a potential solution to cycle time reduction and uniform curing of thick composites. Electromagnetic radiation has been exploited in curing binders used in fiber mats<sup>79-83</sup>; however, to date, microwaves have not been utilized in the curing stage of RTM processing.

# 1.3.2. Polymer Matrices

Performance characteristics, processability, and cost must all be considered when selecting a polymer system. As is evident from Table 1.3, parts manufactured by RTM have a wide range of performance criteria and, therefore, demand a wide range of resin

performance characteristics. Epoxy or polyester resins are typically used; however, RTM is adaptable to numerous thermosets, including polyurethanes, phenolics, bismaleimides, and methacrylates<sup>84</sup>.

Epoxies typically exhibit physical properties, such as toughness, flexibility, and strength, required for higher performance parts. Additionally, epoxies offer good surface quality, chemical resistance, excellent adhesion, low shrinkage, and high service temperature. Bisphenol A-based resins constitute the majority of the epoxy resins used with RTM.

# 1.3.3. Fiber System

The selection of the reinforcement for a composite dictates the composite performance properties such as specific gravity, tensile strength, and modulus.

Additionally, since the fibers can constitute over half of the part volume fraction, the reinforcement significantly impacts the part cost.

Typical fibers used in RTM include E-glass, S-glass, carbon, and aramid. E-glass and S-glass exhibit high tensile strengths, good chemical resistance, and excellent insulating properties. Carbon fibers are very attractive for high performance applications due to the high tensile modulus, low coefficient of thermal expansion, and high fatigue strengths. Aramid fiber is a general term for an aromatic polyamide fiber. This fiber system offers exceptionally high strength, low density, and toughness.

Selections of the fiber reinforcement and resin system are not independent. The adhesion promoter sizing on the fibers must be compatible with the resin system.

Achieving intimate resin-fiber contact is essential to maximizing mechanical properties of

the final composite. Poor resin-fiber contact results in diminished part performance due to weakened interlaminar shear strength and fiber pull-out under stress.

#### **CHAPTER TWO**

#### **THEORY**

# 2.1. Maxwell's Equations

The study of electrostatics reveals that a stationary volume charge density,  $\rho$ , results in an electric field,  $\vec{E}$ , about the charge volume. Analogously, the study of magnetostatics shows that a constant volume current density,  $\vec{J}$ , throughout a test volume produces a magnetic flux density,  $\vec{B}$ . If  $\vec{J}$  in a fixed volume varies with time,  $\rho$  will change as well with time according to the conservation of electric charge:

$$\nabla \cdot \vec{\mathbf{J}}(\vec{\mathbf{r}},t) + \frac{\partial}{\partial t} \rho(\vec{\mathbf{r}},t) = 0.$$
 [2.1]

Since J and  $\rho$  are coupled through Equation [2.1],  $\vec{E}$  is coupled to  $\vec{B}$  for time-varying electric sources. The equations that define the relation between  $\vec{E}$  and  $\vec{B}$  as a function of J and  $\rho$  are termed Maxwell's equations, named after the theoretician James Clerk Maxwell. Maxwell's equations provide the foundation for electromagnetism.

For solving time-varying fields, a common representation of Maxwell's equations is in complex phasor form, valid at any point † in the defined system. For fields produced by a source of constant angular frequency, ω, the Maxwell field equations are represented as follows:

$$\nabla \times \vec{\mathbf{E}}(\vec{\mathbf{r}}) = -j\omega \vec{\mathbf{B}}(\vec{\mathbf{r}})$$
 [2.2]

$$\nabla \cdot \vec{\mathbf{B}}(\vec{\mathbf{r}}) = 0 \tag{2.3}$$

$$\nabla \times \vec{\mathbf{H}}(\vec{\mathbf{r}}) = \vec{\mathbf{J}}(\vec{\mathbf{r}}) + \mathbf{j}\omega\vec{\mathbf{D}}(\vec{\mathbf{r}})$$
 [2.4]

$$\nabla \cdot \vec{\mathbf{D}}(\vec{\mathbf{r}}) = \rho(\vec{\mathbf{r}}) \tag{2.5}$$

where  $\vec{E}(\vec{r})$  = electric field strength [=] volts/m,  $\vec{D}(\vec{r})$  = electric flux density [=] coulombs/m<sup>2</sup>,  $\vec{H}(\vec{r})$  = magnetic field strength [=] amperes/m,  $\vec{B}(\vec{r})$  = magnetic flux density [=] webers/m<sup>2</sup>,  $\vec{J}(\vec{r})$  = volume current density [=] amperes/m<sup>2</sup>,  $\rho(\vec{r})$  = volume charge density [=] coulombs/m<sup>3</sup>,  $\vec{J}$  = imaginary number  $\sqrt{-1}$ , and  $\vec{J}$  = angular frequency [=] radians/s.

Using a series of vector operations and Equation [2.1], it can be shown that Equations [2.2] through [2.5] actually represent only two independent vector equations.

 $\vec{D}$  and  $\vec{B}$  can be eliminated by introducing the following constitutive equations for linear "simple" matter<sup>85</sup>:

$$\vec{\mathbf{D}} = \mathbf{\epsilon}^{\bullet}(\mathbf{\omega})\vec{\mathbf{E}}$$
 [2.6]

$$\vec{\mathbf{B}} = \boldsymbol{\mu}^{\bullet}(\boldsymbol{\omega})\vec{\mathbf{H}} \tag{2.7}$$

Here,  $\epsilon^*(\omega)$  is called the complex permittivity, and  $\mu^*(\omega)$  is termed the complex permeability. The behavior of  $\epsilon^*(\omega)$  is dependent on the material medium. Details on  $\epsilon^*(\omega)$  are given in Section 2.3. For non-magnetic material,  $\mu^*(\omega)$  is simply the permeability of free space,  $\mu_0$ .

# 2.2. Wave Propagation

Electromagnetic energy is transmitted from regions in space via electromagnetic modes. An electromagnetic mode is a distinct field pattern that is classified as one of four possible categories: transverse electric (TE), transverse magnetic (TM), transverse electromagnetic (TEM), and hybrid (HE). Physically, a TE mode does not have an electric field component in the direction of propagation, and a TM mode does not have a magnetic field component in the direction of propagation. Both electric and magnetic field components in the propagation direction are zero for the TEM mode and non-zero for the HE mode.

Mathematically, the fundamental equations that define the electric and magnetic field behavior are Maxwell's equations. These equations coupled with the proper assumptions (e.g., perfect reflection at metallic boundaries), mode classification (i.e., TE, TM, TEM, or HE) and boundary conditions define a boundary-value problem with a harmonic eigenvalue solution.

At any material interface, the tangential component of the E-field is continuous and the normal component of the B-field is continuous. A special case of these boundary conditions is a dielectric-conductor interface. Since the E-field and the H-field, or B-field, are essentially non-existent in the conductor, the tangential E-field and normal H-field at the dielectric-conductor interface are zero.

The following two sections present two specific systems for transporting, storing, or transferring electromagnetic energy: the rectangular waveguide and the rectangular

cavity resonator. Details of the derivations for the equations shown in the next two sections are outlined in Appendices A and B.

# 2.2.1. Rectangular Waveguide

A waveguide is a structure with, typically, either a rectangular or a circular cross section defined by conductive boundaries that is used to transport electromagnetic energy. Waveguides have also been used to heat material. Energy from a microwave generator travels through the waveguide and is partially absorbed by the process material. The remainder of the energy is directed to a terminating load. Waveguide applicators are primarily used for continuous processing of high loss material; low loss materials require an excessively long waveguide or slow processing speed to absorb the necessary energy.

For TE modes in a rectangular waveguide, the E-field components are given in phasor notation by:

$$E_x = C_1 k_y \cos(k_x x) \sin(k_y y) \exp(-jk_z z), \qquad [2.8]$$

$$E_v = -C_1 k_x \sin(k_x x) \cos(k_y y) \exp(-jk_z z), \text{ and}$$
 [2.9]

$$\mathbf{E}_{\mathbf{z}} = \mathbf{0}, \tag{2.10}$$

where  $C_I = a$  constant,

$$k_x = \left(\frac{m\pi}{a}\right), m = 0, 1, 2, \dots,$$
 [2.11]

$$k_y = \left(\frac{n\pi}{b}\right)$$
,  $n = 0, 1, 2, ...$ , and [2.12]

$$k_{z} = \sqrt{\omega^{2} \varepsilon_{0} \mu_{0} (\varepsilon' - j\varepsilon'') - \left(\frac{m\pi}{a}\right)^{2} - \left(\frac{n\pi}{b}\right)^{2}}.$$
 [2.13]

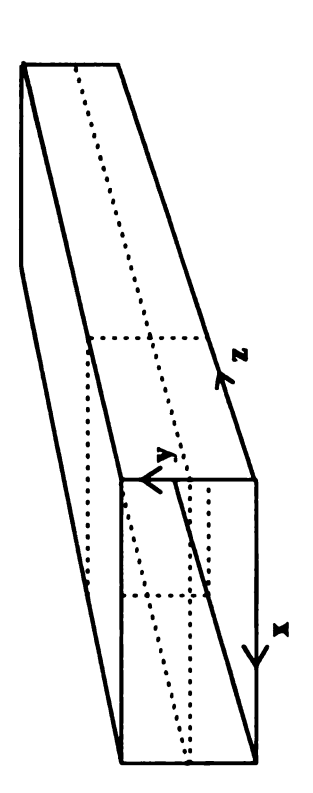
These expressions define the E-field for a positive z traveling wave in a waveguide with an x-length of a and y-length of b, where  $a \ge b$ . Additionally, m or n can be zero; however, both m and n may not be zero.

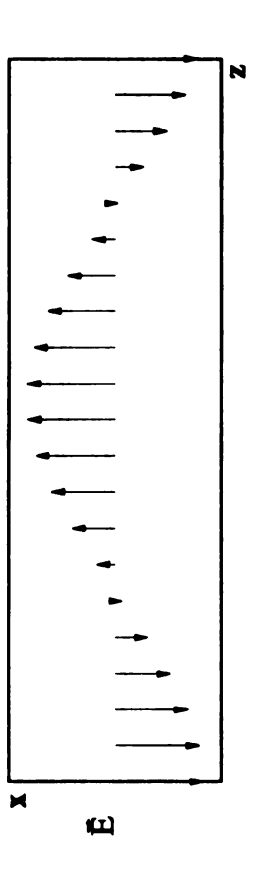
The traveling wave behavior is illustrated with vector E-field plots in Figure 2.1 for the TE<sub>01</sub> mode in a rectangular waveguide. For the TE<sub>01</sub> mode, the E-field is independent of x and varies sinusoidally with y. As indicated by the eigenvalue indices, there are zero variations in the x-direction and one half-wave variation in the y-direction. The boundary condition of zero tangential E-field at conductive boundaries is also evident from Figure 2.1.

Confining a region with conductive boundaries places a constraint on the applicable source frequency. In a waveguide, electromagnetic modes propagate above the cutoff frequency; below the cutoff frequency, modes are evanescent, or nonpropagating. Propagation of electromagnetic energy for a given mode through a waveguide is only permissible using source frequencies above the cutoff frequency. The mode becomes nonpropagating, or evanescent, below the cutoff frequency. For a rectangular waveguide filled with a dielectric material, the cutoff frequency is a function of the waveguide dimensions, the electromagnetic mode, and the dielectric constant of the material as given by

$$f_{c} = \frac{1}{2} \frac{1}{\sqrt{\epsilon_{0} \mu_{0} \epsilon'}} \sqrt{\left(\frac{m}{a}\right)^{2} + \left(\frac{n}{b}\right)^{2}}.$$
 [2.14]

This relationship for the lower order TE and TM modes are shown in Figure 2.2.





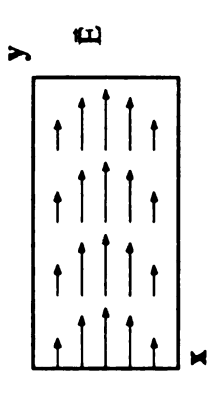


Figure 2.1. Instantaneous Vector E-field Plots for the TE<sub>01</sub> Mode in a Rectangular Waveguide.

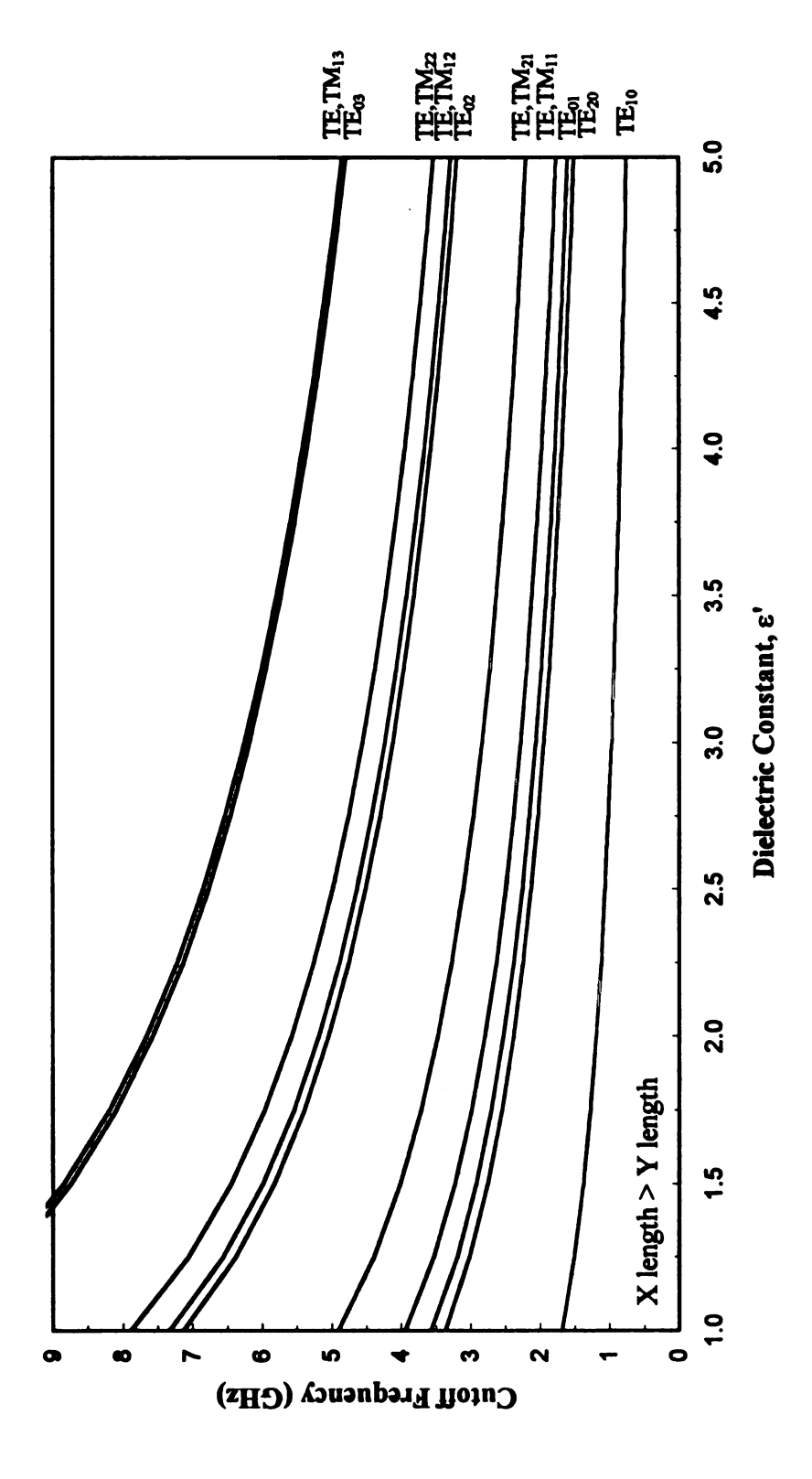


Figure 2.2. Cutoff Frequency Versus Dielectric Constant for a Dielectric-Filled Waveguide with a Cross-Section of 3.8 cm x 8.7 cm.

# 2.2.2. Rectangular Resonant Cavity

The resonant cavity is a system, enclosed by conductive boundaries, that can store or transfer electromagnetic energy. Typically, resonant cavities are excited by a coupling probe or an aperture. The superposition of incident and reflected waves creates a standing wave phenomenon, or resonance, in the cavity.

For processing applications in a resonant cavity, the heating uniformity inside dielectric materials is a strong function of the heating mode. The E-field for the TE modes in a rectangular resonant cavity is given in phasor notation by:

$$E_x = C_1 k_y \cos(k_x x) \sin(k_y y) \sin(k_z z), \qquad [2.15]$$

$$E_v = -C_1 k_x \sin(k_x x) \cos(k_y y) \sin(k_z z), \text{ and}$$
 [2.16]

$$\mathbf{E}_{z}=\mathbf{0},\qquad \qquad [2.17]$$

where  $C_I = a$  constant,

$$k_x = \left(\frac{m\pi}{a}\right), m = 0, 1, 2, ...,$$
 [2.18]

$$k_y = \left(\frac{n\pi}{h}\right)$$
,  $n = 0, 1, 2, ...$ , and [2.19]

$$k_z = \left(\frac{p\pi}{c}\right), p = 0,1,2,...$$
 [2.20]

By convention, a < b < c, where a, b, and c refer to the x-length, y-length, and z-length of the cavity, respectively. Additionally, m or n can be zero; however, both m and n may not be zero.

A plot of the TE<sub>011</sub> mode in a rectangular cavity is illustrated by vector plots for various x-y planes in Figure 2.3. Only the x component of the E-field is present for the

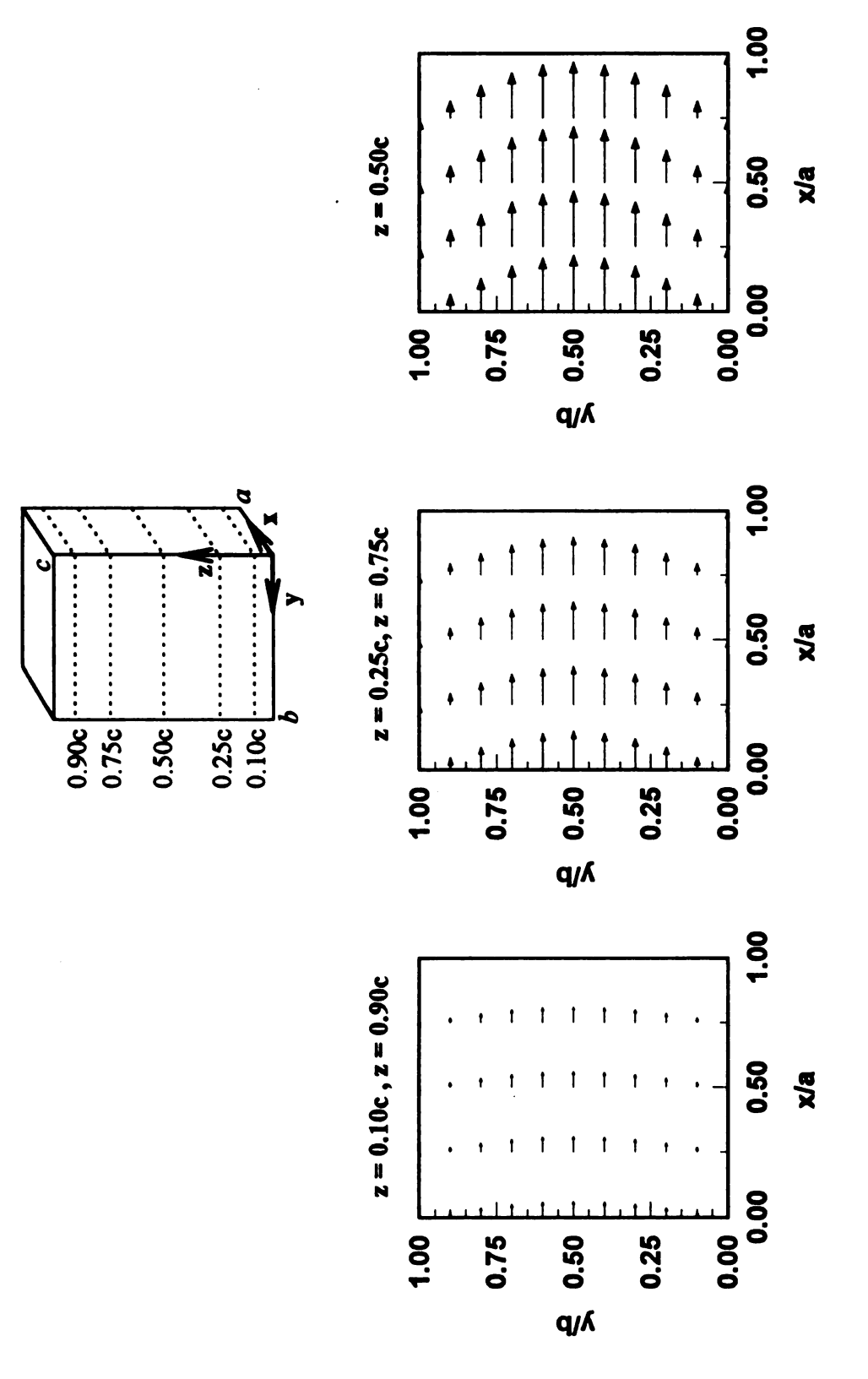


Figure 2.3. Vector Plots of E-field for the TE<sub>011</sub> Mode in a Rectangular Resonant Cavity.

TE<sub>011</sub> mode. In accordance with the eigenvalue indices, there are no E-field variations in the x-direction, one half-wave variation in the y-direction, and one half-wave variation in the z-direction. The strongest E-field is located at the intersection of the planes at y = 0.5 b and z = 0.5 c (i.e., the cavity center). The E-field diminishes to zero at y = 0, y = 0, and z = 0 due to the zero tangential E-field boundary condition at conductive surfaces.

Resonant conditions for a specific mode in a cavity can be attained by adjusting the source frequency or cavity dimensions to satisfy the following relationship.

$$f_{r} = \frac{1}{2} \frac{1}{\sqrt{\epsilon_{0} \mu_{0} \epsilon'}} \sqrt{\left(\frac{m}{a}\right)^{2} + \left(\frac{n}{b}\right)^{2} + \left(\frac{p}{c}\right)^{2}}$$
 [2.21]

Figure 2.4 illustrates this relationship for a 6.4 cm by 7.6 cm cavity.

#### 2.3. Microwave Energy Absorption Mechanisms

In the microwave frequency range, there are primarily two types of mechanisms for dissipating microwave radiation: dielectric loss heating in electrically insulating material and electrical resistive heating in conductive material. Microwave power absorption in polymeric materials is typically either purely dielectric heating or a summed contribution of dielectric and resistive heating if the composite is partially composed of conductive materials such as carbon fibers or metal filings.

With conductive materials, the free electrons move in response to the E-field causing power absorption due to electrical resistive heating; whereas, dielectric materials principally absorb microwave radiation via reorientation and distortion of induced or

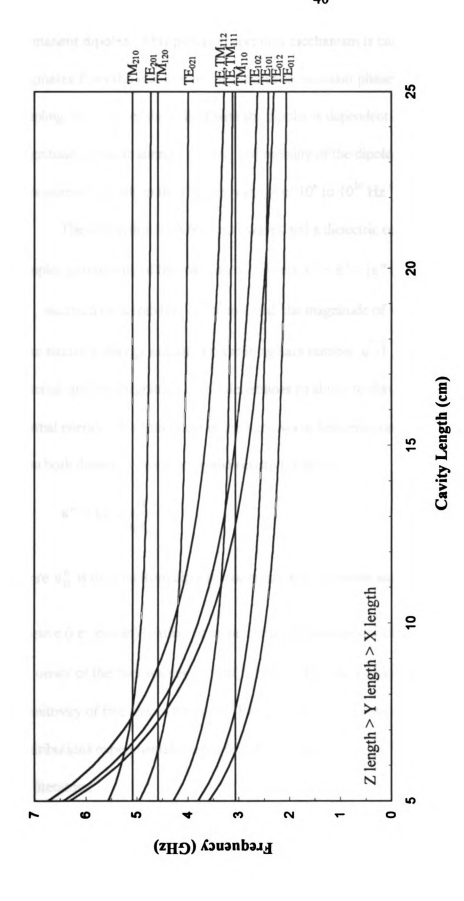


Figure 2.4. Mode Chart for a Rectangular Resonant Cavity with a Cross-Section of 6.4 cm x 7.6 cm.

permanent dipoles. This power absorption mechanism is called loss heating, which originates from the inability of the dipoles to maintain phase with the electric field. The coupling efficiency of the E-field with the dipoles is dependent on the dipole moment magnitude, concentration of dipoles, and mobility of the dipoles. Dielectric loss due to dipole relaxation is typically in the frequency range of 10<sup>6</sup> to 10<sup>10</sup> Hz (32).

The interaction between microwaves and a dielectric or a conductor is dictated by the complex permittivity of the material,  $\varepsilon^*$ , where  $\varepsilon^* = \varepsilon' - j\varepsilon''$ .  $\varepsilon'$  is the real permittivity (i.e., electrical polarizability) of the material, the magnitude of which reflects its ability to store electrical energy as heat; j is the imaginary number  $\sqrt{-1}$ ;  $\varepsilon''$  is the loss factor of the material, and the magnitude of this determines its ability to dissipate electrical energy into thermal energy. The loss factor in the microwave frequency range captures the contributions from both dielectric loss heating and resistive heating:

$$\mathbf{\varepsilon''} = \mathbf{\varepsilon_D''} + \frac{\sigma}{\omega \mathbf{\varepsilon_o}} , \qquad [2.22]$$

where  $\varepsilon_D''$  is the loss from dipolar reorientation polarization and  $\frac{\sigma}{\omega \varepsilon_o}$  is the loss due to resistive (i.e., ohmic) heating.  $\sigma$  is the electrical conductivity of the material,  $\omega$  is the angular frequency of the microwaves ( $\omega=2\pi f$ , where f is the microwave frequency), and  $\varepsilon_o$  is the permittivity of free space (8.85×10<sup>-12</sup> Fm<sup>-1</sup>). Separation of the dipolar and resistive heating contributions experimentally is not feasible. Therefore, only  $\varepsilon''$  is reported for materials in the literature.

Microwave power dissipation per unit volume of homogeneous material, derived from the first law of thermodynamics and Poynting's theorem, is given by

$$P_{MW} = \frac{1}{2} \varepsilon_{o} \omega \left( \varepsilon_{D}^{"} + \frac{\sigma}{\varepsilon_{o} \omega} \right) E_{o}^{2}, \qquad [2.23]$$

where  $P_{MW}$  = power absorption [=] watts/m³,  $\epsilon_o$  = permittivity of free space [=] farads/m,  $\omega$  = angular frequency [=] radians/s,  $\epsilon_D''$  = dipolar loss,  $\sigma$  = electrical conductivity [=] siemens/m, and

= electric field strength

From this expression, one can deduce that microwave power absorption is directly

[=] volts/m.

field strength.

# 2.4. Penetration Depth

E,

In composite and polymer processing, microwave power penetration is often of great practical interest. Electromagnetic penetration into the material is crucial for energy to couple with the process material.

proportional to the microwave frequency, dielectric loss, and the square of the electric

The power penetration depth,  $D_p$ , is defined as the distance from the surface of an infinite plane at which the power diminishes to  $1/e~(\approx 37\%)$  of the surface power. As electromagnetic energy passes through lossy material, the E-field magnitude decreases as a result of the transfer of energy to thermal energy. Assuming zero reflected energy, the power penetration depth in a lossy, homogeneous, and infinite medium is calculated by

$$D_{p} = \frac{1}{\omega \sqrt{2\mu_{o}\mu'\epsilon_{o}\epsilon'\left(\sqrt{1+\left(\frac{\epsilon''}{\epsilon'}\right)^{2}}-1\right)}},$$
 [2.24]

where  $\mu_{o}$  is the permeability of the free space,  $4\pi x 10^{-7}$  Hm<sup>-1</sup>; and  $\mu'$  is the relative permeability of the medium which equals one for non-magnetic materials. As is evident from Equation [2.24], penetration depth in an unconfined region is inversely proportional to the frequency.

Placing a constraint on the boundaries of propagation alters the penetration depth calculation. The penetration depth in a lossy waveguide is given by

$$D_{p} = \frac{1}{\sqrt{2R(\sqrt{1+(I/R)^{2}}-1)}},$$
 [2.25]

where 
$$R = \omega^2 \epsilon_0 \mu_0 \epsilon' - \left(\frac{m\pi}{a}\right)^2 - \left(\frac{n\pi}{b}\right)^2$$
 [=]  $1/m^2$ , [2.26]  $I = -\omega^2 \epsilon_0 \mu_0 \epsilon''$ , [2.27]

m = mode index for x-direction,

n = mode index for y-direction,

a = x-dimension of waveguide [=] m, and

b = y-dimension of waveguide [=] m.

For an unconfined system (i.e.,  $a = b = \infty$ ), Equation [2.25] reduces to Equation [2.24]. The penetration depth in a lossy waveguide decreases with increasing frequency above an optimum frequency where the penetration depth is a maximum,  $f_{opt}$ . Below  $f_{opt}$ , the penetration depth decreases to zero at the cutoff frequency. This behavior is illustrated in Figure 2.5 for a 4.2 cm x 8.9 cm waveguide filled with a material of various complex permittivities. From this figure, one can see that for a given dielectric constant, the

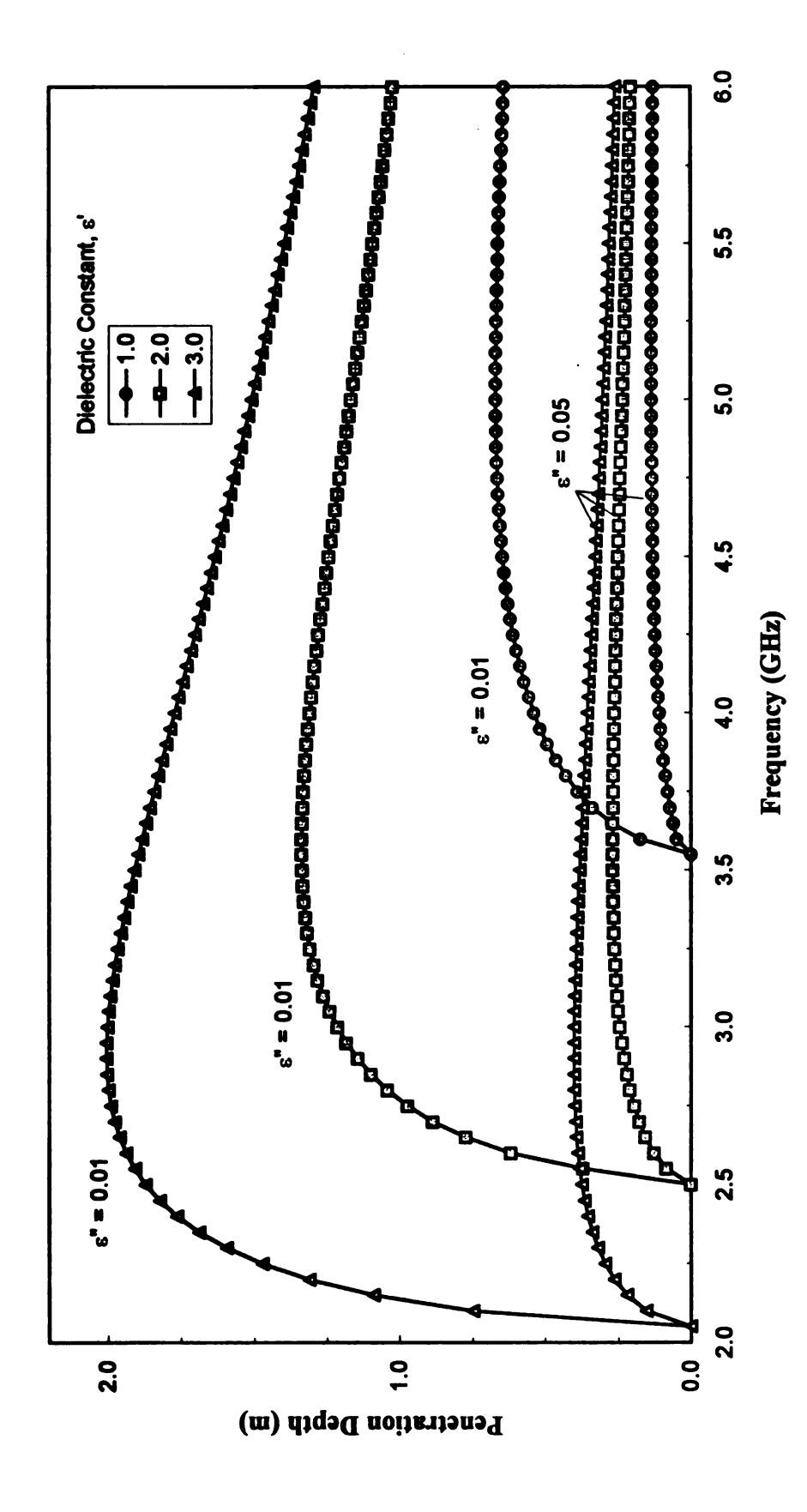


Figure 2.5. Power Penetration Depth for the TE<sub>01</sub> mode in a 4.2 cm by 8.9 cm Dielectric-Filled Waveguide.

penetration depth increases with a decreasing dielectric loss at a constant frequency. Additionally, the cutoff frequency decreases for an increasing dielectric constant, consistent with Figure 2.2. Details of the derivation of equations [2.24] and [2.25] are shown in Appendix C.

#### **CHAPTER THREE**

#### EXPERIMENTAL

### 3.1. Experimental System

The development of the part-shaped applicator consists of two phases: cavity characterization and curing demonstration. The purpose of the former is to acquire an understanding of the electromagnetic behavior in the process material. A portion of the cavity characterization is theoretical, using concepts presented in Chapter 2. These theoretical issues are addressed in Chapter 4. This chapter focuses on the details of the laboratory experimental system for both the cavity characterization and curing demonstration.

The microwave processing system is comprised of microwave applicators (e.g., part-shaped cavity and external applicators), microwave circuitry, thermometry system, and process material. These components and systems are discussed in detail in the following five sections.

# 3.1.1. Part-Shaped Cavity

The brass part-shaped cavity, as illustrated in Figure 3.1, is capable of processing a parallelopipedic 31.8 cm x 8.9 cm x 4.2 cm part. The numbers in brackets in this section refer to the various features in Figure 3.1.

Electromagnetic radiation is admitted to the process material in the cavity
through external applicators and aperture plates that can be secured to a centrally located

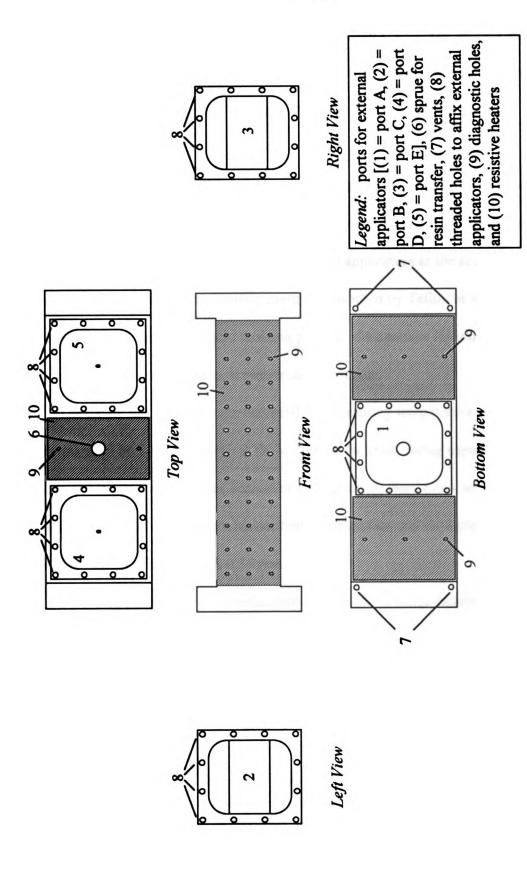


Figure 3.1. Drawing of the Part-Shaped Cavity.

port (i.e., port A [1]), an end port (i.e., ports B [2] and/or C [3]), and an off-center port (i.e., ports D [4] and/or E [5]). The aperture acts as a shunt admittance device to the mold interior. In this thesis, ports with an external applicator will be referred to as "active" ports.

During cavity characterization experiments and curing runs, all non-active ports were sealed with a brass plate. To provide a resin barrier, all liquid molding experiments used Teflon spacers between the cavity and external applicators at the active ports. An insignificant amount of electromagnetic energy is absorbed by Teflon as its dielectric loss is 0.0003 <sup>(86)</sup>. In an industrial liquid molding process, the aperture should be filled with a more rigid low-loss material such as reinforced polyimide.

The cavity has 74 diagnostic holes [9] for measuring temperature inside the process material or E-field strength at the wall. For the resin curing experiments, these holes are either filled with silicone sealant or with glass capillary tubes with one sealed end. The capillary tubes provide a barrier between the resin and the temperature probes. The wall thickness of the tubes is 0.75 mm.

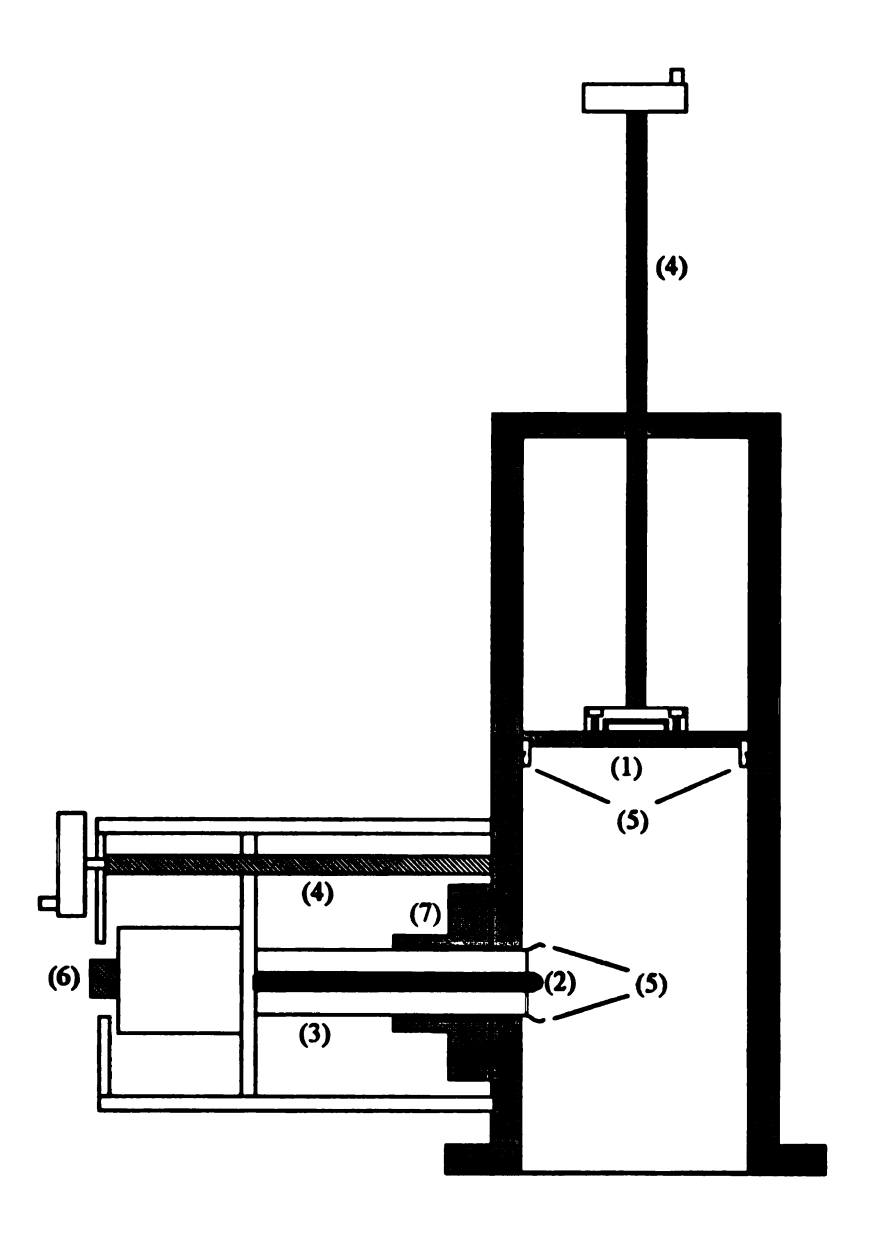
Conventional heating is achieved from five flexible silicone heaters [10] affixed to the external surfaces of the cavity. The heaters are wired to deliver a total power of 1280W. When conventional heating is employed, the heater duty is controlled via a Digi-sense proportional controller with a type K thermocouple attached to the cavity exterior near port A.

A centrally located sprue [6] is placed on the top of the cavity for resin transfer.

Four vents [7] are located at the each of the bottom corners of the cavity to ensure proper wetting of the fiber mats.

# 3.1.2. External Applicators

The external applicator, as shown in Figure 3.2, is a single-mode cavity with one open surface through which electromagnetic energy is fed to the part-shaped cavity. Resonant conditions are attained in the external applicator by mechanically adjusting the depth of the microwave coupling probe [2] and the height of the traveling short [1] to match the impedance of the input radiation. For all experiments, the external applicators were tuned by minimizing reflected power near a cavity length of 10.3 cm, the theoretical TE<sub>011</sub> cavity length. Resonance in the external applicators is affected by the dielectric properties of the material in the part-shaped cavity. Since the dielectric properties of the process material are functions of temperature, the external applicators required slight tuning during each run to maintain heating efficiency. A microwave excitation probe. consisting of an aluminum inner conductor with a diameter of 0.95 cm and an outer brass conductor with a diameter of 2.26 cm, can be adjusted from a depth of 0 to 6.37 cm. A grounding contact ring (Instrument Specialties 97-154) is soldered to the outer conductor to provide electrical contact with the external applicator walls. The external applicator length is fixed by a 7.6 cm x 6.4 cm shorting plate that is mechanically adjusted. Electrical contact between the external applicator walls and the traveling short



Legend: (1) traveling short, (2) inner conductor, (3) outer conductor, (4) threaded shafts, (5) grounding contacts, (6) type N coaxial connector, and (7) choke

Figure 3.2. Cross-section of the external applicator.

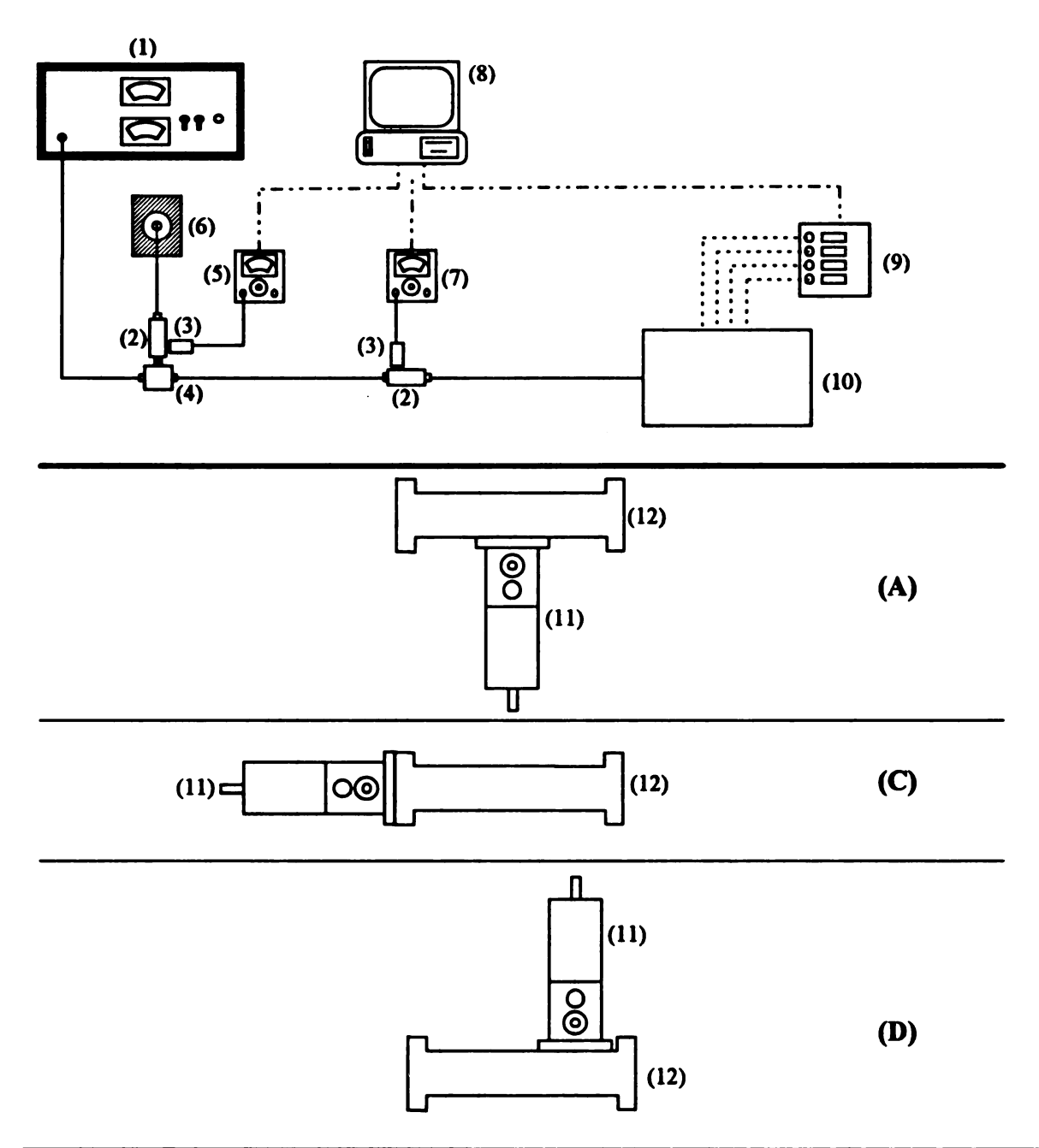
is attained by grounding contact strips (Instrument Specialties 97-139) soldered to the perimeter of the short.

# 3.1.3. Experimental Setup and Microwave Circuitry

The external applicator configuration dictates the type of wave propagation in the process material. For instance, activating one port and sealing all other ports results in a potential standing wave inside the cavity. Electromagnetic wave reflection at all sealed ports in superposition with incident waves from the external applicator could create the standing wave phenomenon. The circuitry and three standing wave configurations, which were investigated, are illustrated in Figure 3.3.

During runs with two or more active ports, incident energy is directed to one external applicator through an SP5T electromechanical switch. All other external applicators act as a matched termination. Therefore, the waves inside the cavity are primarily incident waves. The cavity in this configuration becomes a traveling wave applicator. The curing demonstration utilized the traveling wave configuration, as shown in Figure 3.4. Cavity characterization experiments were performed for both traveling wave and standing wave configurations.

A magnetron microwave generator (Opthos MPG 4) with a fixed frequency of 2.45 GHz and a power of 120 W served as a high power microwave source for all experiments. 50-ohm impedance coaxial transmission lines are used to transmit power from the power source to the external applicator. The power source and the microwave switch are protected from reflected energy by a circulator. Incident and reflected signals



Legend: (1) 120 W magnetron microwave generator, (2) directional coupler, (3) power sensor, (4) circulator, (5) reflected power meter, (6) terminal resistor, (7) input power meter, (8) computer, (9) Luxtron thermometry system, (10) part-shaped cavity with external applicator, (11) external applicator, (12) part-shaped cavity, [———] coaxial transmission lines, [·····] silica temperature probes, [-····] computer data transmission lines, (A) port A heating configuration, (C) port C heating configuration, and (D) port D heating configuration.

Figure 3.3. Microwave Circuitry and Cavity Configurations for Standing Wave Operation.

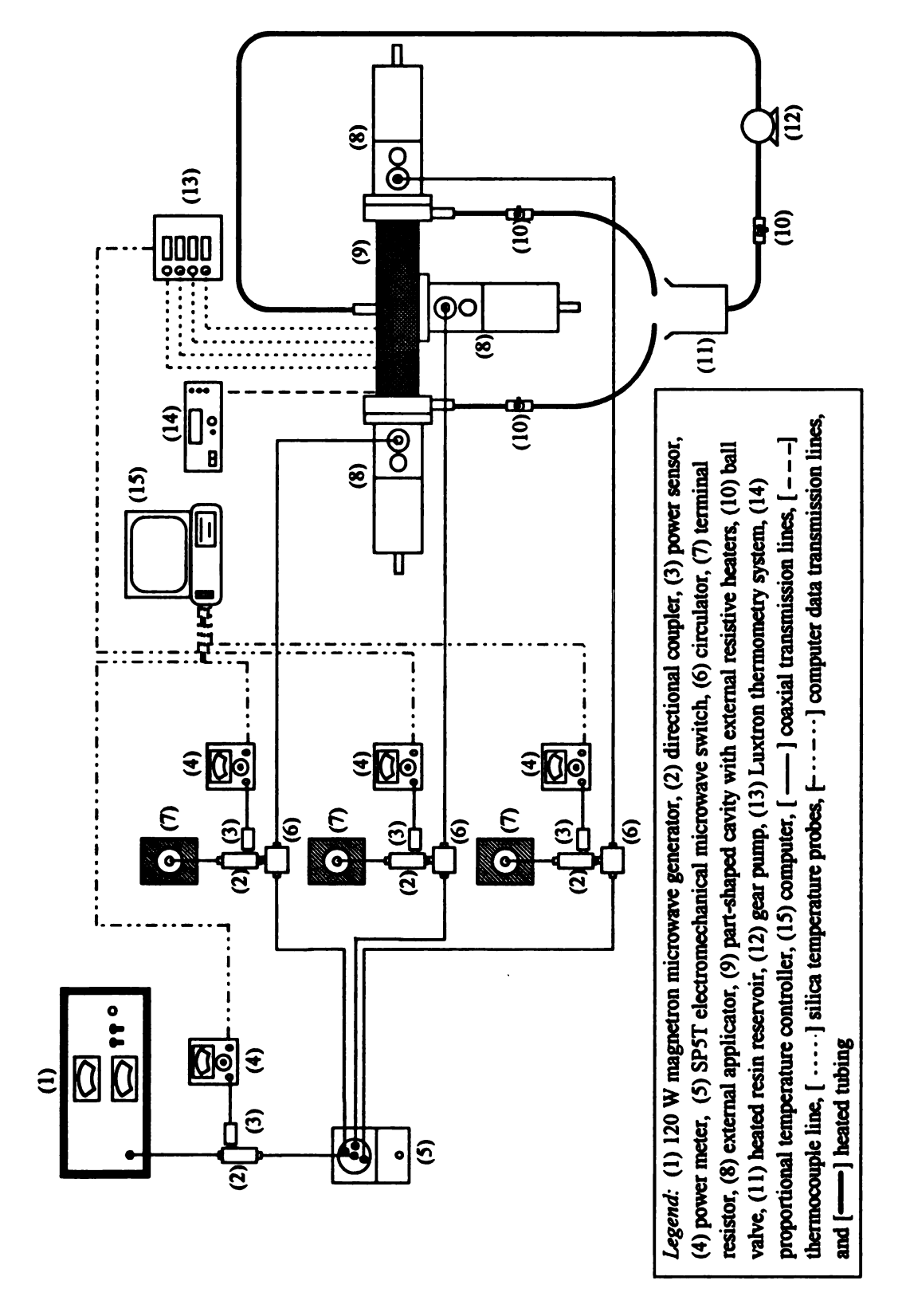


Figure 3.4. Microwave Circuitry and Pumping Configuration for Traveling Wave Operation.

from the Opthos generator and the cavity, respectively, are sampled by Narda coaxial direction couplers with a 20 dB attenuation and measured using 3.5 W power meters (HP 435B). Power meter data and temperature data are stored in a computer.

Liquid resin is transferred to the cavity via a pumping system comprised of a Sherwood bronze gear pump, driven by a 1-hp U.S. Unimount 125 electric motor. The motor is capable of a rotation speed of 3475 RPM and is controlled with a Magnetek GPD 403 variable frequency drive, which allows the user to control the pump speed at a constant torque.

# 3.1.4. Thermometry System

Temperature measurements are sampled inside the part-shaped cavity using a Fluoroptic thermometry system (Luxtron 750 and 755) with temperature probes constructed of silica fibers coated with Teflon. The E-field is essentially unaffected by the temperature probes, as both silica and Teflon are very low loss materials.

The thermometry unit contains a xenon flashlamp that emits a blue-violet light, which travels through the fiber optic probe body, at specified intervals. A manganese-activated magnesium fluorogermanate material, located in the probe tip, absorbs the blue-violet light and emits a deep red fluorescence for a given time period which is a function of temperature. The decay time of the red fluorescence is measured and correlated with the temperature at the probe tip. Data acquisition of the temperature is achieved via an RS-232 interface to a personal computer.

#### 3.1.5. Process Material

For the cavity characterization experiments, fully cured glass-reinforced polyester plates are used as a dielectric media in the cavity. Eleven 31.8 cm x 8.9 cm x 0.32 cm plates are stacked and heated in the cavity. The complex permittivity of glass-reinforced polyester at 2.45 GHz and 25°C is 4.30 - j 0.049. The permittivity was measured by the cavity perturbation technique using the  $TM_{012}$  mode in a cylindrical cavity with a diameter of 15.24 cm.

For RTM applications, a common composite is a glass-reinforced epoxy system, specifically diglycidyl ether of bisphenol A (DGEBA). A DGEBA resin, Epon 828 (Shell Chemical Co.), cured with diaminodiphenyl sulfone (DDS) and reinforced with continuous random E-glass fibers (Unifilo U101), served as the composite system for the curing demonstration. The chemical structures of difunctional DGEBA and tetrafunctional DDS are given in Figure 3.5.

The crosslinked structure of an epoxy is formed by step-growth polymerization.

An epoxy resin, which typically has two or more epoxide functionalities, reacts with a curative which is capable of opening the epoxide ring via nucleophilic substitution.

Typical curatives include amines and anhydrides. During polymerization of an epoxy with an amine, for example, the predominant reaction consists of the amine opening the epoxide ring and transferring a hydrogen to the oxygen of the epoxide ring.

Respectively, a primary or a secondary amine after this reaction becomes a secondary or tertiary amine.

# Diaminodiphenyl Sulfone (DDS)

# Diglycidyl Ether of Bisphenol A (DGEBA)

Figure 3.5. Chemical Structure of Diglycidyl Ether of Bisphenol A and Diaminodiphenyl Sulfone.

# 3.2. Cavity Characterization Methods

Achieving uniform and rapid heating rates for a given process material is one of the main objectives in the development of the part-shaped cavity. Some of the dominant process variables that influence heating patterns and rates include the following:

- microwave power,
- microwave frequency,
- aperture width,
- aperture orientation relative to the coupling probe,
- aperture configuration (e.g., single vs. double aperture),
- number of external applicators,
- location of external applicators,
- resonant mode in the external applicator,
- process material dielectric properties,
- geometry of fill material in the aperture, and
- dielectric properties of fill material.

Experimental efforts for the cavity characterization are focused on determining the effect of aperture width and orientation on the E-field pattern behavior and, hence, heating patterns and rates. Additionally, the number and location of external applicators are investigated, as explained in Section 3.1.3.

Qualitative heating patterns are determined by securing thermal paper to each polyester plate. The thermal paper begins to indicate at 60°C and progressively darkens at higher temperatures. This allows a fingerprint of the heating zones to be taken during a run.

The unsteady-state energy balance for a reactive process material in the mold is given by:

$$\rho C_{p} \frac{\partial T}{\partial t} = \nabla \cdot (k \nabla T) + P_{MW} + S_{Rxn}, \qquad [3.1]$$

where  $\rho$  is the material density  $C_p$  is the material heat capacity  $C_p$  is the material heat capacity  $C_p$  is the material temperature  $C_p$  is time  $C_p$  is the material temperature  $C_p$  is the material heat capacity  $C_p$  is the material temperature  $C_p$  is the

At the beginning of a run, the thermal conduction term,  $\nabla \cdot (k\nabla T)$ , can be neglected due to the insignificant temperature gradients throughout the cavity volume. Additionally, the reaction source term is zero since the polymer plates are non-reactive; therefore, the initial heating rate, dT/dt, is directly proportional to the microwave power absorption:

$$\frac{\mathrm{dT}}{\mathrm{dt}} = \frac{1}{\rho C_p} P_{MW}. \tag{3.2}$$

By recording temperature as a function of time at a fixed location in the cavity, one can determine an indication of microwave power absorption for the polyester plates as a function of a processing parameter, such as aperture width.

#### 3.3. Glass Fiber-Reinforced DGEBA/DDS Processing

Three methods of curing composites are demonstrated in the part-shaped applicator: conventional, microwave, and hybrid. With conventional curing, resistive heaters affixed to the cavity surface provide the thermal energy for processing. During the microwave curing run, microwave radiation provides the energy for promoting crosslinking. Hybrid curing combines conventional and microwave curing techniques.

The resin is prepared according to the manufacturer recommendation of 4.0 g of DGEBA per 1.0 g of DDS, corresponding to a mixture with excess DGEBA. Epon 828 has an epoxide equivalent weight of 185 to 192, and the molecular weight of DDS is 248.3. Each molecule of DDS has four reactive sites that can react with one of the two epoxide groups per molecule of DGEBA.

Approximately 2000g of DGEBA is placed in an insulated 4-liter beaker, agitated, and heated to 130°C on a hot plate. When the resin reaches 130°C, 500 g of DDS is slowly added to the DGEBA, while maintaining the mixture temperature near 130°C. After the DDS is fully dissolved in DGEBA, the resulting mixture is degassed in a vacuum oven at approximately 100°C for 15 minutes to minimize void formation during processing.

As shown in Figure 3.4, the resin reservoir and the tubing is heated. The resin temperature is maintained above 60°C to facilitate resin transfer; at lower temperatures, the viscosity is too high for pumping.

To aid in part removal, the cavity is treated with Mono-Coat RPM 711 sealer and Mono-Coat RPM 115 mold release agent (Chem-Trends, Inc.). The cavity is charged with 30 E-glass fiber mats and heated to 100°C. Five capillary tubes are placed inside the cavity through the diagnostic holes. Four tubes are located in the center of the cavity near port A (2 tubes), port B (1 tube), and port C (1 tube). The fifth tube is located near the mold wall. The resin is transferred to the cavity via the gear pump, powered by a 1-hp electric motor controlled with a variable frequency drive. Upon filling the cavity with resin, the vent valves are closed and pumping is terminated.

For each curing method, the process cycle consisted of cure and post-cure stages.

The manufacturer recommendation of a five hour cure cycle at 125°C and a one hour post-cure cycle at 200°C is observed.

### 3.4. Mechanical Strength Tests

For comparison of part strength for each of the three processing methods, the modulus of elasticity of samples was determined by the three-point bending test using procedure A in accordance with ASTM 790. Figure 3.6 illustrates the approximate locations of the samples that were removed from the cured composite. Ten samples with a length of 76.2 mm and a width of 25.4 mm were sized with a D.R. Bennett, model PX, table saw using a water-soluble oil coolant system to prevent any thermal effect during sample preparation. A depth of approximately 3.18 mm was achieved using a Struers Abramin polisher and a Leco BG-20 belt grinder equipped with a water cooling system.

The three-point bending tests were performed on an SFM 20 United Testing System unit using a 1000-lb loadcell. The diameter of both the loading nose and the supports is 6.35 mm. With a support span of 50.8 mm, samples were deflected at a rate of 1.27 mm/min.

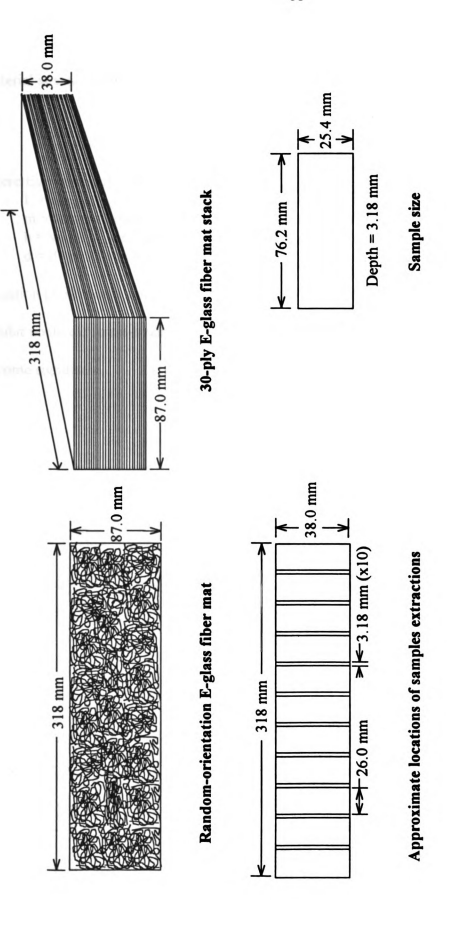


Figure 3.6. Fiber Mat Orientation and Sample Locations for Curing Experiments in Part-Shaped Cavity.

Assuming that the glass-reinforced epoxy specimens behave as a linear elastic material at small deflections, the modulus of elasticity is given by:

$$E_{\rm B} = \frac{L^3 \rm m}{4 \rm b d^3}, \qquad [3.3]$$

where  $E_B$  = modulus of elasticity [=] N/m<sup>2</sup>, L = support span [=] m,

m = tangent of the initial linear portion of the load-deflection curve [=] N/m,

b = width of specimen [=] m, and d = depth of specimen [=] m.

Equation [3.3] is only valid at small deflections. At large deflections, composites usually exhibit nonlinear stress-strain behavior<sup>87</sup>. Additionally, friction forces at the supports become significant.

### CHAPTER FOUR

#### **RESULTS AND DISCUSSION**

## 4.1. Cavity Characterization Results

### 4.1.1. Temperature Profiles and Heating Patterns

As described in Chapter 3, the E-field is characterized inside the part-shaped cavity by studying heating rates and heating patterns using the E-glass reinforced polyester plates. Figures 4.1 through 4.3 illustrate the temperature profiles for microwave heating of the eleven plates using the standing wave cavity configurations shown in Figure 3.3. The approximate location of each temperature probe is shown in the figures; each probe is located in the center of the middle plate.

As is evident in Figures 4.1 through 4.3, heating rates diminish at distances farther away from the microwave source (i.e., the active port). This observation in Figures 4.1 and 4.2 can be attributed to energy absorption. Through lossy material, the E-field intensity decreases in the direction of propagation due to the conversion of electromagnetic energy to thermal energy.

Temperature probe 1 in Figure 4.3 detects no rise in temperature over the 8.5 minute experiment. This is not due to microwave energy attenuation, but rather the electromagnetic fields are not coupling with the entire length of the cavity. However, temperature probes 2 and 3 indicate that the E-field couples very well with the polyester plates near port D.

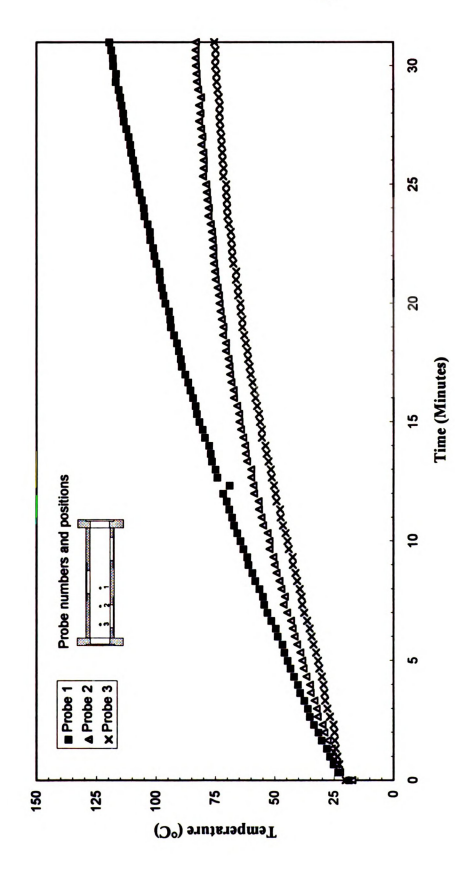


Figure 4.1. Glass-Reinforced Polyester Temperature Profiles for Heating Runs With One External Applicator at Port A and an Aperture Width of 4.19 cm.

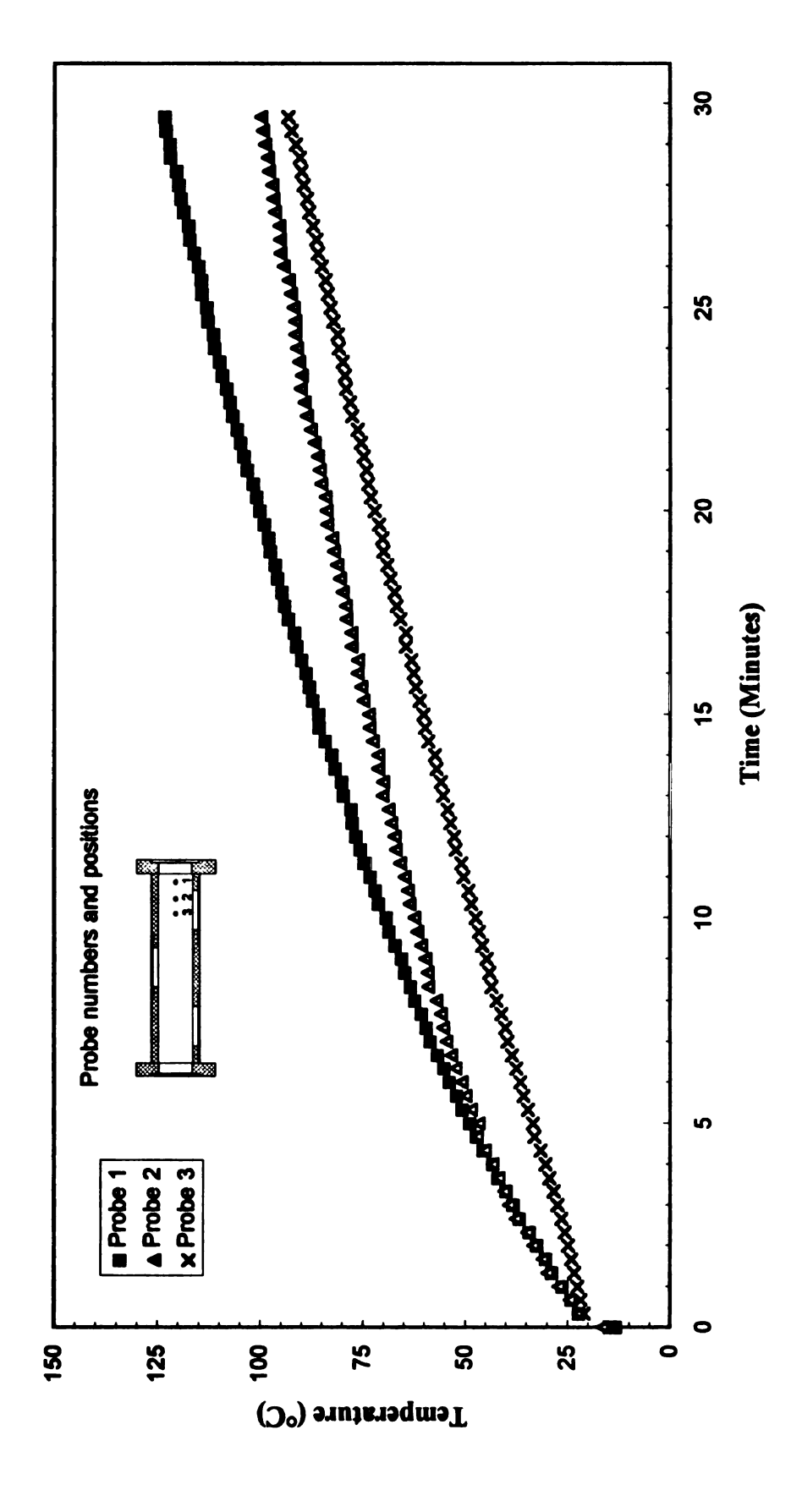


Figure 4.2. Glass-Reinforced Polyester Temperature Profiles for Heating Runs With One External Applicator at Port C and an Aperture Width of 4.19 cm.

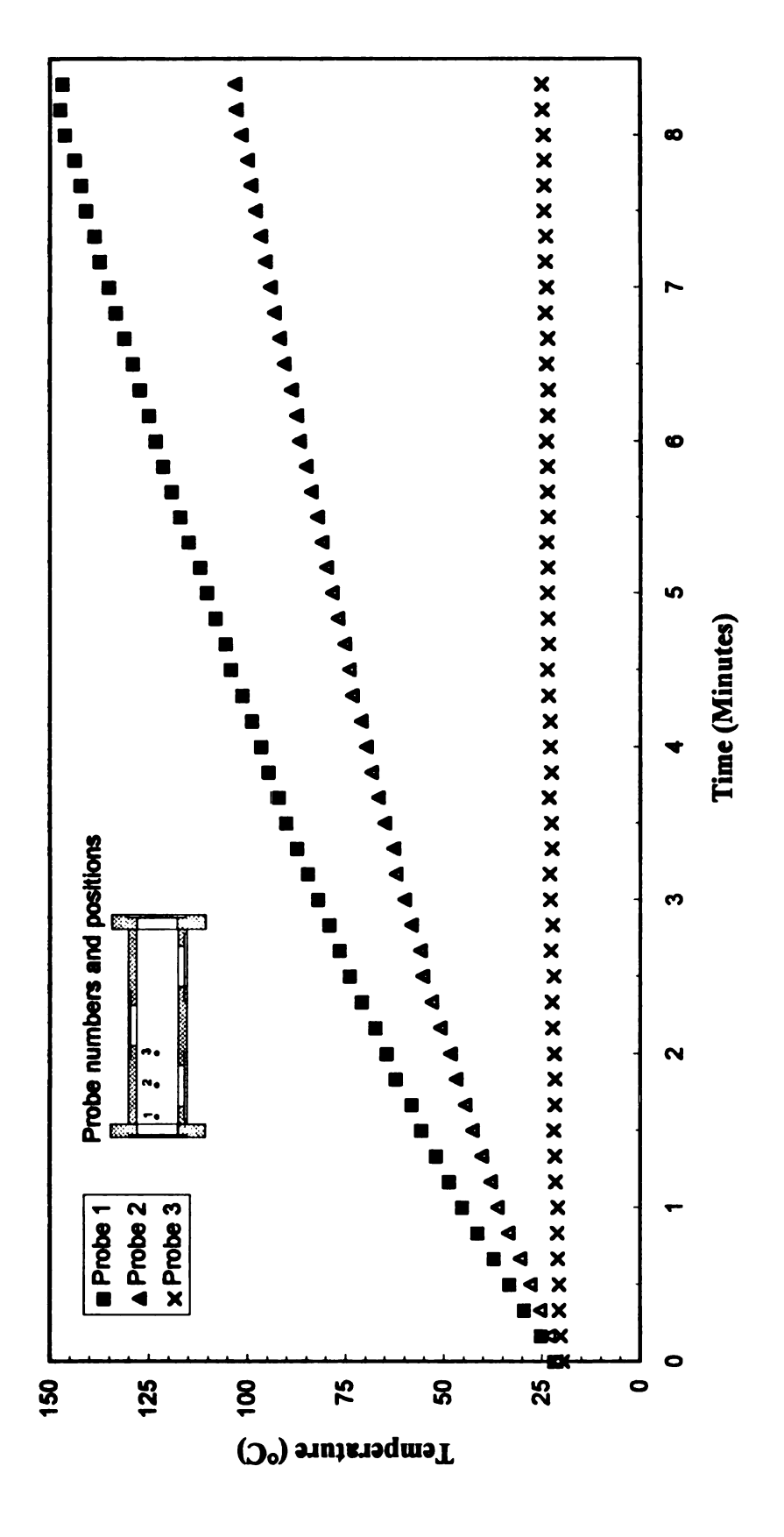


Figure 4.3. Glass-Reinforced Polyester Temperature Profiles for Heating Runs With One External Applicator at Port D and an Apperture Width of 4.06 cm.

A map of the heating patterns throughout the cavity can be determined by placing temperature-sensitive thermal paper on each of the eleven plates. Figure 4.4 shows images from the center plate for heating runs using one external applicator at ports A, C, or D. The dielectric properties of the polyester plates allow propagation of the observed heating mode. The distinct lobes on the images from heating the polyester plates demonstrate the standing wave phenomenon.

Diminishing E-field magnitude and heating intensity are particularly evident for the runs with the external applicator at port C. The heating intensity is the greatest at the center of the cavity near the source and the least near the top and bottom of the cavity. Thermal paper on the top and bottom plates for most runs provided no indication of heating above 60°C.

For the experimental system, greater heating uniformity can be realized by admitting electromagnetic energy from more than one port: namely ports A, B, and C. As explained in Chapter 3, heating with this configuration results in a traveling wave. A traveling wave is an incident wave, and a standing wave is the result of the superposition of an incident wave and a reflected wave. One would expect, for a given power source, the heating rates to be lower for the traveling wave operation. This is evident in comparing Figure 4.5 with Figure 4.1 and Figure 4.6 with Figure 4.2.

Thermal paper images from heating the polyester plates in the traveling wave operation, as shown in Figure 4.7, exhibit a more uniform heating pattern relative to the standing wave operation; the lobes are not as sharply defined for the former. Slight reflection inside the cavity system from the aperture plates and from the non-active

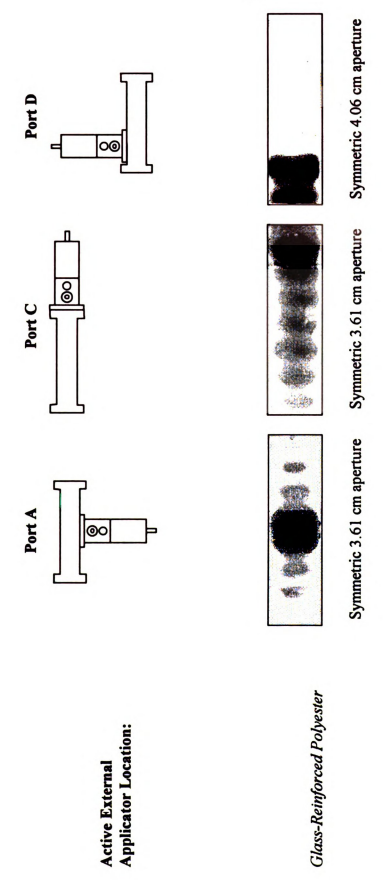


Figure 4.4. Thermal Paper Images for Polyester Plates in the Part-Shaped Cavity. Standing Wave Operation.

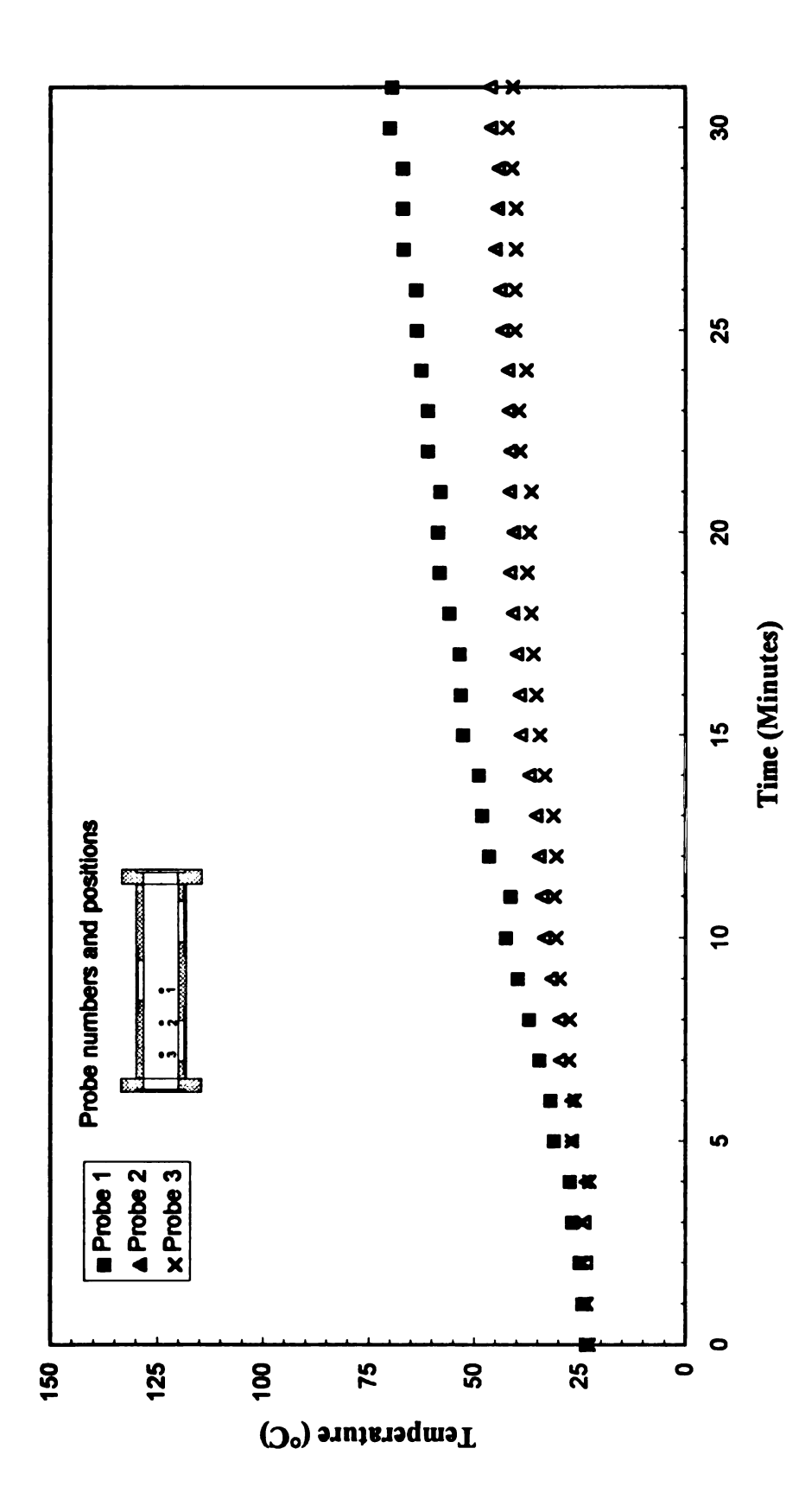


Figure 4.5. Glass-Reinforced Polyester Temperature Profiles for Heating Runs With an Active External Applicator at Port A and Non-Active External Applicators at Ports B and C With an Aperture Width of 3.61 cm.

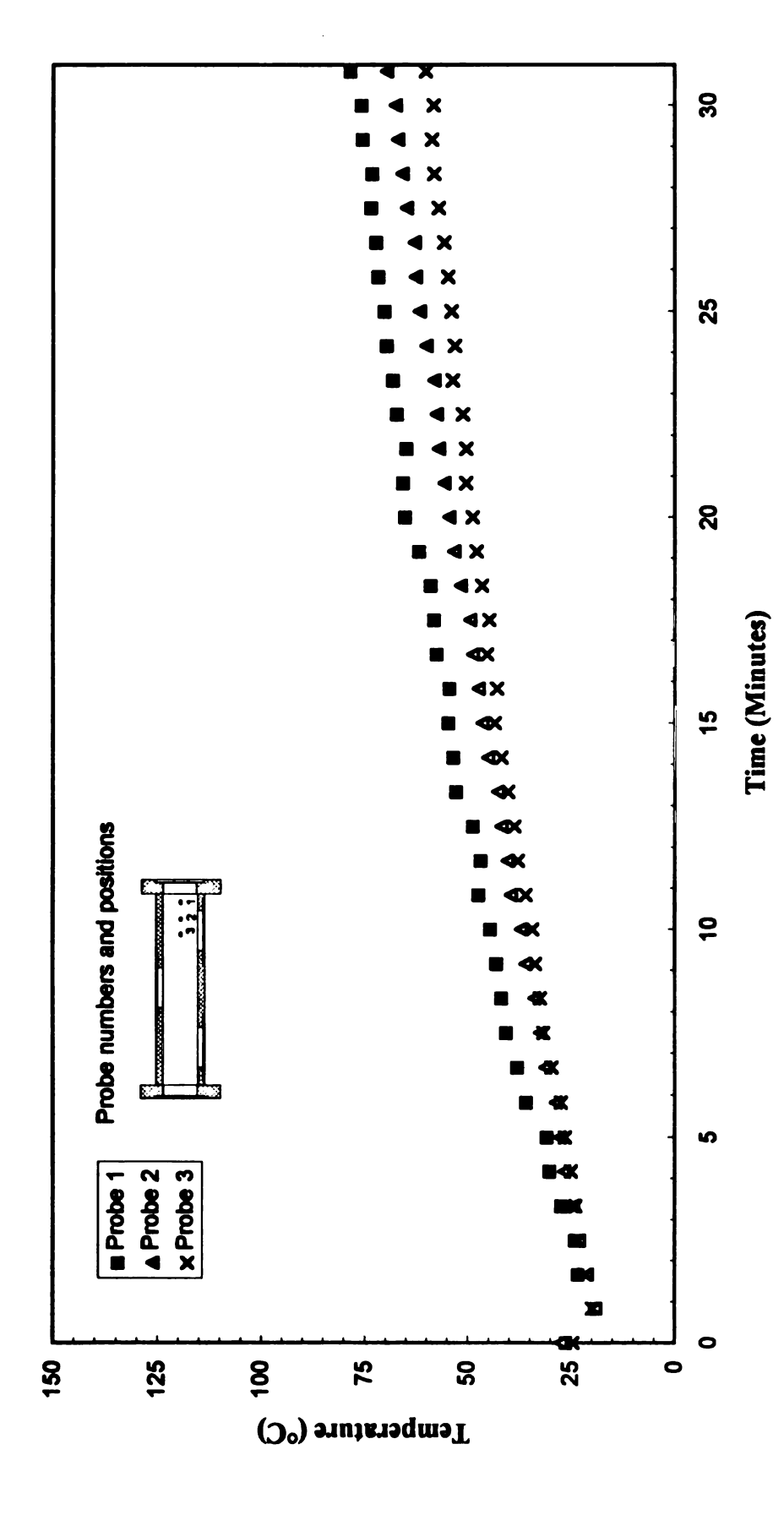
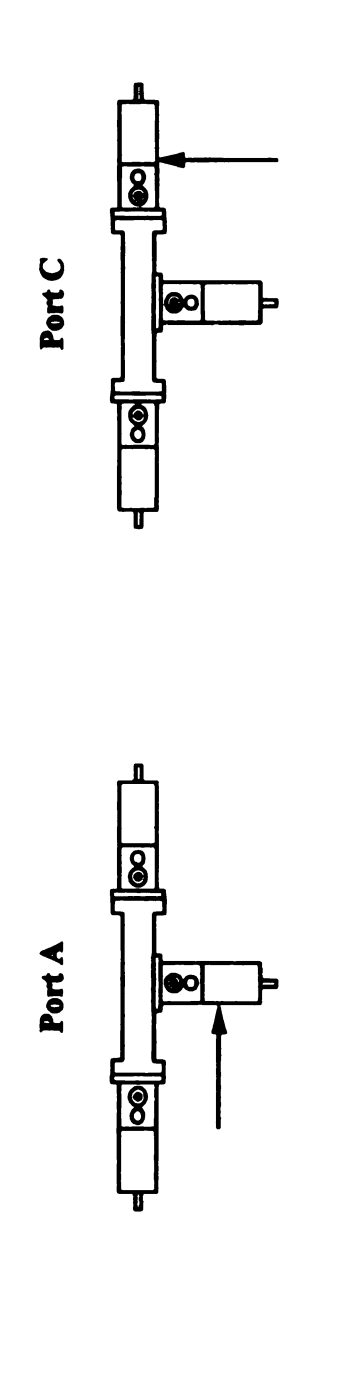


Figure 4.6. Glass-Reinforced Polyester Temperature Profiles for Heating Runs With an Active External Applicator at Port C and Non-Active External Applicators at Ports A and B With an Aperture Width of 3.61 cm.



Active External Applicator Location:

Symmetric 3.61 cm aperture

Glass-Reinforced Polyester

Symmetric 3.61 cm aperture

Figure 4.7. Thermal Paper Images for Polyester Plates in the Part-Shaped Cavity: Traveling Wave Operation.

external applicators creates the lobed heating patterns when using more than one external applicator.

The image from heating with the external applicator at port C illustrates the terminating nature of the non-active external applicator. The high temperature indication ceases where port A is located, mid-way across the plate. The incident energy from port C couples with the external applicator at port A and is directed to a dummy load.

# 4.1.2. Aperture Effects

As explained in Section 3.2, the initial microwave heating rate of a non-reactive, dielectric material is directly proportional to the microwave power absorption. A straight-line behavior near the initiation of a heating experiment is evident in Figures 4.1 through 4.3. As the heating progresses, however, the dielectric properties change with temperature, heat losses at the mold surfaces increase, and thermal conduction becomes significant due to temperature gradients. These phenomena create the non-linear temperature behavior at longer times.

Part of the cavity characterization study focused on the effect of aperture orientation, configuration, and width on the heating rates and patterns. Aperture orientation refers to the orientation of the opening in the aperture plate with respect to the excitation probe. The three configurations investigated were single symmetric, single asymmetric, and double symmetric apertures. The investigated aperture characteristics are illustrated in Figure 4.8.

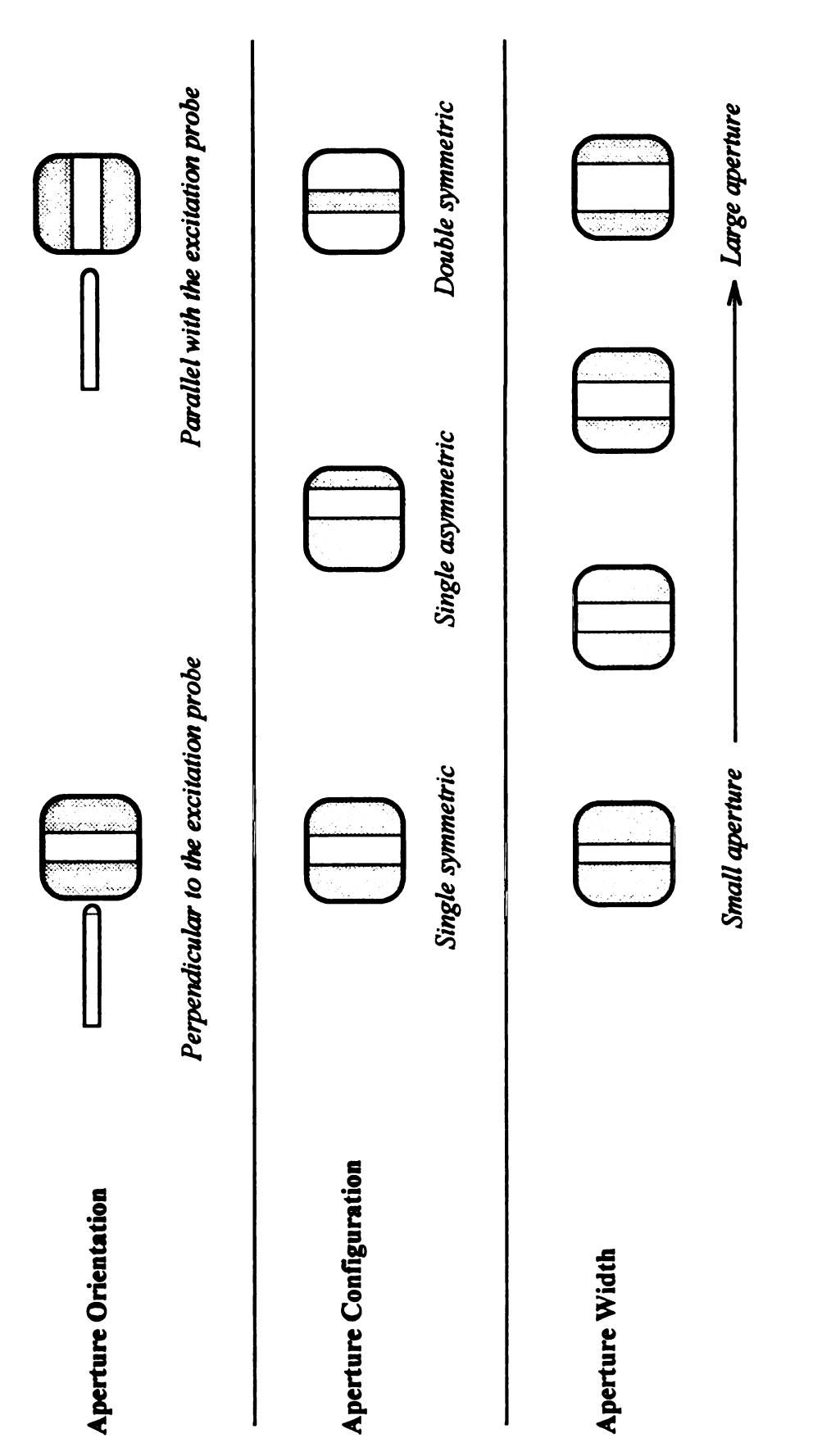


Figure 4.8. Investigated Aperture Characteristics.

The desired resonant mode in the external applicator using a double symmetric aperture or an aperture perpendicular to the probe is difficult to excite. The resonance curve for these cases had a very narrow bandwidth. As a result, very frequency tuning during heating was required. Single apertures parallel to the excitation probe provide a more stable configuration for the desired resonance mode.

A single asymmetric aperture at port D proved to diminish the intense heating pattern characteristic of the off-center port. By locating the aperture closer to the center of the cavity, the E-field could be dissipated over more material.

For single symmetric apertures oriented parallel with the excitation probe, the initial heating rates are plotted versus aperture width in Figure 4.9 through 4.11 to identify the effect of aperture width on the microwave power absorption. At each type of port (i.e., center, off-center, or end), the initial heating rate increases with aperture width at small apertures. Above an aperture width of 5.0 cm at port A, the near-field heating appears to become more intense.

The thermal paper images for three experiments utilizing different aperture widths demonstrate that microwave heating patterns are essentially independent of aperture width. As shown in Figure 4.4, characteristic of each run using the external applicator at port A is a near-field heating effect directly below the port. On either side of the central heating lobe, three lobes appear, diminishing in intensity away from the central lobe. The width of the aperture controls the admitted E-field and, hence, the heating rates. As outlined in Table 4.1, the locations of the E-field lobes are

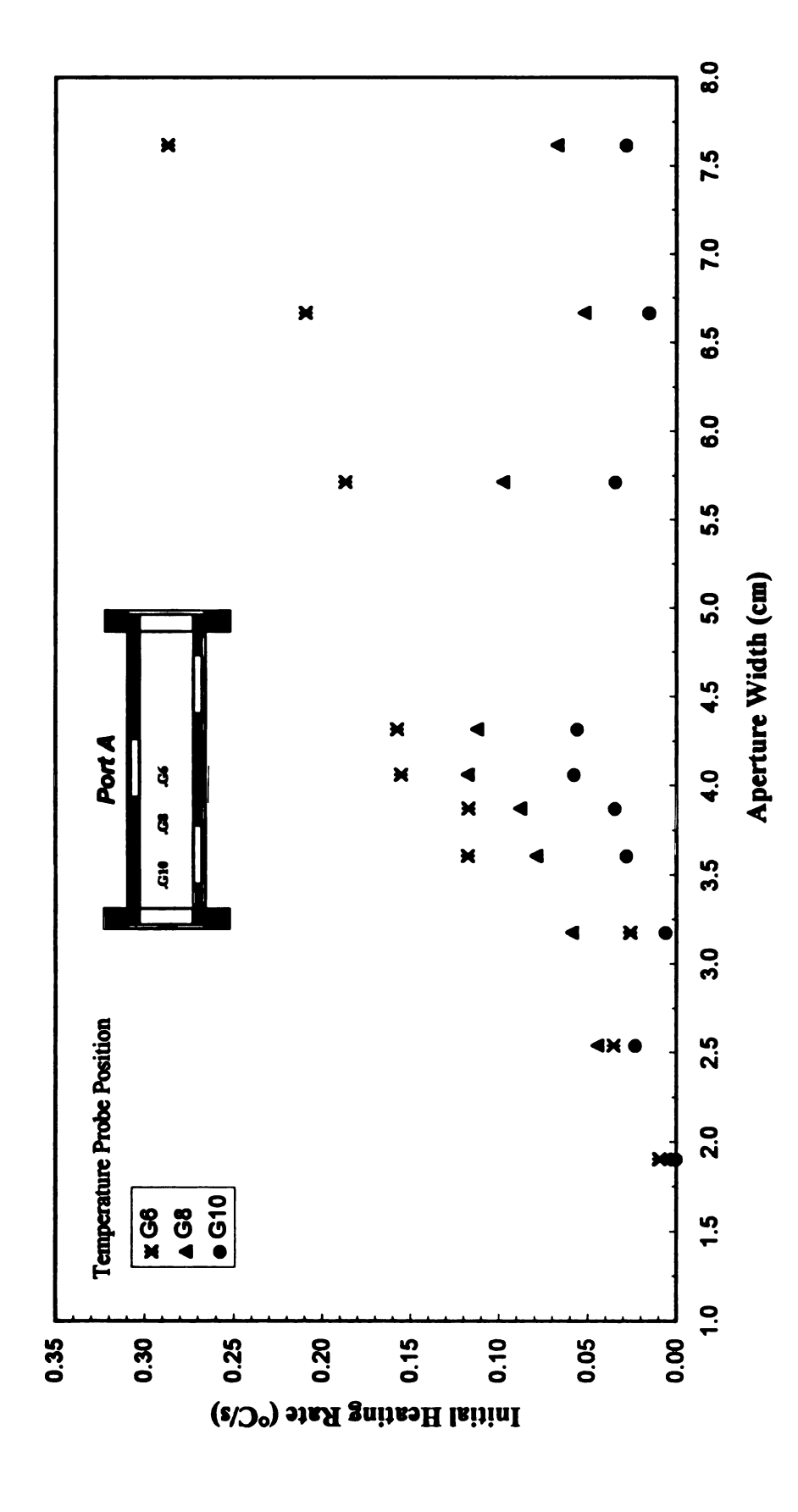


Figure 4.9. Initial Temperature Profile as a Function of Aperture Width at Port A.

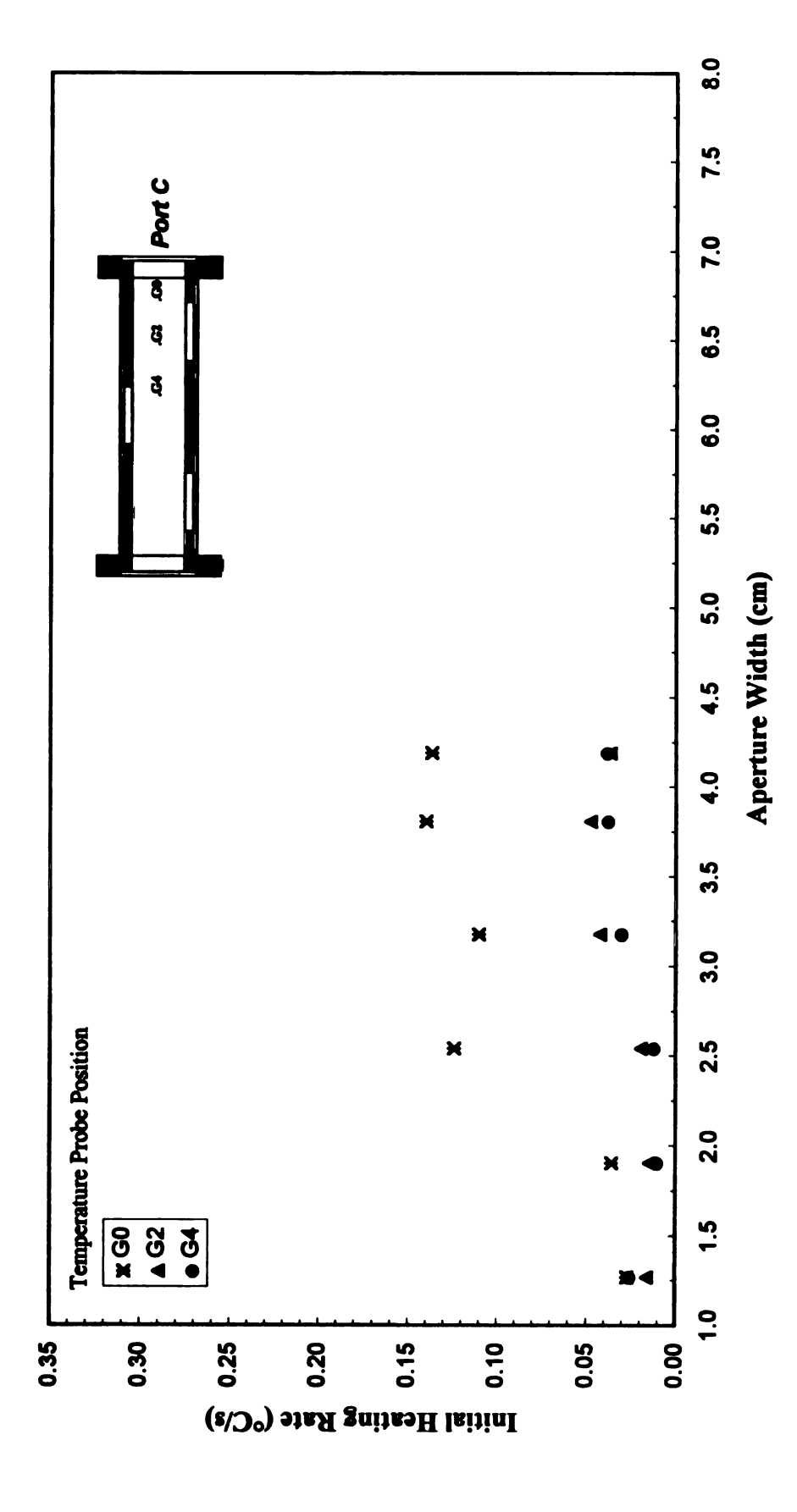


Figure 4.10. Initial Temperature Profile as a Function of Aperture Width at Port C.

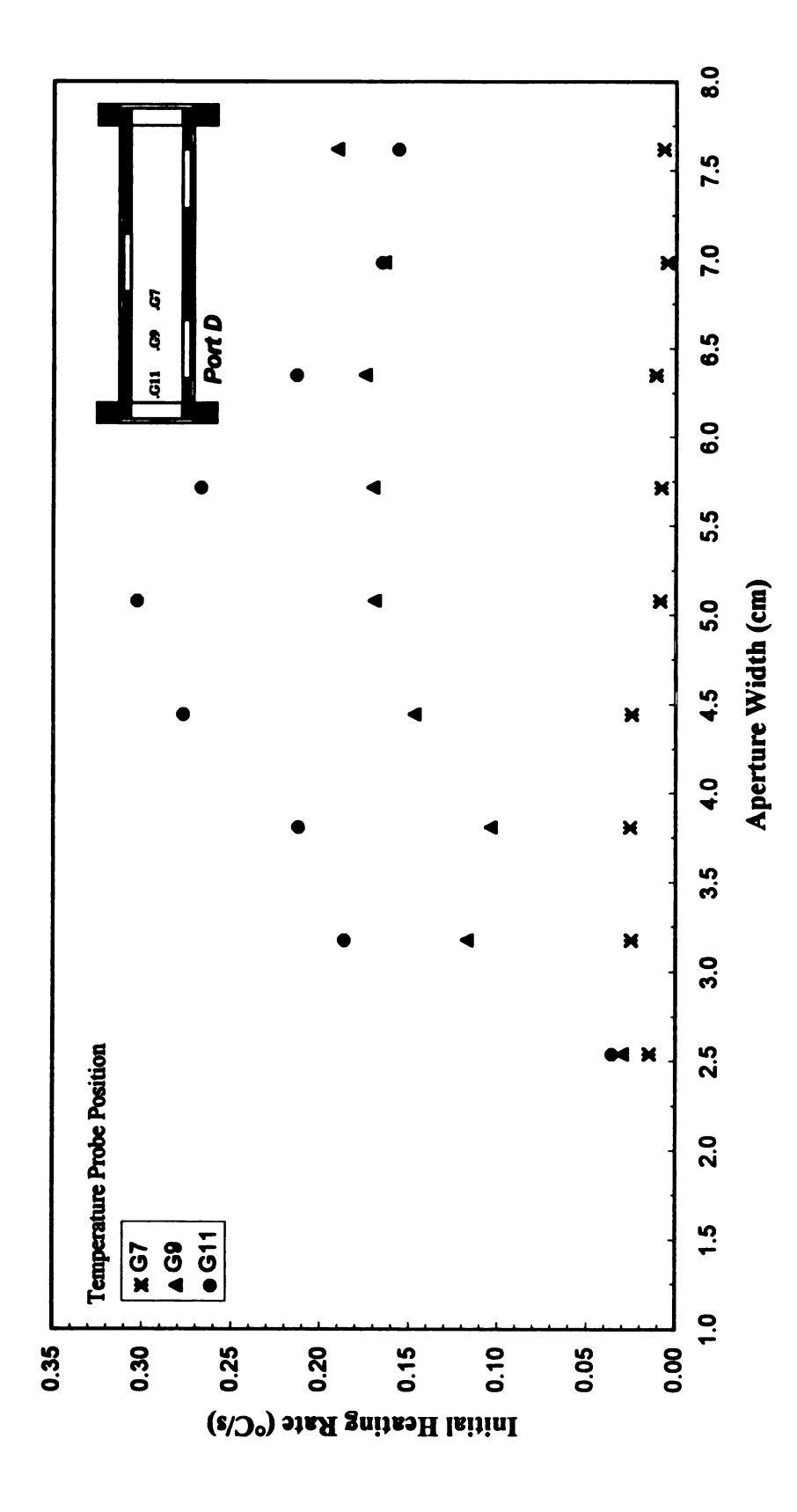


Figure 4.11. Initial Temperature Profile as a Function of Aperture Width at Port D.

Table 4.1. Thermal Paper Images for Various Aperture Widths.

Thermal Paper Image	Aperture Width (cm)	2° lobe location (cm)	3° lobe location (cm)	4° lobe location (cm)
	3.61	6.4	10.6	14.4
	4.19	5.8	10.6	14.5
	5.08	6.3	10.5	14.6

approximately the same, within measurement uncertainty. This observation indicates that the electromagnetic mode in the cavity is not affected by the aperture width.

#### 4.2. Theoretical Calculations

### 4.2.1. Electromagnetic Modes in the External Applicators

A resonant cavity is described in Chapter 2 as being a system, enclosed by conductive boundaries, that can store or transfer electromagnetic energy. Because the external applicator is not completely enclosed by conductive boundaries, strictly speaking, it is not a resonant cavity. The presence of process material directly below the aperture creates a partially reflective surface. However, analysis of the theoretical cavity modes provides instructive information on the electromagnetic behavior inside the cavity.

Experimentally, two modes can be excited in the external applicators: one at lengths ranging from 7.0 to 9.6 cm and one ranging from 18.7 to 19.5 cm. As is evident from the mode chart shown in Figure 4.12 for a resonant cavity with the cross-sectional dimensions of the external applicator, 6.4 cm x 7.6 cm, three modes should be excited over the range of the external applicator length at 2.45 GHz. Excitation of the TE<sub>011</sub>,TE<sub>101</sub>, and TE<sub>012</sub> modes is possible at 10.3 cm, 20.8 cm, and 20.6 cm, respectively. The heating characterization runs and curing experiments all used the observed mode near the theoretical TE<sub>011</sub> mode.

The theoretical TE<sub>011</sub> mode resonates with an E-field component in the x-direction only and zero E-field at z=0 and z=c, where c is the length of the cavity in the z-direction. In the external applicator, the excitation probe and the aperture length are oriented parallel with the x-direction, as shown in Figure 4.13. At z=c, the E-field in the

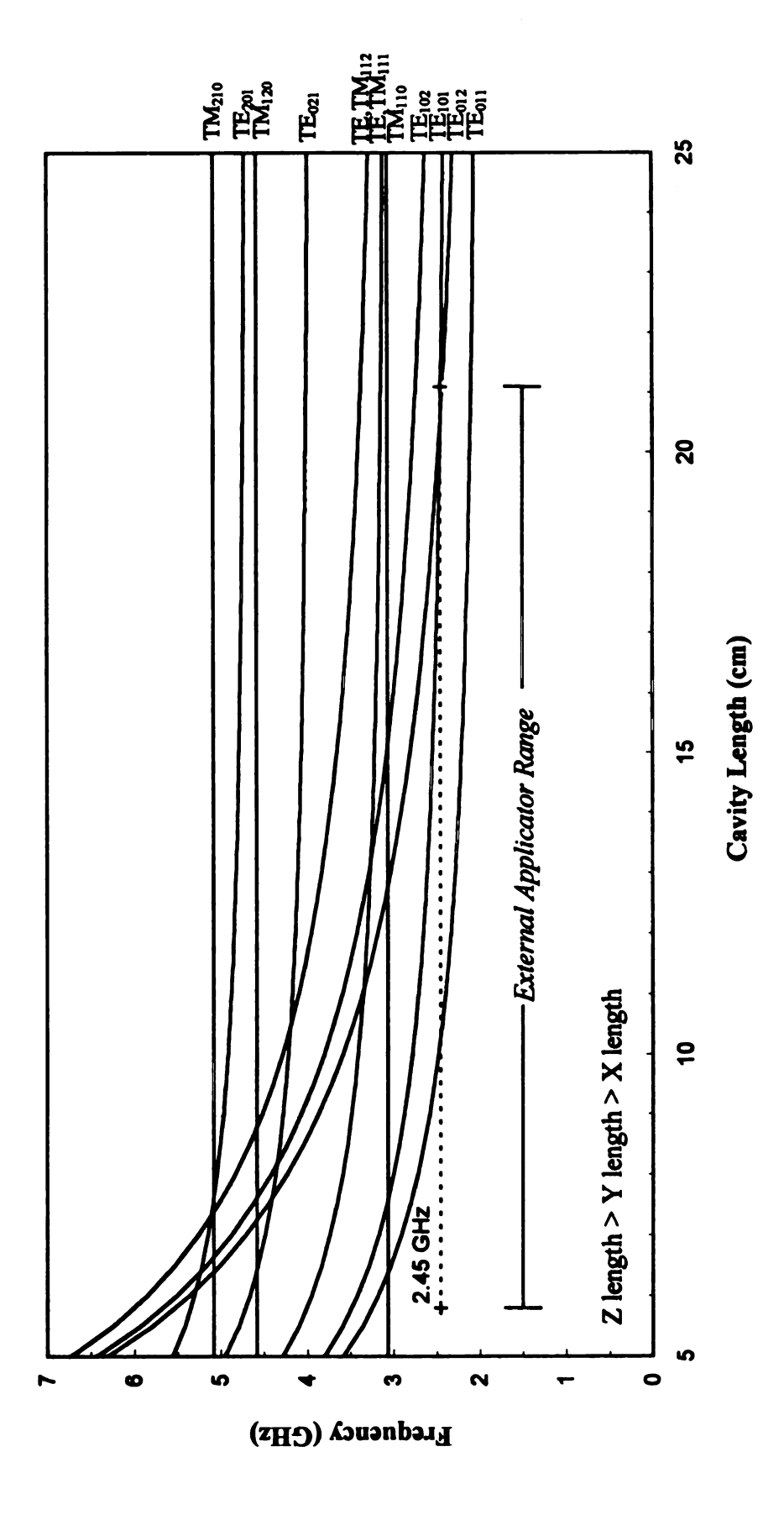


Figure 4.12. Theoretical Mode Chart for a 6.4 cm x 7.6 cm Rectangular Cavity.

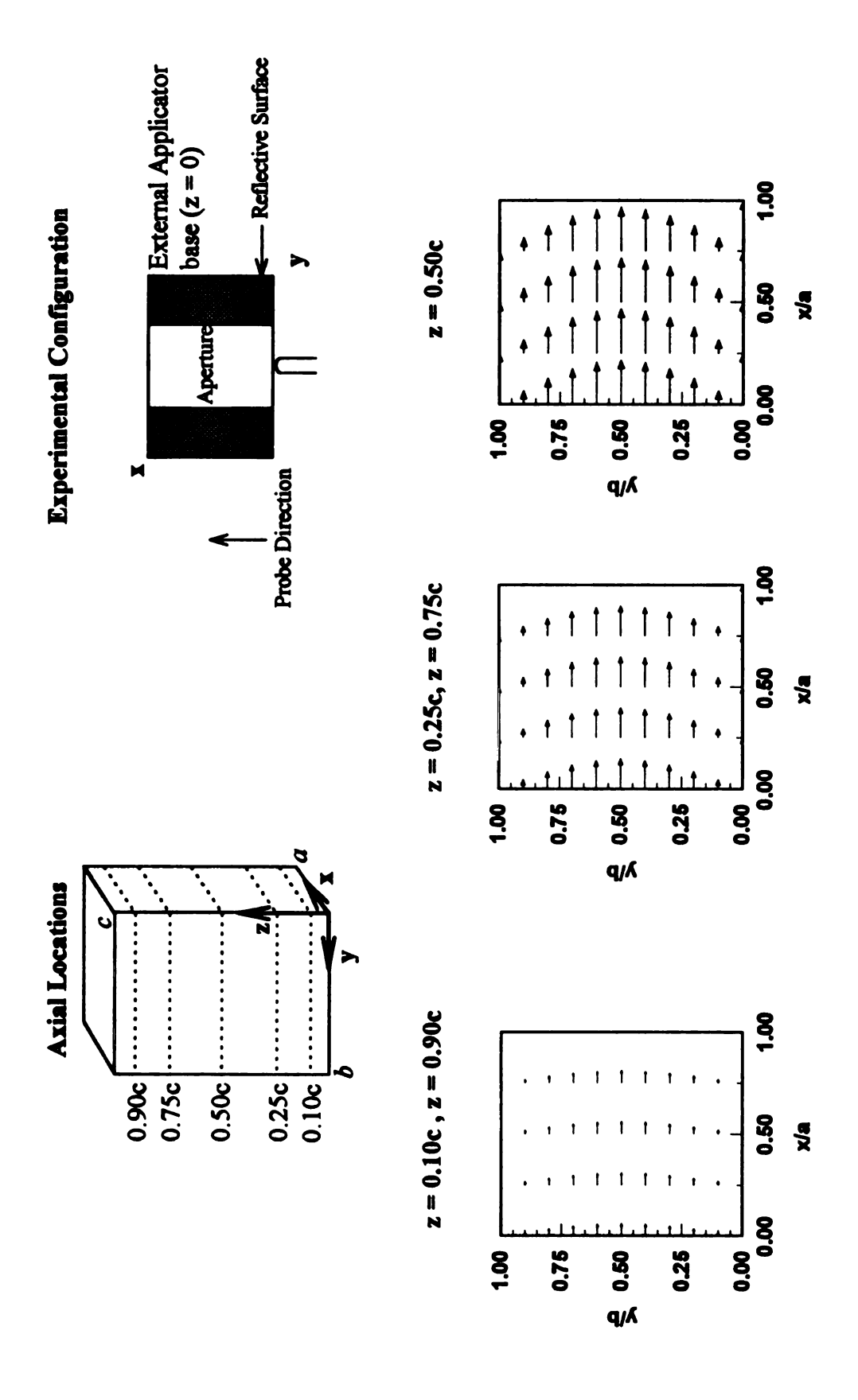


Figure 4.13. Theoretical Vector Plots of E-field for the TE<sub>011</sub> Mode and the Aperture Configuration.

external applicator is zero due to the conductive boundary; however, at z=0, admittance of the E-field to the cavity would not be possible if the E-field were zero. Therefore, the E-field is zero on the conductive aperture plate and non-zero at the aperture. The theoretical E-field vectors shown in Figure 4.13 do not strictly represent the actual E-field magnitudes. Due to the aperture, deviation from the theoretical calculations would be most evident near z=0.

## 4.2.2. Electromagnetic Modes in the Cavity

Propagation of electromagnetic energy in the cavity is defined by waveguide theory, as the cavity is a dielectric-filled waveguide. In a waveguide, electromagnetic modes propagate above the cutoff frequency, below the cutoff frequency, modes are evanescent, or nonpropagating.

Cutoff frequency calculations, theoretical E-field calculations, thermal paper images, and heat transfer analysis are used in determining the propagating mode in the cavity. Using the cross-sectional dimensions of the cavity, 4.2 cm x 8.9 cm, Figure 4.14 illustrates the cutoff frequencies for a range of dielectric constants typical of polymeric systems. Over this range, five modes could potentially propagate through the cavity at 2.45 GHz: TE<sub>10</sub>, TE<sub>20</sub>, TE<sub>01</sub>, TE<sub>11</sub> or TM<sub>11</sub>, and TE<sub>21</sub> or TM<sub>21</sub>. The glass-reinforced polyester used for heating characterization has a complex permittivity of 4.3 - j0.049. With a dielectric constant of 4.3, any of the aforementioned modes could propagate through the cavity at 2.45 GHz.

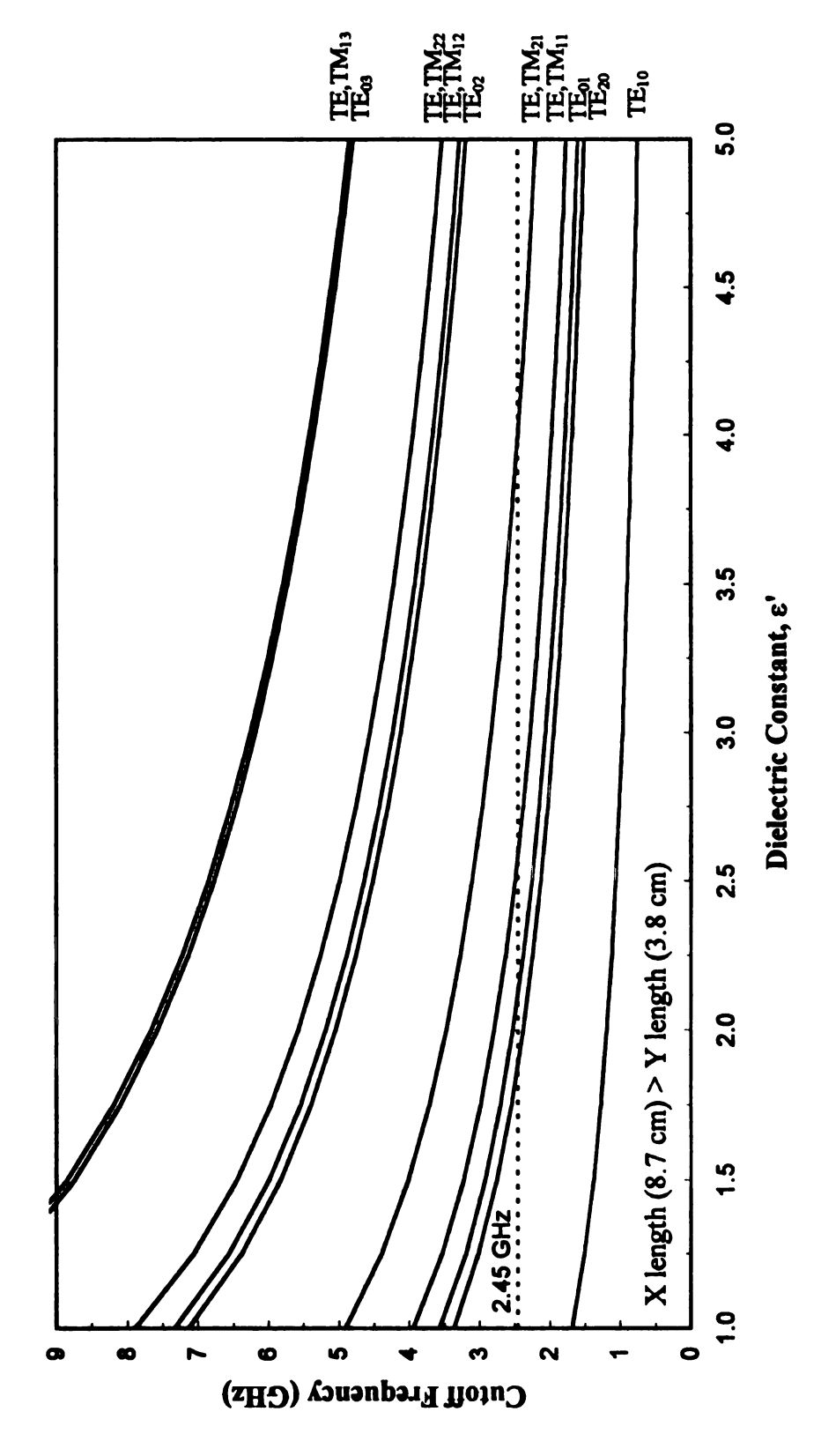


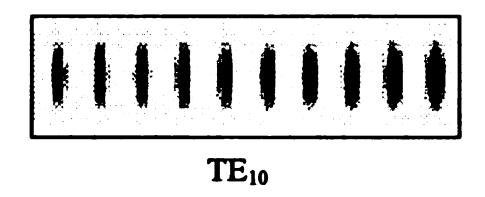
Figure 4.14. Cutoff Frequency in the Cavity as a Function of the Process Material Dielectric Constant.

The E-field intensity patterns for the seven lowest order modes for the cavity are calculated and plotted to theoretically determine the areas of heating intensity. The E-field strength plots, shown in Figure 4.15, are x-z plots with attenuation in the negative x direction. The dark regions indicate areas of higher E-field intensity. For comparison, a thermal paper image is included in Figure 4.15. As is evident from comparison of the heating pattern to the E-field strengths, TE<sub>20</sub>, TE<sub>11</sub>, TE<sub>21</sub>, and TM<sub>21</sub> are not the modes of propagation observed experimentally.

The plots in Figure 4.15 show the Euclidean norm of the E-field as a function of space in an x-z plane. Vector plots of the TE<sub>10</sub>, TE<sub>01</sub>, and TM<sub>11</sub> modes, illustrated in Figure 4.16 for an x-y plane, provide more detail about the direction of the E-field.

Assuming that a mode similar to the TE<sub>011</sub> mode is resonating in the external applicator, only an x-component of the E-field exists in the external applicator. This suggests that the TE<sub>01</sub> mode is propagating in the cavity since the TE<sub>01</sub> E-field has an x-component only. As shown in Figure 4.16, a y-component only exists for the TE<sub>10</sub> mode. The TM<sub>11</sub> mode has an x-, y-, and z-component. Additionally, the z-location of the E-field nodes for the TM<sub>11</sub> mode is a function of y. Experimentally, the thermal paper from each plate indicated identical positions of the intense heating regions.

The theoretical E-field magnitude for the TE<sub>01</sub> mode is constant in the x-direction. However, from the thermal paper images, the heating patterns indicate high temperatures at the center of the cavity and diminishing temperatures near the cavity wall in both the x- and y-directions. To elucidate this observed phenomenon with the heating



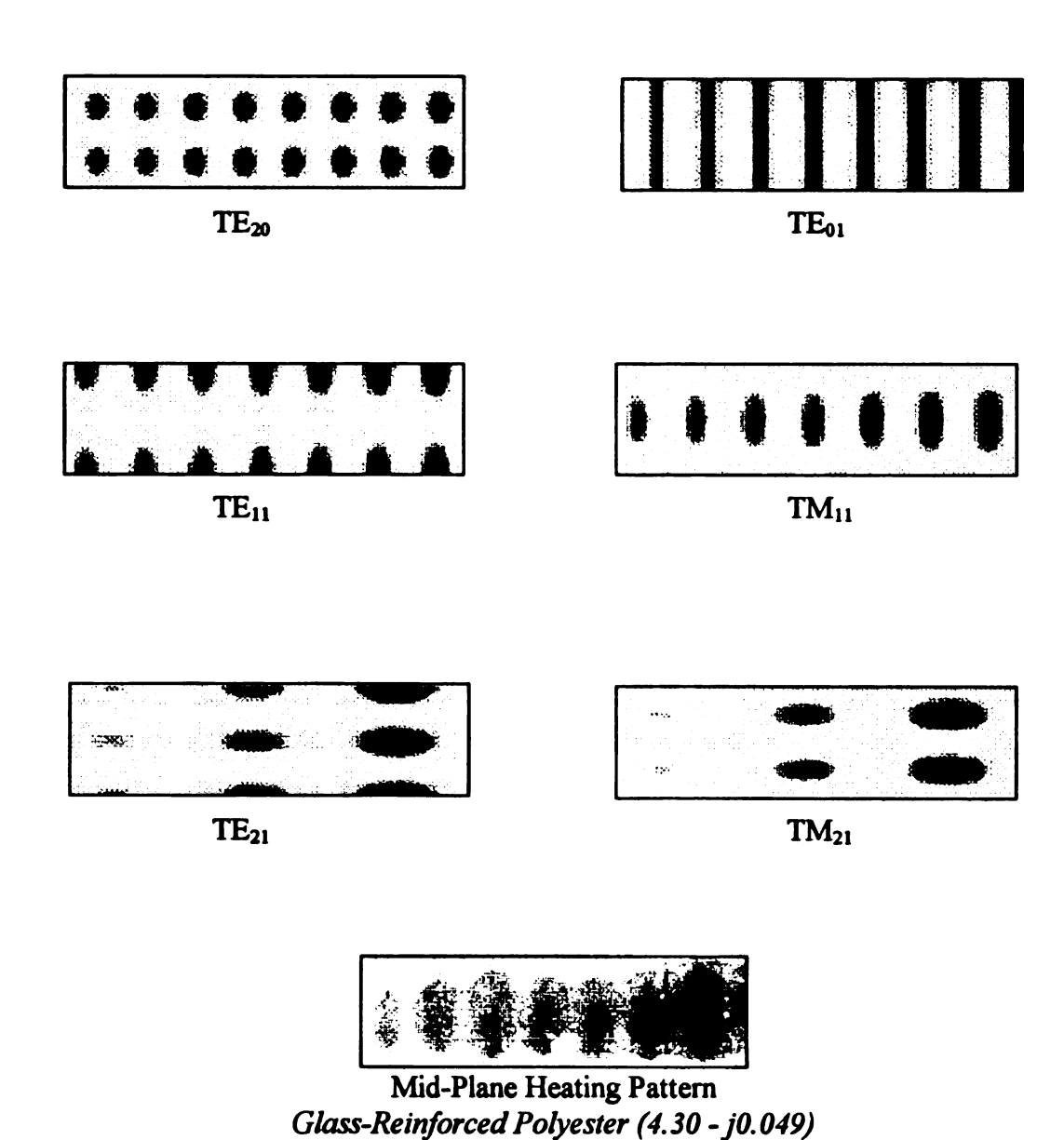


Figure 4.15. Theoretical E-field Strength Plots and Thermal Paper Image For the Mid-Plane (i.e., y = 0.5 b) of a 4.2 cm x 8.9 cm Waveguide filled With Dielectric Material ( $\epsilon^{\circ}$  = 4.30-j0.049).

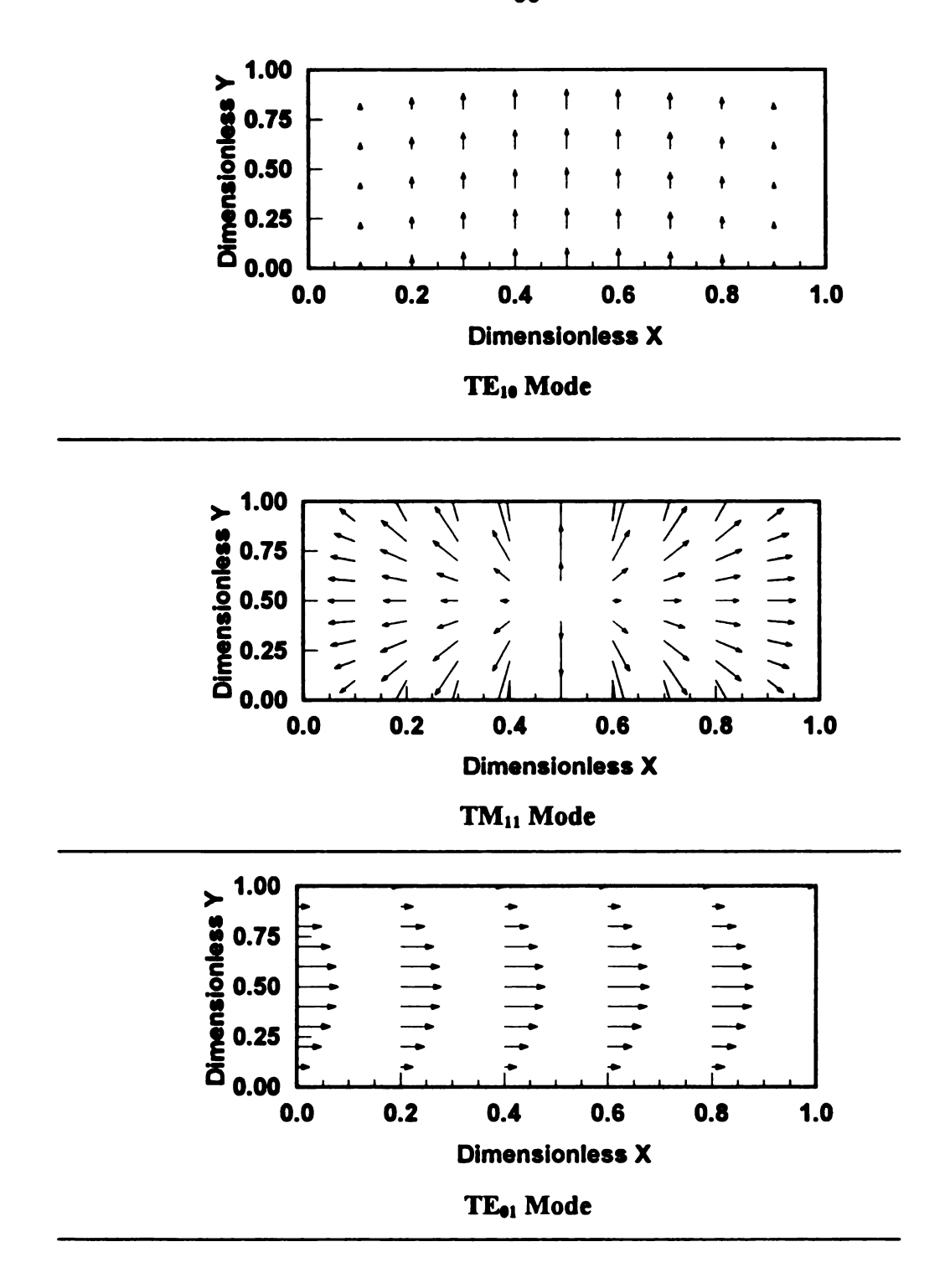


Figure 4.16. X-Y Vector Plots for the TE<sub>10</sub>, TM<sub>11</sub>, and TE<sub>01</sub> Modes.

patterns and demonstrate the virtues of microwave heating, a one-dimensional finite difference model was developed based on the energy balance:

$$\rho C_{p} \frac{\partial T}{\partial t} = k \nabla^{2} T + P_{MW}, \qquad [4.1]$$

where  $\rho$  is the material density  $C_p$  is the material heat capacity  $C_p$  is the material temperature  $C_p$  is the m

This model assumes an isotropic thermal conductivity and no heat of reaction. The physical system is an 8.9 cm slab of polymer between two 1.25 cm slabs of brass, which are the dimensions of the cavity and brass walls in the x-direction. The details of the boundary conditions and the FORTRAN code are outlined in Appendices F and G, respectively.

The half-wave E-field variation in the y-direction for the TE<sub>01</sub> mode is responsible for the strong center heating and absence of heating near the cavity wall at y=0 cm and y=4.2 cm. The E-field in the x-direction, however, is invariant with position. The relative differences in heating intensity in the x-direction can be explained using the heat transfer model. A constant microwave power input of 0.115 W/cm<sup>3</sup> was selected based on matching the simulated rate of temperature rise with that of experiments with an external applicator at port C. Using a free-convective boundary condition of 5.0 W/m<sup>2</sup>-K, the model predicts the temperature profiles shown in Figure 4.17. At short times, the temperature profile is relatively flat, due to the insignificant temperature gradients. During this regime, the heating rate is equal to the constant microwave power

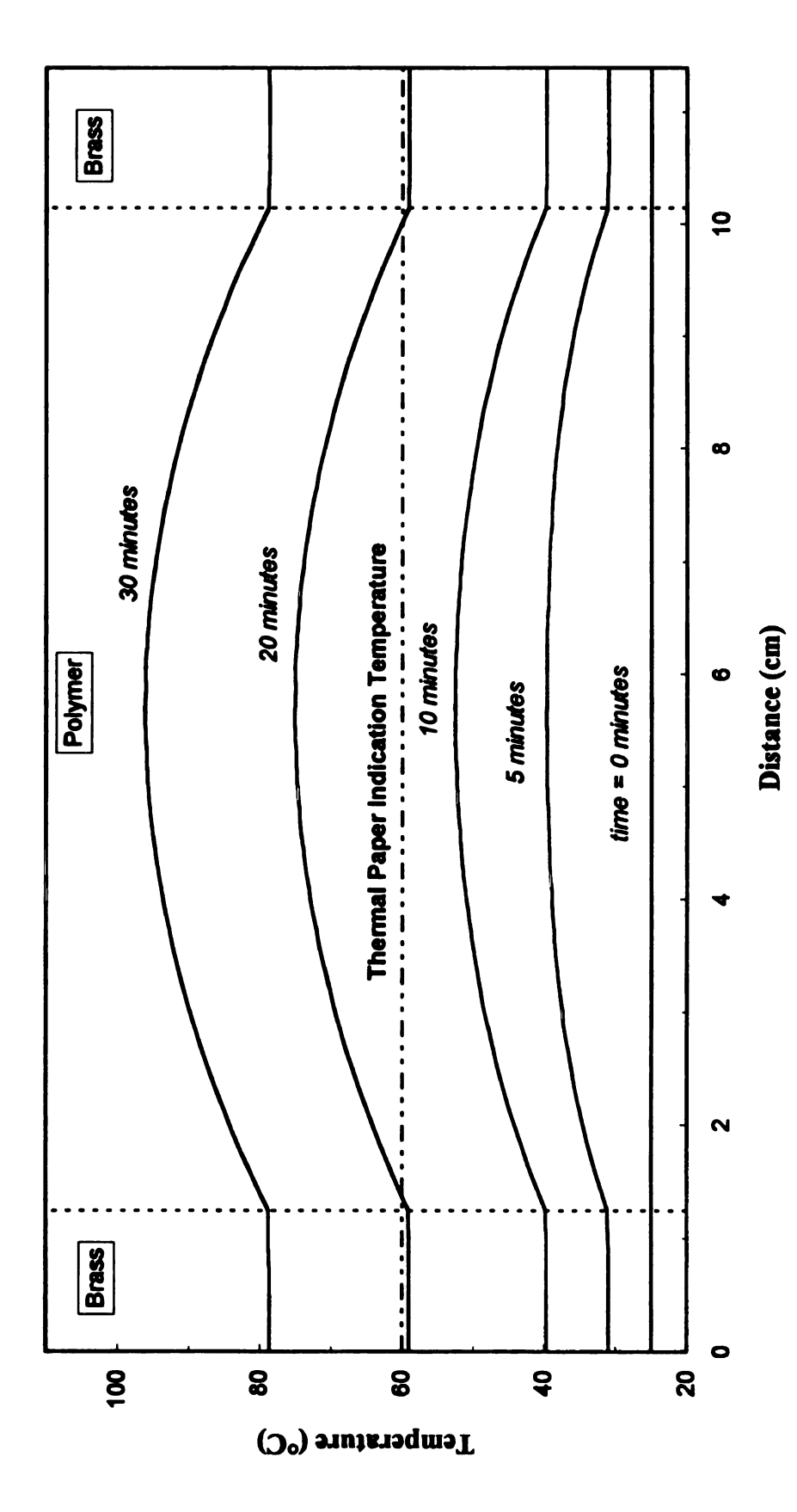


Figure 4.17. Theoretical Temperature Profiles at Various Times for a Constant Microwave Power Input of 0.115 W/cm<sup>3</sup> in an Infinite Slab of Polymer Between Brass Boundaries.

absorption. When the temperature of the polymer increases, energy is transferred outward toward the brass walls and into the surroundings. When conduction becomes significant, the low thermal conductivity of the polymer creates a resistance to heat transfer and, eventually, a temperature gradient. A constant E-field does not necessarily translate into constant temperature profiles.

## 4.3. Processing of Glass-Reinforced DGEBA/DDS

## 4.3.1. Complex Permittivity

The complex permittivity of DGEBA/DDS as a function of E-glass fiber content at 25°C was measured by the cavity perturbation technique using the TM<sub>012</sub> mode at 2.45 GHz in a cylindrical cavity with a diameter of 15.24 cm<sup>(35)</sup>. The Teflon cylinder used to introduce the epoxy-fiber sample into the cavity has an inner diameter of 1.12 cm and a length of 2.60 cm. Resin samples were prepared with the 3:4 amine to epoxy ratio. Epoxy-fiber sample volumes were calculated based on the densities of each component in the mixture. Assuming volume additivity in a two-component system, the sample volume is given by

$$V_{\text{mix}} = \frac{M_{\text{mix}}}{\rho_{\text{mix}}} = M_{\text{mix}} \left( \frac{1}{\rho_{\text{resin}}} (1 - \chi_{\text{fiber}}) + \frac{\chi_{\text{fiber}}}{\rho_{\text{fiber}}} \right), \quad [4.2]$$

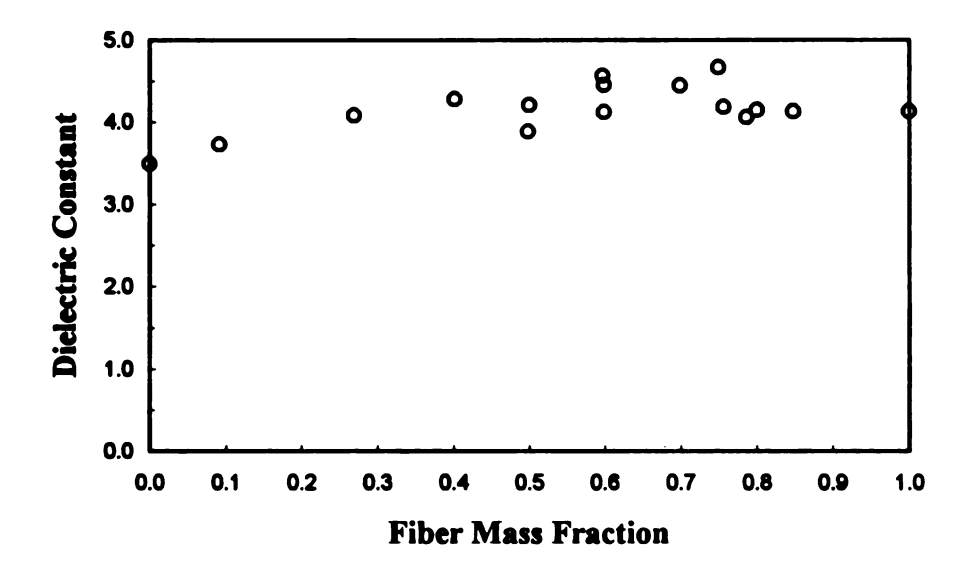
where  $M_{mix}$  is the mass of the fibers and resin,  $\chi_{fiber}$  is the fiber mass fraction,  $\rho_{resin}$  is 1.09 g/cm<sup>3</sup>,  $\rho_{fiber}$  is 2.54 g/cm<sup>3</sup>. Air pockets in the epoxy-fiber mixture at fiber mass fractions greater than 0.5 introduce uncertainty in the measurement of sample volume.

The complex permittivity of the E-glass fibers in resin appears to behave linearly with fiber mass fraction for mass fractions below 0.5 as is evident in Figure 4.18. At room temperature and zero extent of cure, DGEBA/DDS in a 3:4 amine to epoxy ratio has a larger dielectric loss and a smaller dielectric constant relative to the fibers. For instance, a fiber mass fraction of 0.25 increases the dielectric constant of the unloaded DGEBA/DDS sample by 15% and reduces the loss by 8%. The uncured DGEBA/DDS samples have a complex permittivity of 3.50 - j0.23.

## 4.3.2. Curing Results

By conventional, microwave, and hybrid heating, three E-glass-reinforced DGEBA/DDS composites are cured. Temperatures during cure are measured at locations near ports A, B, and C in the center of the part and at a wall location near the cavity center. Temperatures at the select locations inside the cavity were used to provide a basis for manual control of the microwave power input for microwave and hybrid heating. Figures 4.19 through 4.21 illustrate the various temperature profiles for the three types of heating. A comparison of the average axial-to-wall temperature gradients, from using three curing methods in the part-shaped cavity, is shown in Figure 4.22.

Over one hour is required for the composite to achieve the cure temperature, 125°C, using conventional heating. Microwave and hybrid heating techniques heated the composite to 125°C in 10 minutes or less, corresponding to more than an 85% reduction in the time required to attain the cure temperature.



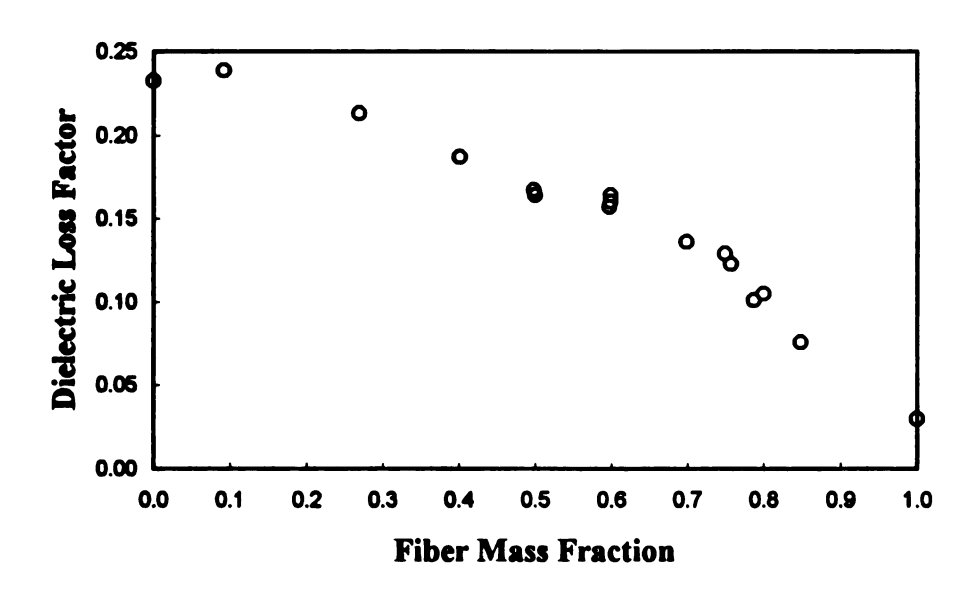


Figure 4.18. Complex Permittivity of Uncured DGEBA/DDS at 25°C as a Function of Fiber Content.

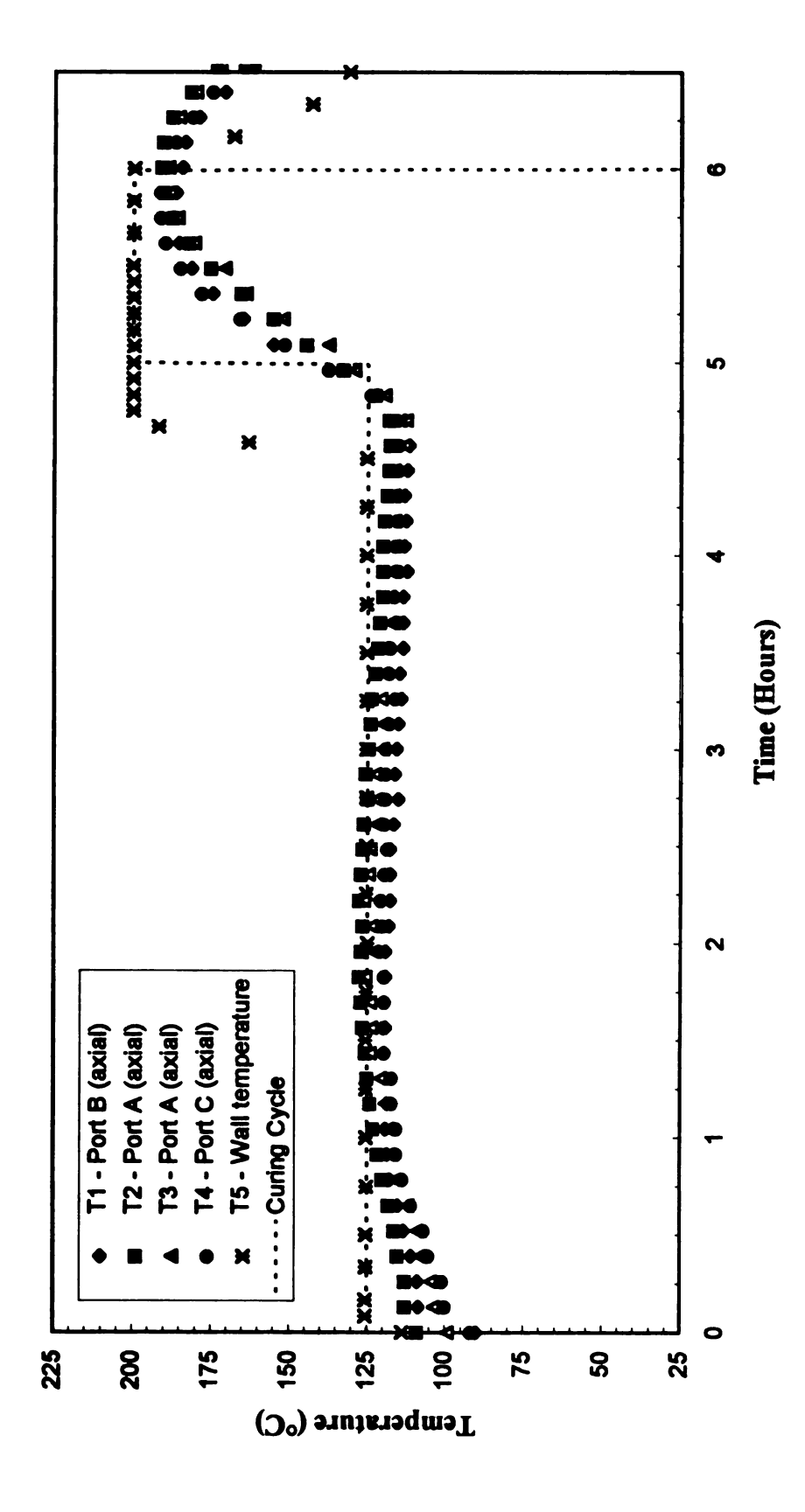


Figure 4.19. Temperature Profiles for Conventional Curing of E-glass-Reinforced DGEBA/DDS in the Part-Shaped Cavity.

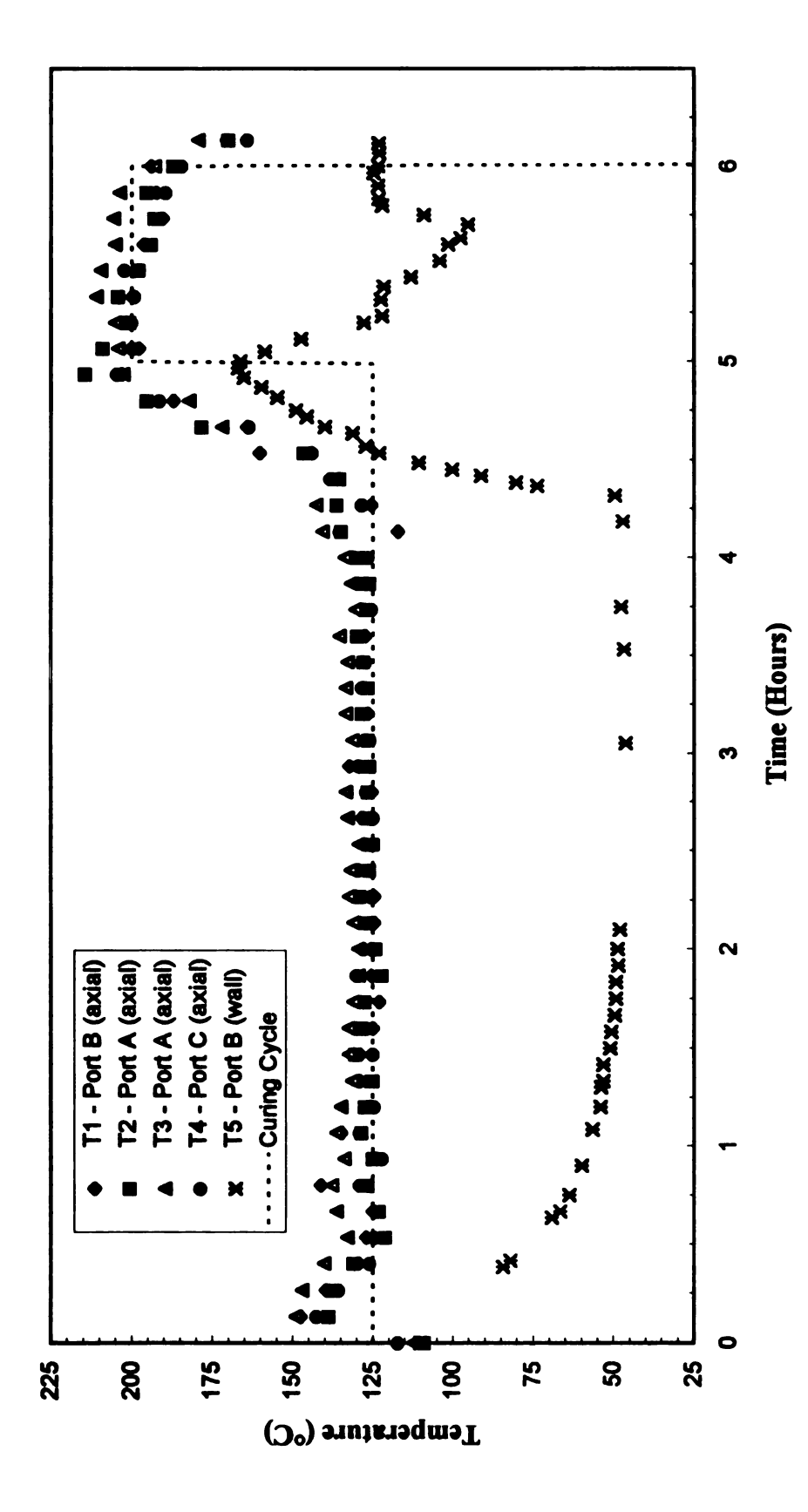


Figure 4.20. Temperature Profiles for Microwave Curing of E-glass-Reinforced DGEBA/DDS in the Part-Shaped Cavity.

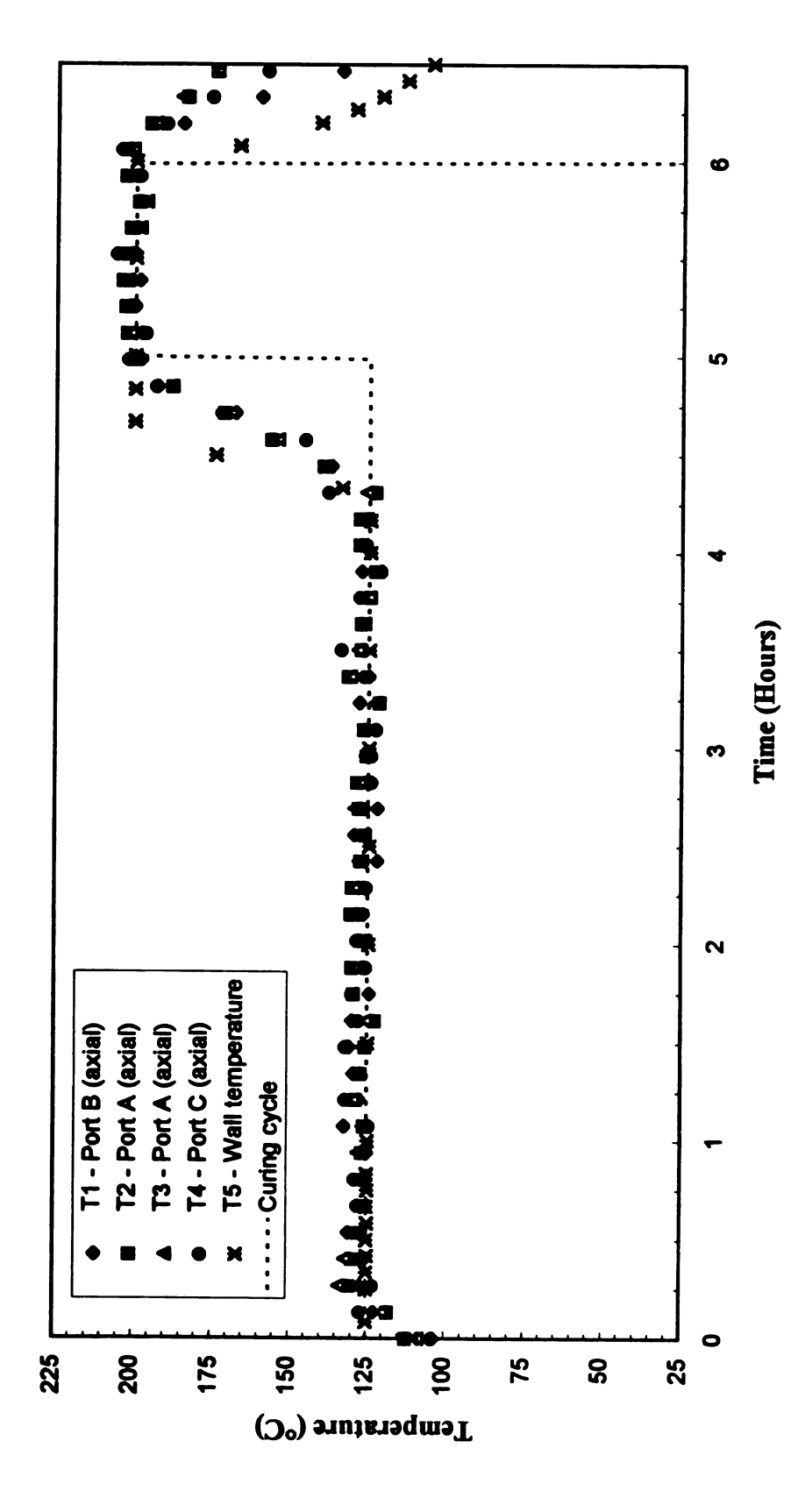


Figure 4.21. Temperature Profiles for Hybrid Curing of E-glass-Reinforced DGEBA/DDS in the Part-Shaped Cavity.

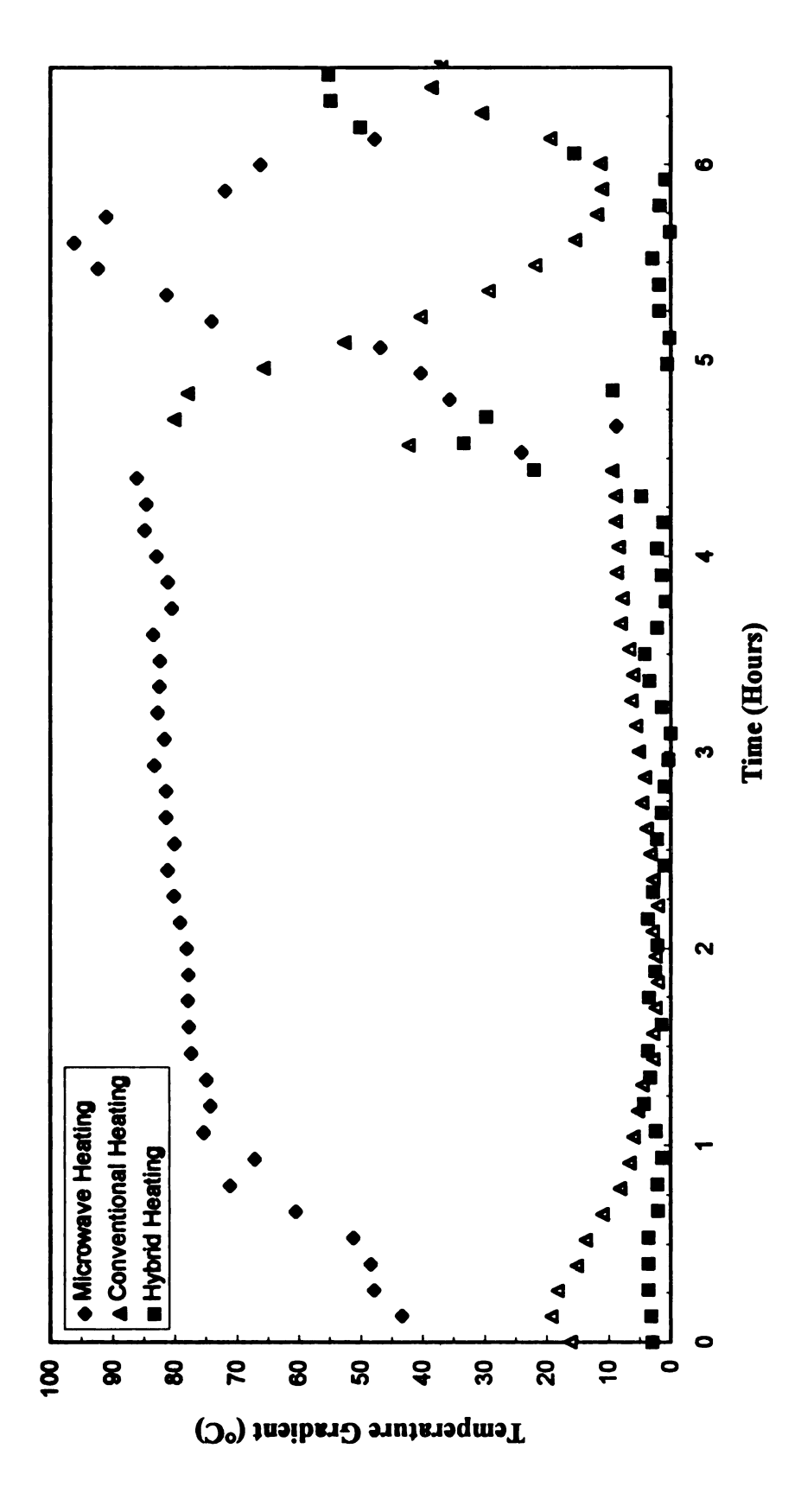


Figure 4.22. Average Center-to-Wall Temperature Gradient for Microwave, Conventional, and Hybrid Curing of E-glass-Reinforced DGEBA/DDS in the Part-Shaped Cavity.

At the beginning of the cure cycle, the relatively large dielectric loss of the composite provided excellent coupling of the electromagnetic energy with the process material molecules. As the reaction progressed, the loss decreased due to a decrease in the molecular mobility (i.e., crosslinking). A thermal boost from the heaters on the cavity was required to attain the post-cure temperature during the microwave heating run. A microwave source larger than 120 W is required to achieve the 200°C post-cure temperature due to the decrease in the microwave power absorption combined with heat losses to the external applicators and the surroundings.

Microwave heating resulted in the largest average axial-to-wall temperature gradient throughout the cure and post-cure cycles. As explained in Section 4.2.2., this gradient develops due to the heat loss at the cavity boundaries coupled with the low thermal conductivity of the composite. Gradients can also develop as a result of the type of electromagnetic mode propagation inside the cavity.

Hybrid heating provided the most uniform temperature profiles for the three processing methods. Initially, the conventional heating technique results in a temperature gradient between the center and the mold wall is formed. The heat transfer model can be applied as a semi-quantitative tool in the temperature profile analysis.

Table 4.2 outlines the parameters used in the model for each process method.

The simulation of conventional heating, as shown in Figure 4.23, clarifies the observed initial temperature gradient. Because of the low thermal conductivity of the polymer, the temperature of the midplane lags the rising temperature of the brass wall.

Table 4.2. Heat Transfer Model Parameters for Conventional, Microwave, and Hybrid Heating.

Parameter	Conventional Heating	Microwave Heating	Hybrid Heating	
Physical Properties				
Polymer				
Thermal conductivity	2.0	2.0	2.0	
(W/m <sup>2</sup> -K) Density (kg/m <sup>3</sup> )	1100	1100	1100	
Density (kg/m)	1100	1100	1100	
Heat capacity (J/kg-K)	2000	2000	2000	
Brass				
Thermal conductivity (W/m²-K)	110	110	110	
Density (kg/m³)	8500	8500	8500	
Heat capacity (J/kg-K)	380	380	380	
Physical System				
Convective heat transfer	1000	5.0	1000	
coefficient				
(W/m <sup>2</sup> -K) Polymer thickness (cm)	8.9	8.9	8.9	
1 orymor unormoss (om)	0.7	0.7	0.7	
Brass thickness (cm)	1.25	1.25	1.25	
Initial system temperature	25.0	25.0	25.0	
(°C)				
Ambient temperature	125.0	25.0	125.0	
(°C)	0.0	2.0	2.0	
Microwave power input (W/cm³)	0.0	2.0	2.0	
Finite Difference				
X-interval (cm)	0.178	0.178	0.178	
Time-step (s)	0.10	0.10	0.10	

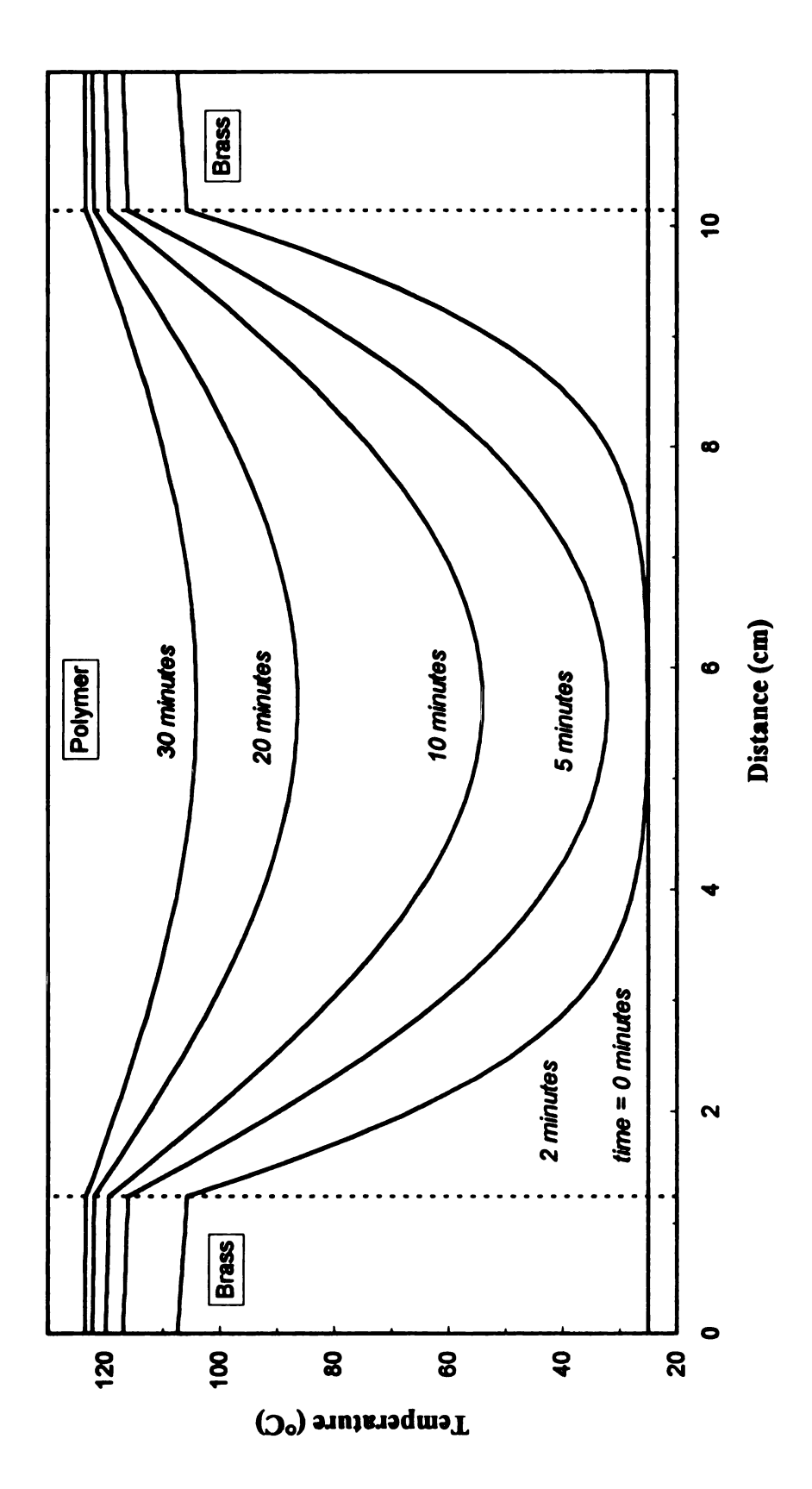


Figure 4.23. Theoretical Temperature Profiles at Various Times for Conventionally Heating an Infinite Slab of Polymer Between Brass Boundaries.

Conductive heat transfer in the material near the wall is greater than that near the midplane.

A simulation of microwave heating with a constant microwave power absorption of 2.0 W/cm<sup>3</sup> is performed. This microwave heating simulation employs a greater power absorption than the previous one in Section 4.2.2. Comparing Figures 4.24 and 4.17 shows the same type of temperature profile: maximum in the center and minimum at the walls. For the TE<sub>01</sub> mode, greater microwave power results in faster heating times and more uniform temperatures. Energy input due to microwave power becomes the dominant energy transfer mechanism, and the effects of conductive heat transfer are only seen near the mold walls.

As observed experimentally, minimizing temperature gradients and reducing the heating time are feasible by combining microwave and conventional heating. The same behavior is demonstrated theoretically, as shown in Figure 4.25. With hybrid heating, the large outward flux of thermal energy near the mold wall associated with microwave heating is offset by the large inward flux of energy near the mold walls associated with conventional heating.

# 4.4. Mechanical Strength Tests

Ten test samples from each cured composite were prepared according to the description given in Section 3.4. During each test, the normal load on the sample surface and the deflection of the sample midpoint are recorded. An example of the typical load-deflection relationship is shown in Figure 4.26. As is evident from this plot, the sample

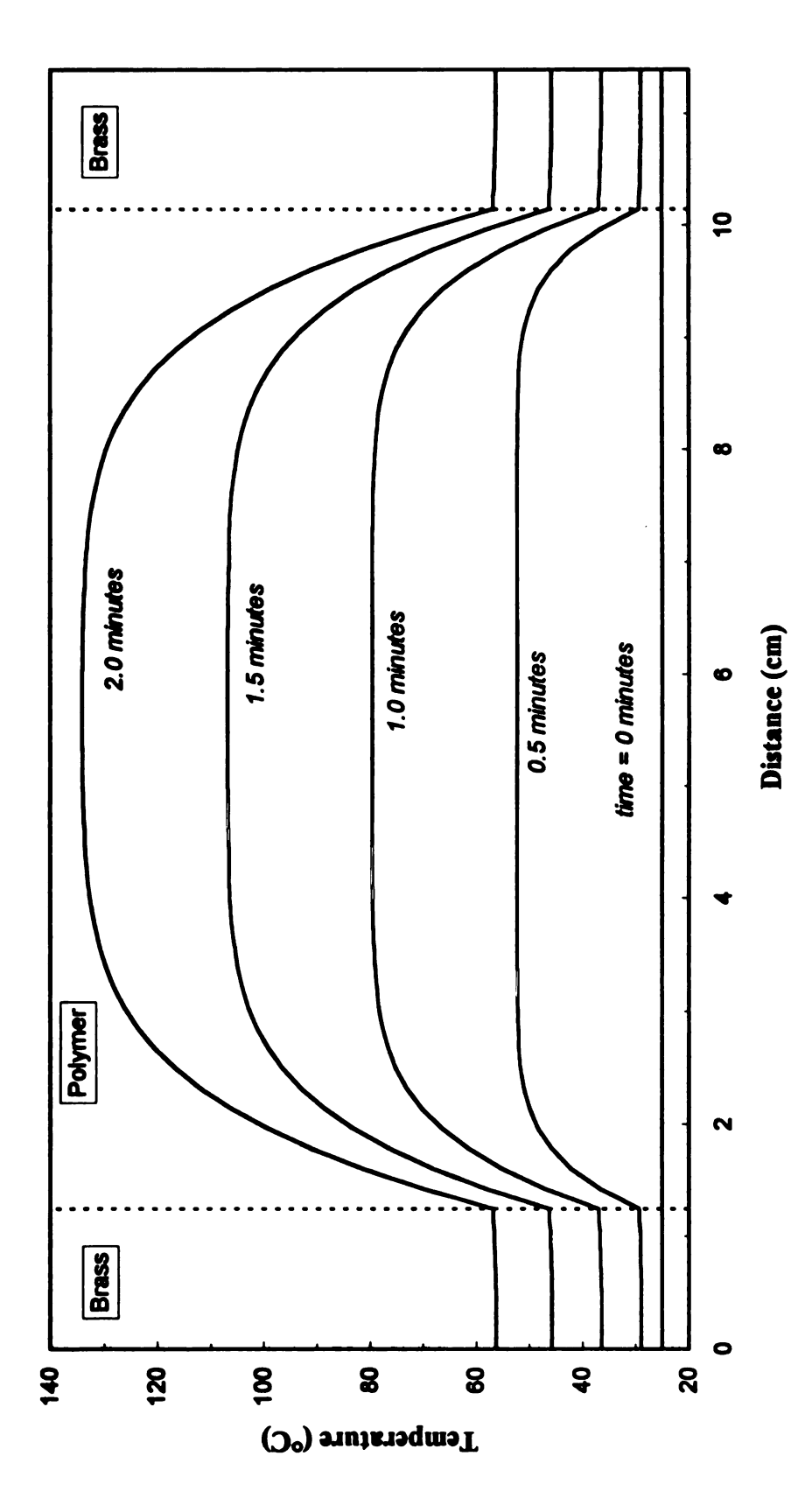


Figure 4.24. Theoretical Temperature Profiles at Various Times for a Constant Microwave Power Input of 2.0 W/cm<sup>3</sup> in an Infinite Slab of Polymer Between Brass Boundaries.

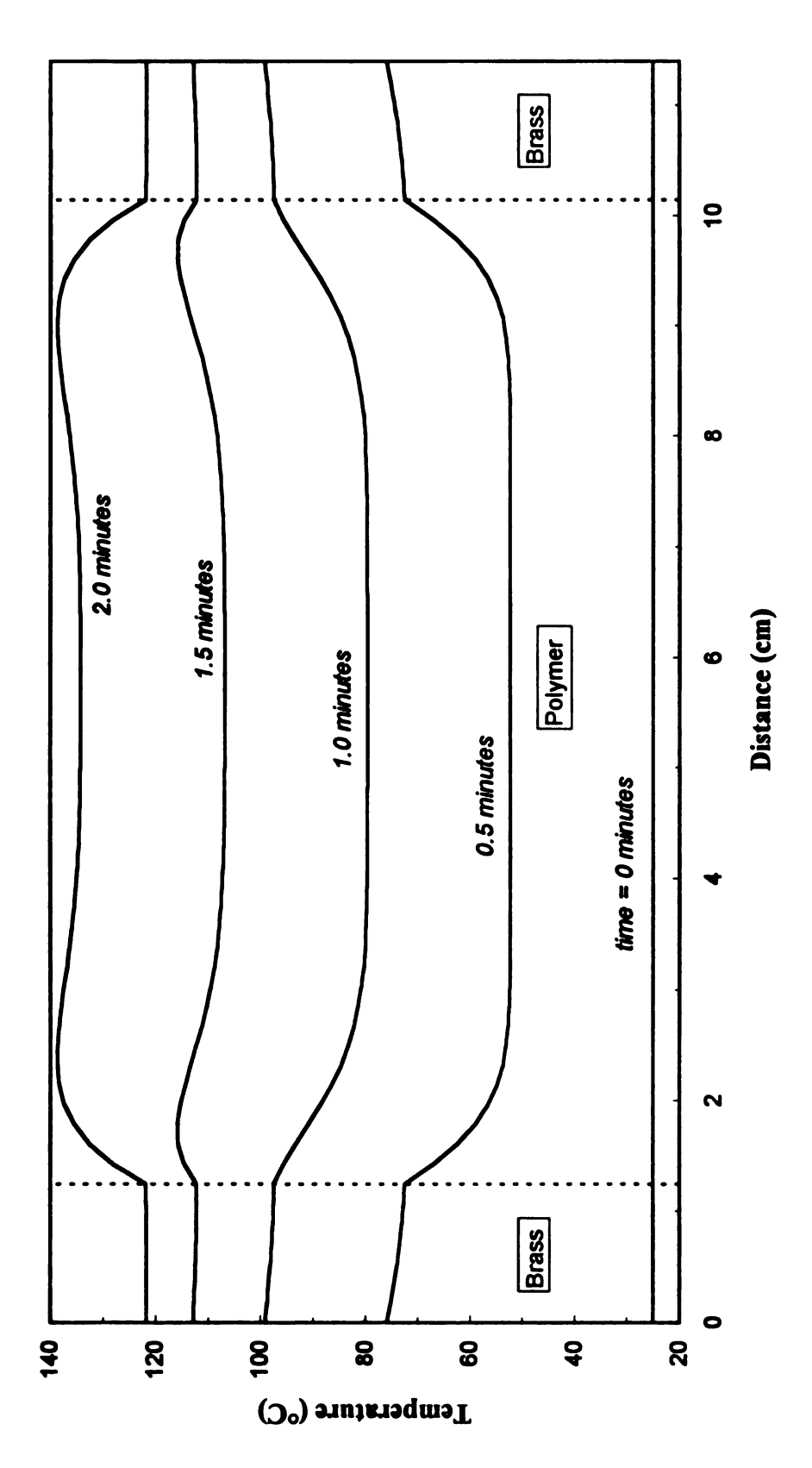


Figure 4.25. Theoretical Temperature Profiles at Various Times for Hybrid Heating With a Constant Microwave Power Input of 2.0 W/cm<sup>3</sup> in an Infinite Slab of Polymer Between Brass Boundaries.

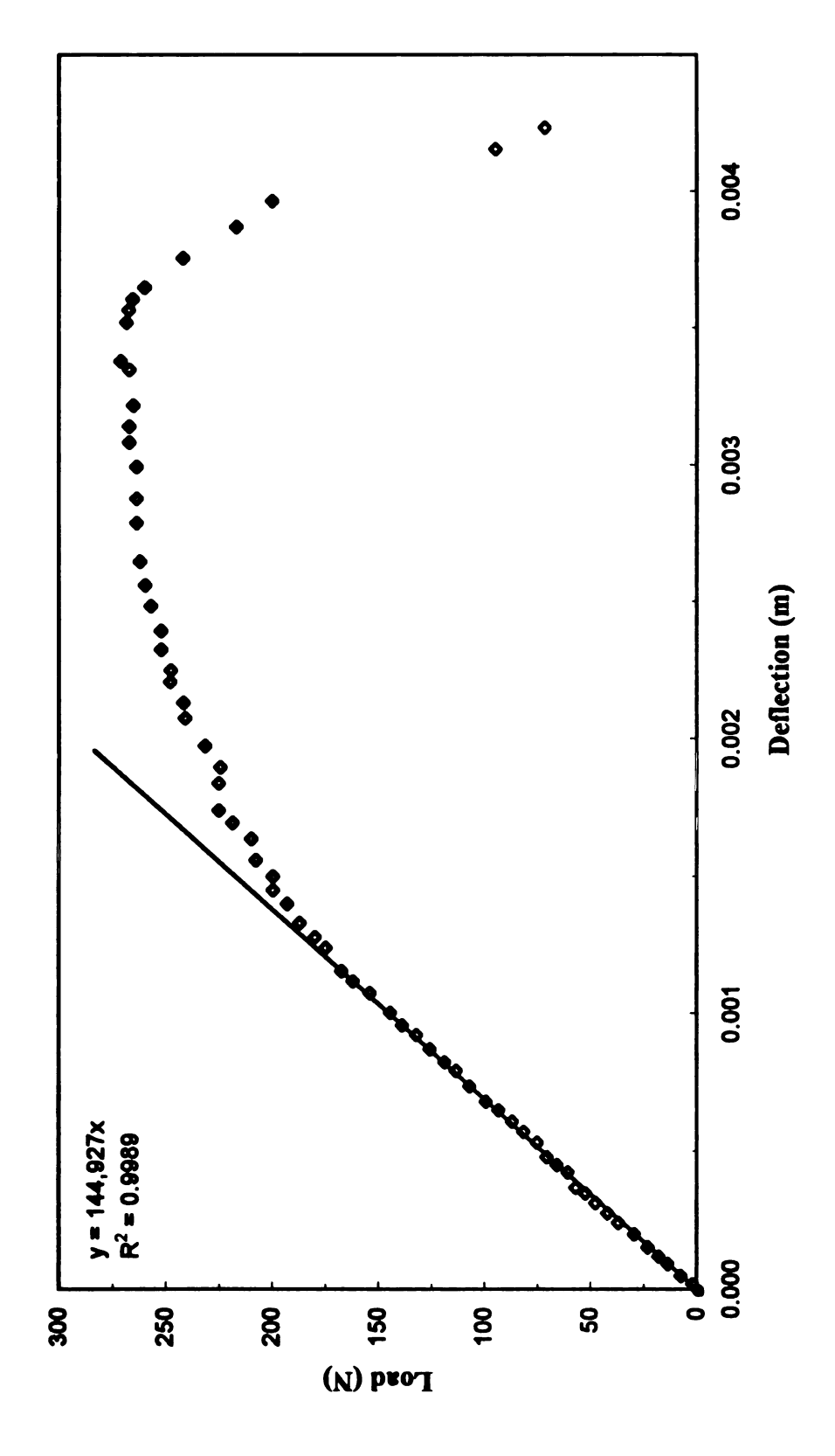


Figure 4.26. Load-Deflection Data With Initial Slope for Sample 7H (Hybrid Cured E-glass-Reinforced DGEBA/DDS).

deflection behaves linearly with the applied normal load, for this particular sample, to approximately 12 mm. The deflection range from 0 to 12 mm is defined as the region of linear elastic behavior. This slope is used in the calculation of the modulus of elasticity as given in Equation 3.3.

The moduli of elasticity for samples cured by conventional, microwave, and hybrid heating are  $6.56 \pm 0.30$  GPa,  $6.68 \pm 0.26$  GPa, and  $6.47 \pm 0.22$ GPa, respectively. Only the samples in Table 4.3 that are designated as 'valid data' are used in the calculation of these averages. The invalid samples contained three or more visible microvoids; voids can affect data accuracy. By observing the manufacturer recommendation for the cure cycle, each of the three processing methods have the capability of producing composites with comparable moduli of elasticity.

Table 4.3. Modulus of Elasticity Data for E-glass-Reinforced DGEBA/DDS.

Sample	Width (mm)	Length (mm)	Depth (mm)	Number of Visible Microvoids	Valid Data	Modulus of Elasticity (GPa)
Convention	onal Cure					
1 <b>C</b>	2.53	7.62	0.324	0	Yes	6.22
2C	2.53	7.60	0.303	1	Yes	6.84
3C	2.52	7.62	0.354	1	Yes	6.23
4C	2.53	7.62	0.309	11	No	6.64
5C	2.53	7.61	0.326	50	No	6.45
6C	2.52	7.61	0.283	50	No	6.54
7C	2.53	7.62	0.336	20	No	6.30
8C	2.53	7.62	0.358	0	Yes	6.50
9C	2.53	7.62	0.329	0	Yes	6.89
10C	2.53	7.63	0.332	0	Yes	6.69
					Average:	$6.56 \pm 0.30$
Microwan	ve Cure					
1 <b>M</b>	2.54	7.62	0.336	1	Yes	6.84
2M	2.54	7.61	0.277	0	Yes	6.69
3M	2.53	7.62	0.324	0	Yes	6.84
4M	2.54	7.51	0.324	0	Yes	6.86
5M	2.54	7.62	0.330	0	Yes	6.91
6M	2.54	7.62	0.381	50	No	5.96
7M	2.53	7.59	0.326	15	No	6.38
8M	2.50	7.62	0.310	2	Yes	6.26
9 <b>M</b>	2.53	7.62	0.290	0	Yes	6.39
10 <b>M</b>	2.54	7.62	0.329	3	No	6.49
					Average:	$6.68 \pm 0.26$
Hybrid C	ure					
1 <b>H</b>	2.46	7.60	0.286	0	Yes	6.75
2H	2.54	7.64	0.329	0	Yes	6.64
3H	2.53	7.63	0.330	0	Yes	6.26
4H	2.52	7.59	0.343	0	Yes	6.62
5H	2.53	7.62	0.336	25	No	6.36
6H	2.53	7.63	0.307	25	No	6.16
7H	1.88	7.61	0.338	0	Yes	6.54
8H	2.19	7.61	0.333	0	Yes	6.31
9H	1.71	7.60	0.362	0	Yes	6.16
10H	2.55	7.62	0.331	1 (large void)	No	6.09
					Average:	$6.47 \pm 0.22$

#### **CHAPTER FIVE**

#### CONCLUSIONS

# 5.1. Part-Shaped Cavity Processing Capabilities and Limitations

The experimental part-shaped cavity has demonstrated:

- more than an 85% reduction in the time required to heat the center of a thick cross-section part to the cure temperature, which translates to a potential reduction in the cycle time, and
- the ability to produce composite parts by conventional, microwave, and hybrid heating with comparable moduli of elasticity.

The geometry of the experimental cavity is a simple, parallelopipedic shape, permitting the propagating electromagnetic mode. In order for microwave energy to couple with the process material, the geometry of the mold must be able to support an electromagnetic mode. Additionally, the process material must have dielectric properties that allow mode propagation through the mold cavity. Knowledge of  $\varepsilon$  over the cure cycle is crucial, as the dielectric properties of polymers significantly during cure.

# 5.2. Project Status

To date, this project has investigated the ability of the part-shaped applicator to heat dielectric materials (e.g., fully cured glass-reinforced polyester) and to cure E-glass-reinforced DGEBA/DDS. The developments for this project have demonstrated the following:

1. a fundamental comprehension of the electromagnetic behavior in the external applicator and the cavity:

- A mode similar to the TE<sub>011</sub> mode resonates in the external applicator, as determined by the theoretical cavity length.
- The pseudo-TE<sub>011</sub> mode is a stable mode when using a single aperture oriented parallel with the coupling probe, and hence the E-field, in the external applicator.
- The magnitude of the admitted E-field to the process material can be controlled by the aperture width.
- The TE<sub>01</sub> mode propagates in the cavity, as determined by thermal paper images, heat transfer analysis, and electromagnetic analysis of the heating intensity locations.
- 2. the ability to cure a glass-reinforced DGEBA/DDS RTM composite by three processing methods, conventional, microwave, and hybrid heating, with the following characteristics:
  - thick cross-sections: 8.9 cm x 4.2 cm (3.5 in. x 1.6 in.)
  - comparable moduli of elasticity:  $6.56 \pm 0.30$  GPa,  $6.68 \pm 0.26$  GPa, and  $6.47 \pm 0.22$  GPa for conventional, microwave, and hybrid heating, respectively
- 3. a theoretical explanation, based on a heat transfer model, of the observed distinctions between the three heating techniques.
  - Conventional heating: Because of the low thermal conductivity of the polymeric process material, the temperature of the midplane lags the rising temperature of the mold wall. Conductive heat transfer in the material near the wall is greater than that near the midplane.
  - Microwave heating: When the temperature of the polymer increases, a flux of energy is directed to the mold walls and into the surroundings. When conduction becomes significant, the low thermal conductivity of the polymer creates a resistance to heat transfer and, eventually, a temperature gradient. The center temperature is greater than the wall temperature due to the resistance of heat transfer through the process material.

- Hybrid heating: The outward flux of thermal energy near the mold wall associated with microwave heating alone is offset by the large inward flux of energy near the mold walls associated with conventional heating. Hybrid heating provides the most uniform heating.
- 4. the dielectric characterization of the composite system as a function of glass content is determined.

Chapter six outlines suggestions for further development of the part-shaped applicator technology.

#### CHAPTER SIX

#### **RECOMMENDATIONS**

The advantages of hybrid heating in the part-shaped applicator have been demonstrated experimentally and theoretically. To fully realize the capabilities of this processing technique, however, methods of cycle time reduction should be investigated. Additionally, hardware modifications are required to improve coupling efficiency from the external applicator to the process material. Some hardware modifications have the potential to improve the heating uniformity as well. The remainder of this chapter presents concrete suggestions on achieving lower cycle times and attaining more efficient coupling and greater heating uniformity.

Because of material costs and mold and material preparation time, optimization should first be explored theoretically using the unsteady-state energy balance. Modeling may also provide additional insights with respect to the processing methods: conventional, microwave, and hybrid heating. Processing schedules should be determined to minimize cycle time while avoiding temperature excursions from the exothermic heat of reaction. Heat transfer, considering the heat of reaction and microwave source term, is defined as:

$$\rho C_{p} \frac{\partial T}{\partial t} = \nabla \cdot (k \nabla T) + (-r_{A})(-\Delta H_{Rxn}) + P_{MW}, \qquad [6.1]$$

where ρ is the material density [=] kg/m³,
C<sub>p</sub> is the material heat capacity [=] J/kg-K,
T is the material temperature [=] K,
t is time [=] s,
k is the material thermal conductivity [=] W/m-K,

-r<sub>A</sub> is the rate of reaction

 $[=] kg/m^3-s,$ 

 $-\Delta H_{Rx}$  is the heat of reaction

[=] J/kg, and

 $P_{MW}$  is the rate of microwave power absorption [=] W/m<sup>3</sup>.

For a non-isothermal, reacting system, equation [6.1] is a non-linear equation. The microwave power absorption is a function of the dielectric loss, which is strongly dependent on the polymer fractional conversion and temperature. The power absorption also depends on the E-field strength. As the dielectric properties change, the E-field is affected. The physical properties and reaction rate change with conversion and temperature. Solving equation [6.1] requires the knowledge of the E-field magnitude, the behavior of the dielectric loss and physical properties as a function of temperature and conversion, and a model of the reaction kinetics and microwave power absorption. These constitutive relationships should be developed, and the optimum cycle time for conventional, microwave, and hybrid heating should be determined.

Aside from thermal runaway due to the heat of reaction, another limitation in the reduction of the process cycle time is premature vitrification. As discussed in Section 1.2.2.2, Boey and Yue<sup>67</sup> demonstrate the importance of engineering a proper microwave power cycle. Curing DGEBA/DDS on glass substrates for several microwave power levels over a range of radiation times, they demonstrated that the shear strength is highly dependent on the processing cycle. For the microwave powers investigated, the maximum shear strength increased with power. At higher power levels, longer irradiation times resulted in a sharp drop of the shear strength due to premature vitrification. Thermosetting polymers must undergo gelation before vitrification to realize optimum physical properties. Thermal runaway is more likely than premature

vitrification when processing thermosets with thick cross-sections. However, physical properties should be tested for each run with the part-shaped cavity to verify this assumption.

Implementing a larger microwave power source will be required for the optimum cure cycle. The post-cure temperature of 200°C for the glass-reinforced DGEBA/DDS system could not be attained for the run with microwave heating with the 120W power source. This could partially be attributed to the decrease in the dielectric loss with conversion, as excellent coupling was realized between microwave energy and resin with low conversion. At greater fractional conversions, the composite temperatures became less sensitive to microwave power input. A larger microwave power source would provide faster control of energy input for the low loss material.

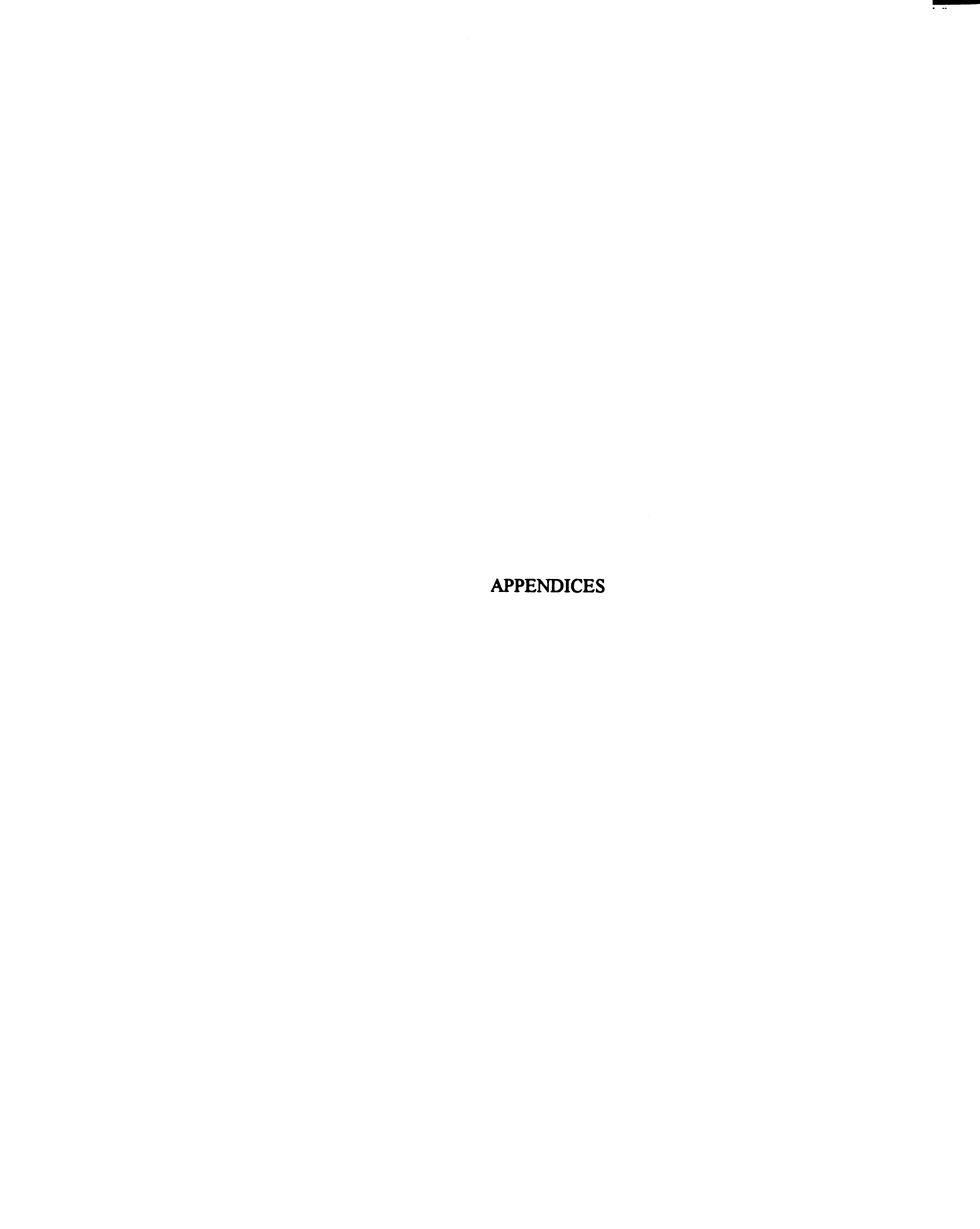
With the current laboratory setup, the external applicators are oriented to excite the TE<sub>01</sub> mode in the cavity. The applicators should be rotated 90° to excite the dominant mode, TE<sub>10</sub>. For the rectangular waveguide, greater penetration depths and smaller wavelengths are feasible with lower order modes. Figure 4.15 illustrates the smaller wavelength of the TE<sub>10</sub> mode relative to the TE<sub>01</sub> mode. By reducing the distance between regions of high E-field intensity, the axial temperature gradients can be reduced. Using a waveguide applicator, Outifa et al. <sup>88</sup> discovered that exciting higher order modes resulted in an uncontrollable energy distribution of hybrid modes.

To date, the development of the part-shaped cavity boasts great potential for cycle time reduction and improved heating uniformity in industrial applications.

However, the experiments have been performed in a parallelopipedic mold. The next

phase of the development should be focused on applying the part-shaped applicator concept to a commercial part with a degree of complexity (e.g., curvature, varying thickness, etc.). Issues of E-field propagation, such as internal reflection and hot spots, in unconventional waveguides should be investigated.

By performing a preliminary economic estimate, Akyel and Bilgen<sup>89</sup> determined that the product costs of microwave curing of polymers and vulcanization of rubber could be reduced by 6 to 23%, depending on the production rate. A more detailed economic evaluation of the part-shaped applicator process should be performed for comparison to the conventional process. Because of the external applicators and the microwave circuitry, microwave tooling will require a greater initial capital investment. However, a smaller total product cost per unit for the part-shaped applicator technology may be attainable due to the feasible increased production rate.



### APPENDIX A

# **VECTOR WAVE EQUATION DEVELOPMENT**

Maxwell's equations in complex phasor form are given by

$$\nabla \times \vec{\mathbf{E}}(\vec{\mathbf{r}}) = -j\omega \vec{\mathbf{B}}(\vec{\mathbf{r}}) \tag{A.1}$$

$$\nabla \times \vec{\mathbf{H}}(\vec{\mathbf{r}}) = \vec{\mathbf{J}}(\vec{\mathbf{r}}) + j\omega \vec{\mathbf{D}}(\vec{\mathbf{r}})$$
 [A.2]

$$\nabla \cdot \vec{\mathbf{D}}(\vec{\mathbf{r}}) = \rho(\vec{\mathbf{r}}) \tag{A.3}$$

$$\nabla \cdot \vec{\mathbf{B}}(\vec{\mathbf{r}}) = 0 \tag{A.4}$$

where  $\vec{E}$  = electric field strength [=] volt/m,  $\vec{B}$  = magnetic flux density [=] weber/m<sup>2</sup>,  $\vec{H}$  = magnetic field intensity [=] ampere/m,  $\vec{J}$  = volume current density [=] ampere/m<sup>2</sup>,  $\vec{D}$  = electric flux density [=] coulomb/m<sup>2</sup>,  $\rho$  = volume charge density [=] coulomb/m<sup>3</sup>, j = imaginary number,  $\sqrt{-1}$ , and  $\omega$  = angular frequency (=2 $\pi$ f) [=] radians/s.

In complex phasor form, a vector is represented as

$$\vec{A}(\vec{r},t) = \text{Re}\left[\vec{A}(\vec{r})e^{j\omega t}\right].$$
 [A.5]

In this development, we will assume that the system is source-free.

$$\rho = \mathbf{J} = 0 \tag{A.6}$$

We will also assume that the system is composed of simple, homogeneous material.

Therefore, the electric and magnetic flux density vectors can be expressed as

$$\vec{\mathbf{D}}(\vec{\mathbf{r}}) = \mathbf{\varepsilon}^* \vec{\mathbf{E}}(\vec{\mathbf{r}}) \tag{A.7}$$

$$\vec{\mathbf{B}}(\vec{\mathbf{r}}) = \mu_0 \vec{\mathbf{H}}(\vec{\mathbf{r}}) \tag{A.8}$$

where  $\epsilon^* = \text{complex permittivity} (\epsilon_o[\epsilon' - j\epsilon''])$  [=] farad/m,

 $\varepsilon'$  = dielectric constant,

 $\varepsilon''$  = dielectric loss,

 $\epsilon_0$  = permittivity of free space, 8.85 x  $10^{-12}$  farad/m, and  $\mu_0$  = permeability of free space, 1.26 x  $10^{-6}$  henry/m.

# Combining Equations [A.1] through [A.8] yields the following:

$$\nabla \times \vec{\mathbf{E}} = -j\omega \mu_0 \vec{\mathbf{H}} \tag{A.9}$$

$$\nabla \times \vec{\mathbf{H}} = \mathbf{j}\omega \mathbf{e}^* \vec{\mathbf{E}}$$
 [A.10]

$$\nabla \cdot \left( \mathbf{\epsilon}^* \mathbf{\vec{E}} \right) = 0 \tag{A.11}$$

$$\nabla \cdot \left( \mu_0 \vec{\mathbf{H}} \right) = 0 \tag{A.12}$$

For isotropic media,

$$\nabla \cdot \vec{\mathbf{E}} = 0 \text{ and}$$
 [A.13]

$$\nabla \cdot \vec{\mathbf{H}} = 0. \tag{A.14}$$

Curling equation [A.9] gives

$$\nabla \times \nabla \times \vec{\mathbf{E}} = -j\omega \mu_0 \nabla \times \vec{\mathbf{H}}$$
 [A.15]

which when combined with equation [A.10] gives

$$\nabla \times \nabla \times \vec{\mathbf{E}} = -j\omega \mu_0 (j\omega \varepsilon^* \vec{\mathbf{E}}) = \omega^2 \varepsilon^* \mu_0 \vec{\mathbf{E}}.$$
 [A.16]

Using a vector identity, [A.16] can be rewritten as

$$\nabla \times \nabla \times \vec{\mathbf{E}} = \nabla (\nabla \cdot \vec{\mathbf{E}}) - \nabla^2 \vec{\mathbf{E}} = \omega^2 \varepsilon^* \mu_0 \vec{\mathbf{E}}.$$
 [A.17]

Combining [A.13] with [A.17] yields

$$\nabla^2 \vec{\mathbf{E}} + \omega^2 \varepsilon^* \mu_0 \vec{\mathbf{E}} = 0.$$
 [A.18]

Similar step can be taken to express the magnetic field intensity in the vector wave equation form. For example, curling equation [A.10] gives

$$\nabla \times \nabla \times \vec{\mathbf{H}} = \mathbf{j} \omega \mathbf{\epsilon}^* \nabla \times \vec{\mathbf{E}} . \tag{A.19}$$

Substituting equation [A.9] results in

$$\nabla \times \nabla \times \vec{\mathbf{H}} = j\omega \epsilon^{\bullet} (-j\omega \mu_0 \vec{\mathbf{H}})$$
 [A.20]

which can be reexpressed as

$$\nabla \times \nabla \times \vec{\mathbf{H}} = \nabla (\nabla \cdot \vec{\mathbf{H}}) - \nabla^2 \vec{\mathbf{H}} = \omega^2 \varepsilon^* \mu_0 \vec{\mathbf{H}}.$$
 [A.21]

Using equation [A.14] in equation [A.21] gives

$$\nabla^2 \hat{\mathbf{H}} + \omega^2 \varepsilon^* \mu_0 \hat{\mathbf{H}} = 0.$$
 [A.22]

Equations [A.18] and [A.22] are the vector wave equations for the electric field intensity and magnetic field intensity, respectively. These equations are second order, homogeneous, partial differential equations. The solution is outlined in the following section.

#### APPENDIX B

# **SOLUTION TO VECTOR WAVE EQUATIONS**

One can reduce equations [A.18] and [A.22] to

$$\nabla^2 \vec{\mathbf{E}} + \mathbf{k}^2 \vec{\mathbf{E}} = 0 \tag{B.1}$$

$$\nabla^2 \vec{\mathbf{H}} + \mathbf{k}^2 \vec{\mathbf{H}} = 0$$
 [B.2]

by letting k, the complex wavenumber, be represented as follows

$$\mathbf{k} = \omega \sqrt{\varepsilon_0 (\varepsilon' - j\varepsilon'') \mu_0} . \tag{B.3}$$

A scalar counterpart to equations [B.1] and [B.2] can be written as

$$\nabla^2 \Psi + \mathbf{k}^2 \Psi = 0. \tag{B.4}$$

For the TE modes in Cartesian coordinates<sup>90</sup>, the E-field and H-field components are:

$$E_x = -\frac{\partial \Psi}{\partial y} \qquad \qquad H_x = \frac{1}{j\omega\mu_0} \frac{\partial^2 \Psi}{\partial x \partial z}$$

$$E_{y} = \frac{\partial \Psi}{\partial x} \qquad \qquad H_{y} = \frac{1}{j\omega\mu_{0}} \frac{\partial^{2}\Psi}{\partial y\partial z}$$
 [B.5]

$$\mathbf{E}_{z} = 0 \qquad \qquad \mathbf{H}_{z} = \frac{1}{j\omega\mu_{0}} \left( \frac{\partial^{2}}{\partial z^{2}} + \mathbf{k}^{2} \right) \Psi$$

Therefore, a solution to [B.4] can indirectly give a solution to the E-field and H-field components.

Because of linearity,

$$\Psi(x,y,z) = X(x)Y(y)Z(z)$$
 [B.6]

Expanding [B.4] gives

$$\nabla^2 \Psi + \mathbf{k}^2 \Psi = \frac{\partial^2 \Psi}{\partial \mathbf{x}^2} + \frac{\partial^2 \Psi}{\partial \mathbf{y}^2} + \frac{\partial^2 \Psi}{\partial \mathbf{z}^2} + \mathbf{k}^2 \Psi = 0.$$
 [B.7]

Substituting [B.6] into [B.7] and dividing by XYZ yields

$$\frac{1}{X}\frac{d^2X}{dx^2} + \frac{1}{Y}\frac{d^2Y}{dy^2} + \frac{1}{Z}\frac{d^2Z}{dz^2} + k^2 = 0.$$
 [B.8]

The wavenumber can be represented as a linear combination of contributions from each Cartesian direction as

$$k^2 = k_x^2 + k_y^2 + k_z^2$$
. [B.9]

Therefore, equation [B.8], after expanding and collecting terms, is

$$\left(\frac{1}{X}\frac{d^2X}{dx^2} + k_x^2\right) + \left(\frac{1}{Y}\frac{d^2Y}{dy^2} + k_y^2\right) + \left(\frac{1}{Z}\frac{d^2Z}{dz^2} + k_z^2\right) = 0.$$
 [B.10]

Setting each of these three terms equal to zero would be a solution.

$$\frac{d^2X}{dx^2} + k_x^2 X = 0$$
 [B.11]

$$\frac{\mathrm{d}^2 Y}{\mathrm{d} y^2} + k_y^2 Y = 0$$
 [B.12]

$$\frac{\mathrm{d}^2 Z}{\mathrm{d}z^2} + k_z^2 Z = 0$$
 [B.13]

The solutions to equations [B.11] through [B.13] depends on the physical system. For a positive z traveling wave in a waveguide with conductive boundaries, Equation [B.6] becomes

$$\Psi = C_1 \cos(k_x x) \cos(k_y y) \exp(-jk_z z)$$
 [B.14]

where  $C_{I}$  is a constant.

According to equation [B.5],

$$E_x = C_1 k_v \cos(k_x x) \sin(k_v y) \exp(-jk_z z)$$
 [B.15]

$$E_y = -C_1 k_x \sin(k_x x) \cos(k_y y) \exp(-jk_z z)$$
 [B.16]

$$\mathbf{E}_{\mathbf{z}} = \mathbf{0} \tag{B.17}$$

For a conductive waveguide with an x-length of a and a y-length of b, the boundary condition of zero tangential E-field results in

$$k_x = \left(\frac{m\pi}{a}\right)$$
 and [B.18]

$$\mathbf{k}_{y} = \left(\frac{\mathbf{n}\pi}{\mathbf{h}}\right)$$
 [B.19]

Therefore, according to equation [B.3] and [B.9],

$$\omega^{2} \varepsilon_{0} \mu_{0} (\varepsilon' - j\varepsilon'') = \left(\frac{m\pi}{a}\right)^{2} + \left(\frac{n\pi}{b}\right)^{2} + k_{z}^{2} \quad \text{or}$$
 [B.20]

$$k_z = \sqrt{\omega^2 \varepsilon_0 \mu_0 (\varepsilon' - j\varepsilon'') - \left(\frac{m\pi}{a}\right)^2 - \left(\frac{n\pi}{b}\right)^2}.$$
 [B.21]

Equation [B.21] is of the form  $\sqrt{R+jI}$ , which can be separated into real and imaginary components as shown below

$$\sqrt{R+jI} = \frac{\pm 1}{\sqrt{2}} \sqrt{\left(R^2 + I^2\right)^{1/2} + R} \pm j \frac{1}{\sqrt{2}} \sqrt{\left(R^2 + I^2\right)^{1/2} - R} = A - jB \quad [B.22]$$

where 
$$R = \omega^2 \epsilon_0 \mu_0 \epsilon' - \left(\frac{m\pi}{a}\right)^2 - \left(\frac{n\pi}{b}\right)^2$$
 [B.23]

$$I = -\omega^2 \varepsilon_0 \mu_0 \varepsilon''$$
 [B.24]

$$A = \frac{\pm 1}{\sqrt{2}} \sqrt{(R^2 + I^2)^{\frac{1}{2}} + R}$$
 [B.25]

$$B = \frac{\mp 1}{\sqrt{2}} \sqrt{(R^2 + I^2)^{1/2} - R} \text{ and } [B.26]$$

$$\mathbf{k}_{\bullet} = \mathbf{A} - \mathbf{j}\mathbf{B}. \tag{B.27}$$

The exponential contributions of equations [B.15] and [B.16] now become

$$\exp(-jk_zz) = \exp(-j[A - jB]z) = \exp(-Bz - jAz).$$
 [B.28]

According to Euler's theorem,

$$\exp(jx) = \cos(x) - j \sin(x), \qquad [B.29]$$

Equation [B.28] can be rewritten as

$$\exp(-Bz - jAz) = \exp(-Bz)[\cos(-Az) + j \sin(-Az)].$$
 [B.30]

Therefore, the E-field components can be written as

$$E_{x} = C_{I} \left(\frac{m\pi}{a}\right) \cos\left(\frac{m\pi}{a}x\right) \sin\left(\frac{n\pi}{b}y\right) \cos(-Az) \exp(-Bz)$$
 [B.31]

$$E_{y} = C_{I} \left(\frac{m\pi}{a}\right) \sin\left(\frac{m\pi}{a}x\right) \cos\left(\frac{n\pi}{b}y\right) \cos(-Az) \exp(-Bz) \text{ and } [B.32]$$

$$E_z = 0$$
. [B.33]

To complete the representation, the E-field in vector notation in Cartesian coordinates is represented with the above components as

$$\vec{E}(\vec{r}) = E_x \underline{e}_x + E_y \underline{e}_y + E_z \underline{e}_z.$$
 [B.34]

### APPENDIX C

#### POWER PENETRATION DEPTH CALCULATION

The power penetration depth is defined as the distance through a dielectric material through which the microwave power is reduced by 1/e (~36.8%). According to Poynting's theorem, the microwave power absorption is directly proportional to the square of E-field intensity or

$$\langle \mathbf{P} \rangle \sim \left| \vec{\mathbf{E}} \right|^2$$
. [C.1]

As shown in Appendix B, the dependence of the E-field on the direction of propagation, the z-direction, is given by

$$\left|\vec{E}\right|^2 \sim \exp(-2Bz). \tag{C.2}$$

Therefore, the distance through which the square of the E-field is attenuated to 1/e is given by

$$z = D_p = \frac{1}{2B}, \qquad [C.3]$$

or

$$D_{p} = \frac{1}{2\frac{1}{\sqrt{2}}\sqrt{(R^{2} + I^{2})^{1/2} - R}} = \frac{1}{\sqrt{2R(\sqrt{1 + (I/R)^{2}} - 1)}}$$
 [C.4]

where R and I are given by [B.23] and [B.24].

# APPENDIX D

# **CUTOFF FREQUENCY**

The cutoff frequency,  $f_c$ , in a lossy waveguide is the frequency below which electromagnetic energy does not propagate. Setting the power penetration depth equal to zero is one method of calculating  $f_c$ .

$$\frac{1}{\sqrt{2R(\sqrt{1+(I/R)^2}-1)}}=0$$
 [D.1]

Equation [D.1] is satisfied if R approaches zero. According to this condition and equation [B.23], the cutoff frequency in the lossy waveguide is given by

$$f_{c} = \frac{1}{2} \frac{1}{\sqrt{\epsilon_{0} \mu_{0} \epsilon'}} \sqrt{\left(\frac{m}{a}\right)^{2} + \left(\frac{n}{b}\right)^{2}}.$$
 [D.2]

### APPENDIX E

## **GUIDED WAVELENGTH**

Examination of Equations [B.31] and [B.32] can provide an expression of the wavelength in the part-shaped applicator. The cosine functions dictate the wavelength in the Z-direction, so the wavelength can be written as:

$$\lambda_{s} = \frac{2\pi}{A} = \frac{2\sqrt{2}\pi}{\sqrt{(R^{2} + I^{2})^{1/2} + R}}$$
 [E.1]

where R and I are given by [B.23] and [B.24].

For a low-loss system where the contribution from  $\varepsilon''$  is insignificant, I can be neglected to give:

$$\lambda_{s} = \frac{2\pi}{\sqrt{R}} = \frac{2\pi}{\sqrt{\omega^{2} \varepsilon_{o} \mu_{o} \varepsilon' - \left(\frac{m\pi}{a}\right)^{2} - \left(\frac{n\pi}{b}\right)^{2}}}$$
 [E.2]

Several algebraic manipulations yield the following:

$$\lambda_{\mathbf{g}} = \frac{\frac{2\pi}{\omega} \frac{1}{\sqrt{\epsilon_{o}\mu_{o}}} \frac{1}{\sqrt{\epsilon'}}}{\sqrt{1 - \frac{1}{\omega^{2}\epsilon_{o}\mu_{o}\epsilon'} \left[ \left( \frac{m\pi}{\mathbf{a}} \right)^{2} + \left( \frac{n\pi}{\mathbf{b}} \right)^{2} \right]}}.$$
 [E.3]

Substituting for the cutoff frequency, source frequency, and the speed of light gives:

$$\lambda_{g} = \frac{\frac{c}{f\sqrt{\epsilon'}}}{\sqrt{1 - \frac{\left(2\pi f_{c}\right)^{2}}{\left(2\pi f\right)^{2}}}} = \frac{\lambda}{\sqrt{1 - \left(\frac{f_{c}}{f}\right)^{2}}},$$
[E.4]

which is a common expression given in the literature, where  $\lambda$  is the wavelength in the infinite dielectric medium,  $f_c$  is the cutoff frequency of the waveguide, and f is the source frequency.

### APPENDIX F

### **UNSTEADY-STATE ENERGY BALANCE DEVELOPMENT**

A heat transfer model is developed to determine the temperature profiles characteristic of the three types of heating investigated for this project: conventional, microwave, and hybrid. The heat transfer model also assists in the interpretation of the heating patterns of the polymer plates, as recorded by thermal paper.

A general energy balance around an arbitrary homogeneous system is given by:

$$\rho C_{p} \frac{\partial T}{\partial t} = \nabla \cdot (k \nabla T) + P_{MW} + S_{Rxn}, \qquad [F.1]$$

where  $\rho$  = the material density [=] kg/m³,  $C_p$  = the material heat capacity [=] J/kg-K, T = the material temperature [=] K, t = time [=] s, k = the material thermal conductivity [=] W/m-K,  $P_{MW}$  = the rate of microwave power absorption [=] W/m³, and  $S_{Rxm}$  = the reaction source term [=] W/m³.

Assuming an isotropic thermal conductivity and non-reactive material, Equation [F.1] can be reduced to

$$\frac{\partial \mathbf{T}}{\partial t} = \alpha \nabla^2 \mathbf{T} + \frac{1}{\rho C_p} \mathbf{P}_{MW}, \qquad [F.2]$$

where  $\alpha$  is the material thermal diffusivity.

Employing the Crank-Nicolson method of finite differences to Equation [F.2] yields the following expression:

$$-\beta T_{i-1,n+1} + (1+2\beta)T_{i,n+1} - \beta T_{i+1,n+1} = \beta T_{i-1,n} + (1-2\beta)T_{i,n} + \beta T_{i+1,n+1} + \frac{\Delta t}{\rho C_p} P_{MW},$$
[F.3]

where i is the spacial index, n is the time index,

$$\beta = \frac{\alpha \Delta t}{2(\Delta x)^2},$$

 $\Delta t = time step, and$ 

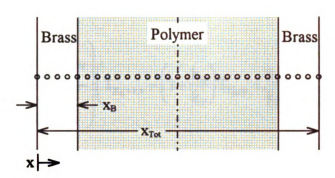
 $\Delta x = spacial increment.$ 

This expression approximates the heat transfer for the interior nodes in the polymer. The microwave power absorption in the brass is negligible; therefore, heat transfer in the brass for the interior nodes can be approximated by Equation [F.3] minus the term defining microwave power absorption.

The nodes at or neighboring the boundaries require special treatment according to the specified boundary conditions, as outlined in Figure F.1. Implementing the convective heat transfer boundary condition at the first node gives the following finite difference expression:

$$\left(\frac{h\Delta x}{k_{\rm B}}+1\right)T_{1_{\rm a+1}}-T_{2,\rm n+1}=\frac{h\Delta xT_{\rm o}}{k_{\rm B}},$$
 [F.4]

where h is the convective heat transfer coefficient and  $k_{\rm B}$  is the brass thermal conductivity.



#### **Boundary Conditions**

1.) Free convection at brass boundaries -

$$-k_{B}\frac{\partial T}{\partial x}\Big|_{x=0} = h[T_{\infty} - T(0,t)]$$

2.) Symmetry about the midplane -

$$\left. \frac{\partial T}{\partial x} \right|_{x = \frac{1}{2} x_{\text{Tot}}} = 0$$

3.) Equal heat fluxes at brass-polymer interface -

$$-k_{\rm B}\frac{\partial T}{\partial x}\bigg|_{x=x_{\bar{\bf h}}} = -k_{\rm P}\frac{\partial T}{\partial x}\bigg|_{x=x_{\bar{\bf h}}}$$

Figure F.1. Boundary Conditions of the One-Dimensional Heat Transfer Model.

Based on the boundary condition of equal heat fluxes between two distinct media, Carnahan et al.<sup>91</sup> developed the expression for the interfacial temperature. The explicit form of this temperature is

$$T_{X_{B,n+1}} = T_{X_{B,n}} + \left(\frac{2\frac{\Delta t}{(\Delta x)^{2}}\alpha_{B}}{\frac{\alpha_{B}}{\alpha_{P}} + \frac{k_{B}}{k_{P}}}\right) \left(T_{X_{B+1,n}} - \left(1 + \frac{k_{B}}{k_{P}}\right)T_{X_{B,n}} + \frac{k_{B}}{k_{P}}T_{X_{B-1,n}}\right)$$
[F.5]

where  $T_{x_n}$  = the interfacial temperature, sub P = polymer physical property, and sub B = brass physical property.

The final boundary condition to apply is the adiabatic condition, which can be applied due to symmetry. Exploiting symmetry increases the program efficiency by cutting the number of calculations in half.

The finite difference equations of the entire system form a tridiagonal matrix.

Solution to this matrix is attained by the Thomas algorithm<sup>92</sup>. The FORTRAN code for the heat transfer model is shown in the following section.

# APPENDIX G

# FORTRAN CODE FOR HEAT TRANSFER MODEL

CCCC	CCCCCCCC	CCCCCCCCCCCCCCCCCCCCCCCCCCCCCCCCCCCCCCC	CCC	CC
C Pro	gram Description	on: Unsteady-state heat conduction in a one-dimension	onal	C
C poly	mer slab with l	brass boundaries and constant microwave power inpu	t to	C
	ymer slab.			C
CCCC	CCCCCCCC	CCCCCCCCCCCCCCCCCCCCCCCCCCCCCCCCCCCCCCC	CCC	CC
C Va	riable Explanati	ions	C	
C			C	
C	A	sub-diagonal coefficient to the tridiagonal matrix	C	
C	ALPHAB	brass thermal diffusivity [=] m <sup>2</sup> /s	C	
C	ALPHAP	polymer thermal diffusivity [=] m <sup>2</sup> /s	C	
C	В	diagonal coefficient to the tridiagonal matrix	C	
C	C	super-diagonal coefficient to the tridiagonal matrix	C	
C	CPB	brass heat capacity [=] J/kg-K	C	
C	CPP	polymer heat capacity [=] J/kg-K	C	
C	D	constant vector	C	
C	DT	time step [=] s	C	
C	DX	interval length [=] m	C	
C	H	convective heat transfer coefficient [=] W/m <sup>2</sup> -K	C	
C	<b>ICOUNT</b>	counting variable	C	
C	<b>IPRINT</b>	printing frequency	C	
C	KB	brass thermal conductivity [=] W/m-K	C	
C	KP	polymer thermal conductivity [=] W/m-K	C	
C	NIB	number of intervals in the brass	C	
C	NIP	number of intervals in the polymer	C	
C	NN	total number of nodes	C	
C	<b>PMW</b>	microwave power absorption [=] W/m <sup>3</sup>	C	
C	RATIOP	polymer constant	C	
C	RATIOB	brass constant	C	
C	RHOB	brass density [=] kg/m <sup>3</sup>	C	
C	RHOP	polymer density [=] kg/m <sup>3</sup>	C	
C	STORE	dummy storage variable	C	
C	T	temperature array [=] K	C	
C	TIME	simulation time [=] s	C	
C	TINF	ambient temperature [=]°C	C	
C	<b>TMAX</b>	maximum center temperature to be computed [=]°C	C	
C	T0	initial system temperature [=] °C, K	C	
C	TOLD	temperature of previous time step [=] K	C	
C	X	x-position [=] m	C	

```
C
                thickness of the polymer [=] cm, m
     XP
PROGRAM 1DHX
* VARIABLE DEFINITIONS
     DIMENSION X(100),A(100),B(100),C(100),D(100),T(100)
     REAL*8 DT, TMAX, RATIOP, RATIOB, DX, H, TINF, TIME, PMW,
     KP,RHOP, CPP,KB,RHOB,CPB,T0,ALPHAB,ALPHAP,TOLD,A,B,
&
&
     C,D,T,XP
     INTEGER NIP, NIB, NN, IPRINT, ICOUNT
     CHARACTER*80 STORE
* INPUT DATA/COMPUTE CONSTANTS
     OPEN(UNIT=21,STATUS='OLD',FILE='1DHX.DAT')
     OPEN(UNIT=22,STATUS='UNKNOWN',FILE='1DTDATA.DAT')
     READ(21,101) RHOP, CPP, KP, RHOB, CPB, KB, XP, T0, TINF, H, PMW,
&
     DT,TMAX,NIP,NIB,IPRINT
     ALPHAP = KP/(RHOP*CPP)
     ALPHAB = KB/(RHOB*CPB)
     XP = (XP/200.0)
     DX = XP/NIP
     RATIOP = DT*ALPHAP/(2.0*DX**2)
     RATIOB = DT*ALPHAB/(2.0*DX**2)
     TINF = TINF + 273.15
     T0 = T0 + 273.15
     TMAX = TMAX + 273.15
     NN = NIB + NIP + 1
     WRITE(22,102)
     REWIND(21)
     READ(21,7) STORE
     READ(21,7) STORE
     DO 20 I = 1,100
           READ(21,7,END=25) STORE
           WRITE(22,7) STORE
```

20

CONTINUE

```
25
      CONTINUE
   COMPUTE COEFFICIENTS
      B(1) = H^*DX/KB + 1.0
      C(1) = -1.0
      D(1) = H*DX*TINF/KB
      DO 30 I = 2, NIB-1
            A(I) = -1.0*RATIOB
            B(I) = 1.0 + 2.0*RATIOB
            C(I) = -1.0*RATIOB
30
      CONTINUE
      A(NIB) = -1.0*RATIOB
      B(NIB) = (1.0+2.0*RATIOB)
      B(NIB+2) = 1.0 + 2.0*RATIOP
      C(NIB+2) = -1.0*RATIOP
      DO 40 I = (NIB+2),(NIB+NIP)
            A(I) = -1.0*RATIOP
            B(I) = 1.0 + 2.0*RATIOP
            C(I) = -1.0*RATIOP
40
      CONTINUE
      A(NN) = -2.0*RATIOP
      B(NN) = 1.0 + 2.0*RATIOP
* SET BOUNDARY CONDITIONS & INITIALIZE TEMPERATURE ARRAY
      DO 50 I = 1,NN
            X(I) = (I-1.0)/(NIB+NIP)
            T(I) = T0
50
      CONTINUE
      TIME = 0.0
      WRITE(22,103) TIME/60.0
      DO 60 I = 1,NN
            WRITE(22,104) X(I),T(I)-273.15
60
      CONTINUE
```

```
* COMPUTE TEMPERATURES - MAIN LOOP
     ICOUNT = 0
70
     CONTINUE
     TIME = TIME + DT
     ICOUNT = ICOUNT + 1
   BRASS
     TOLD = T(NIB+1)
     T(NIB+1) = TOLD + ((2.0*ALPHAB*DT/(DX*DX))/
     (ALPHAB/ALPHAP + KB/KP))*(T(NIB+2)-(1.0+KB/KP)*
&
&
     T(NIB+1) + (KB/KP)*T(NIB))
     DO 80 I = 2,(NIB-1)
           D(I) = RATIOB*T(I-1) + (1.0-2.0*RATIOB)*T(I) +
&
           RATIOB*T(I+1)
80
     CONTINUE
     D(NIB) = RATIOB*T(NIB-1) + (1.0-2.0*RATIOB)*T(NIB) +
     RATIOB*TOLD + RATIOB*T(NIB+1)
&
     CALL TRIDAG(1,NIB,A,B,C,D,T)
   POLYMER
     D(NIB+2) = RATIOP*T(NIB+1) + RATIOP*TOLD +
&
     (1.0-2.0*RATIOP)*T(NIB+2) + RATIOP*T(NIB+3) +
&
     DT*PMW/(RHOP*CPP)
     DO 90 I = (NIB+3),(NIB+NIP)
           D(I) = RATIOP*T(I-1) + (1.0-2.0*RATIOP)*T(I) +
&
           RATIOP*T(I+1) + DT*PMW/(RHOP*CPP)
90
     CONTINUE
     D(NN) = 2.0*RATIOP*T(NN-1) +
&
     (1.0-2.0*RATIOP)*T(NN) + DT*PMW/(RHOP*CPP)
     CALL TRIDAG(NIB+2,NN,A,B,C,D,T)
     IF(ICOUNT.GE.IPRINT)THEN
```

```
WRITE(22,103) TIME/60.0
            DO 100 I = 1,NN
                   WRITE(22,104) X(I),T(I)-273.15
100
            CONTINUE
            ICOUNT = 0
      ENDIF
      IF(T(NN).LE.TMAX) GOTO 70
* FORMAT STATEMENTS
7
      FORMAT(A)
101
      FORMAT(7(/),F8.2,//,F8.2,//,F8.5,4(/),F8.2,//,F8.2,//,F8.5,6(/),
&
      F8.2,//,F8.2,//,F8.2,//,F8.3,//,F12.2,6(/),F9.5,//,F8.2,//,I3,//,
&
      I3,//,I10)
      FORMAT('Output Data for 1DMW.FOR',/,'-----')
102
      FORMAT(' ','TIME (MIN) = ',F9.1)
103
104
      FORMAT(F5.3,2X,F6.1)
STOP
END
SUBROUTINE TRIDAG(IF,L,A,B,C,D,V)
      DIMENSION A(100),B(100),C(100),D(100),V(100),BETA(100),
&
      GAMMA(100)
      REAL*8 A,B,C,D,V,BETA,GAMMA
      BETA(IF) = B(IF)
      GAMMA(IF) = D(IF)/BETA(IF)
      \mathbf{IFP1} = \mathbf{IF} + \mathbf{1}
      DO 200 I = IFP1,L
            BETA(I) = B(I)-A(I)*C(I-1)/BETA(I-1)
            GAMMA(I) = (D(I)-A(I)*GAMMA(I-1))/BETA(I)
200
      CONTINUE
      V(L) = GAMMA(L)
      LAST = L-IF
      DO 210 \text{ K} = 1.\text{LAST}
            I = L-K
             V(I) = GAMMA(I) - C(I)*V(I+1)/BETA(I)
210
      CONTINUE
RETURN
END
```

#### Input Data for 1DHX.FOR

# Physical Constants

## Polymer

Density [=] kg/m<sup>3</sup>

1100.0

Heat Capacity [=] J/kg-K

2000.0

Thermal Conductivity [=] W/m-K

2.0

#### **Brass**

Density [=] kg/m<sup>3</sup>

8500.0

Heat Capacity [=] J/kg-K

380.0

Thermal Conductivity [=] W/m-K

110.0

### **Physical System Definition**

Polymer Thickness [=] cm

8.9

Initial System Temperature [=] °C

25 0

Ambient Temperature [=] °C

25.0

Convective Heat Transfer Coefficient [=] W/m<sup>2</sup>-K

5.0

Microwave Power Absorption [=] W/m<sup>3</sup>

2000000.0

#### Finite Difference Parameters

Time Step [=] s

0.1

Maximum Center Temperature to be Computed [=] C

200.0

Number of X-Direction Intervals in the Polymer

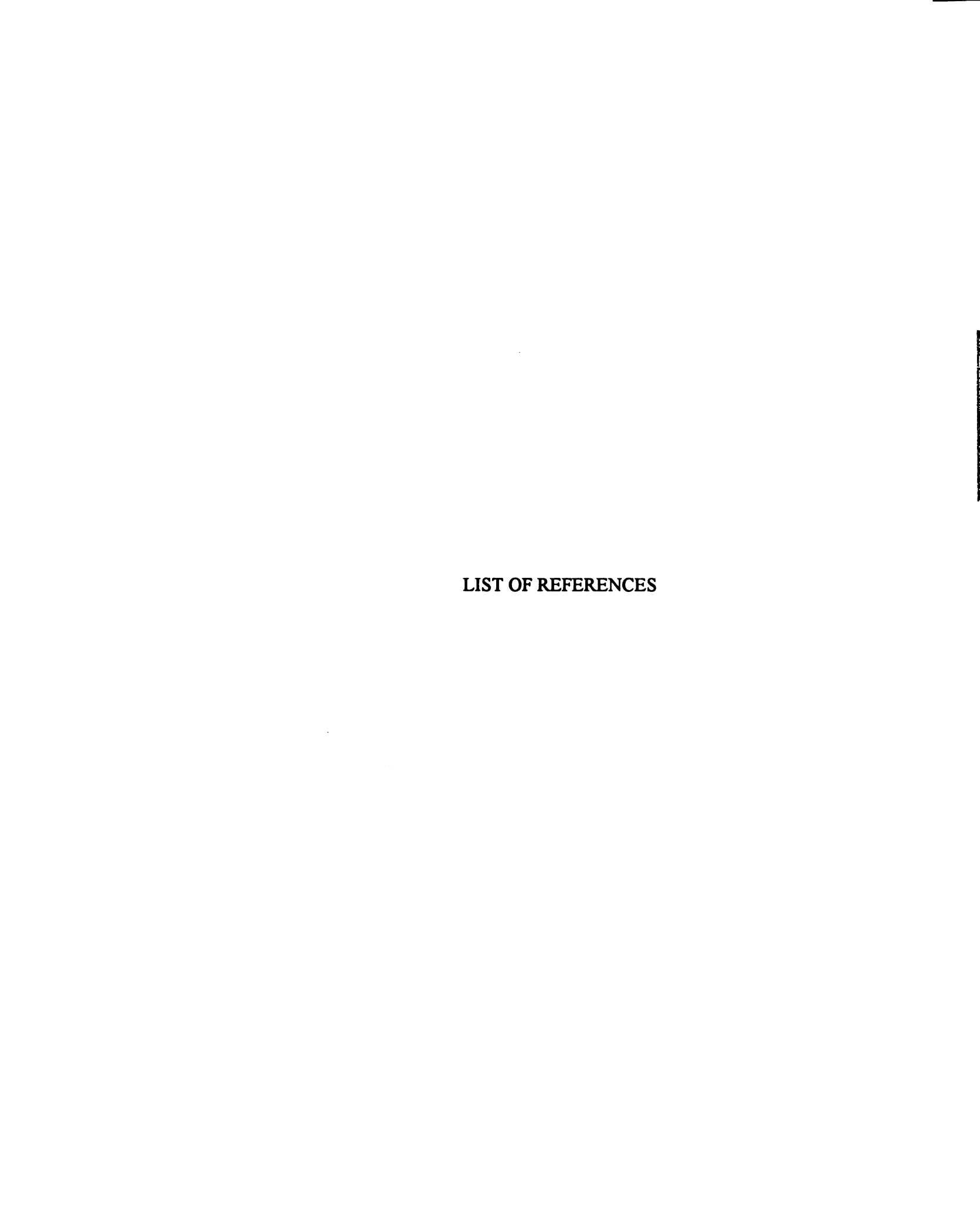
25

Number of X-Direction Intervals in the Brass

7

**Solution Printing Frequency** 

300



#### LIST OF REFERENCES

- 1. Osepchuk J.M., "A History of Microwave Heating Applications", *IEEE Trans Microwave Theory and Tech*, 32(9), pp. 1200-1221 (1984)
- 2. Metaxas A.C., and Meredith R.J. <u>Industrial Microwave Heating</u>, London, U.K.: Peter Peregrinus, Ltd., p. 282, 1983
- 3. Wei J.B., Shidaker T.A., and Hawley M.C., "Recent Progress in Microwave Processing of Polymers and Composites", *Trends in Polymer Science*, 4(1), pp. 18-24 (1996)
- 4. Lewis D.A., and Shaw J.M., "Recent Developments in the Microwave Processing of Polymers", *Mater Res Bull*, pp. 37-40 (November 1993)
- 5. Shidaker T.A., Hawley M.C., and Asmussen J., "Characterization of Microwave Heating Patterns in a Part-Shaped Mold", *Proceedings. 27th International SAMPE Symposium*, 27, pp. 216-226 (1995)
- 6. Hottong U., Wei J., Dhulipala R., and Hawley M.C., "Microwave Processing of Polyester and Polyester/Glass Composites", *Microwaves: Theory and Application in Materials Processing. Am Cer Soc Trans*, 21, (eds. Clark D.E., Gac F.D., and Sutton W.H.), pp. 587-594 (1991)
- 7. Paulauskas F.L., and Meek T.T., "Processing of Thermoset Prepreg Laminates via Exposure to Microwave Radiation", *Mater Res Soc Symp Proc*, 347, pp. 743-751 (1994)

- 8. Boey F.Y.C., and Lye S.W., "Void Reduction in Autoclave Processing of Thermoset Composites; Part 2: Void Reduction in a Microwave Curing Process", CPSOA, 23(4), pp. 266-270 (1992)
- 9. Methven J.M., "Microwave Heating in the Manufacture of Composites", Materials Technology, 9(7/8), pp. 163-165 (1994)
- 10. Sutton W.H., "Microwave Processing of Materials", *Mater Res Bull*, pp. 22-24 (November 1993)
- 11. Mijovic J., and Wijaya J., "Review of Cure of Polymers and Composites by Microwave Energy", *Polym Compos*, 11(3), pp. 184-191 (1990)
- 12. Lewis D. A., "Microwave Processing of Polymers An Overview", Mater Res Soc Symp Proc, 269, pp. 21-31 (1992)
- 13. DeMeuse M.T., Ryan C.L., Occhiello E., Po' R., and Garbassi F., "The Chemistry and Processing of Polymeric Materials at Microwave Frequencies", *Polym News*, 16, pp. 262-265 (1991)
- 14. Fellows L.A., and Hawley M.C., "Microwave Heating of Composites with Complex Geometries in Cylindrical Single-Mode Resonant Microwave Cavities", Proceedings. 29th International Microwave Power Institute Symposium, pp. 91-94 (1994)
- 15. Fellows L.A., and Hawley M.C., "Experimental Design and Preliminary Results of Microwave Heating of Complex Shapes by Mode-Switching Techniques", Proceedings. 25th International SAMPE Conference, pp. 929-943 (1992)
- 16. Qiu Y., Adegbite V., and Hawley M., "Intelligent Composite Processing Using Variable Frequency Method: Preliminary Results", *Proceedings. 27th International SAMPE Symposium*, pp. 173-183 (1995)
- 17. Qiu Y., Adegbite V., and Hawley M., "Microwave Processing Using Intelligent Frequency Switching: System Set-up and Characterization Results", *Proceedings.* 30th International Microwave Power Symposium, pp. 55-58 (1995)

- 18. Qiu Y., Adegbite V., and Hawley M., "Intelligent Microwave Processing Using Variable Frequency", *Proceedings. 11th ESD Advanced Composites Conference*, pp. 155-166 (1995)
- 19. R.K Agrawal, and L.T Drzal, *J Adhesion*, 29, pp. 63-79 (1989)
- 20. Wei J., Ph.D. Dissertation, Michigan State University, pp. 31-78 (1992)
- 21. Wei J.B., Fathi Z., and Hawley M.C., "Non-thermal Effects During Microwave Processing of Materials", *Proceedings. 30th International Microwave Power Symposium*, pp. 11-13 (1995)
- 22. Bush S.F., and Methven J.M., "A Mechanism for Observed Reaction Rate Enhancement in a Microwave Applicator Based on the Concept of a Non-Equilibrated Temperature Reaction (NETR)", *Proceedings. 39th International SAMPE Symposium*, pp. 34-44 (1994)
- 23. Chabinsky I., "Applications of Microwave Energy Past, Present, and Future 'Brave New Worlds'", Mater Res Soc Symp Proc, 124, p. 17-29 (1988)
- 24. Schwarz H.F., Bosisio R.G., Wertheimer M.R., and Couderc D., "Microwave Curing of Synthetic Rubbers", *J Microwave Power*, 8(3/4), p. 303-322 (1973)
- 25. B. Krieger, *Proceedings. American Chemical Society Spring Meeting* 66, Publ. by ACS, Books & Journals Division, Washington, DC, USA., pp. 339-340 (1992)
- 26. Falconer-Flint M.J., "Microwave Heating and Curing", Austr Plast Rubb J, 24(11), pp. 33-36, (1973)
- 27. Metaxas A.C., and Meredith R.J., ibid., p. 300
- 28. Metaxas A.C. and Binner J.G.P., "Microwave Processing of Ceramics", <u>Advanced Ceramic Processing Technology</u>, (ed. Binner), New Jersey: Noyes Publications, 1990
- 29. Metaxas A.C., and Meredith R.J., ibid., p. 298

- 30. George C.E., Lightsey G.R., and Wehr A.G., "Microwave Processing of Polymers and Biomass Materials", Mater Res Soc Symp Proc, 124, pp. 189-194 (1988)
- 31. Metaxas A.C., and Meredith R.J., ibid., p. 302
- 32. Chen M., Siochi E.J., Ward T.C., and McGrath J.E., "Basic Ideas of Microwave Processing of Polymers", *Polym Eng Sci*, 33(17), pp. 1092-1109 (1993)
- 33. Chen M., Siochi E.J., Ward T.C., and McGrath J.E., "The Dielectric Behavior of Glassy Amorphous Polymers at 2.45 GHz", *Polym Eng Sci*, 33(17), pp. 1110-1121 (1993)
- 34. Chen M., Hellgeth J.W., Siochi E.J., Ward T.C., and McGrath J.E., "The Microwave Processability of Semicrystalline Polymers", *Polym Eng Sci*, 33(17), pp. 1122-1131 (1993)
- 35. J. Jow, Ph.D. Dissertation, Michigan State University (1989)
- 36. Strand N.S., "Microwave Polymerization of Thermoset Resins Utilizing Microwave Transparent Tooling", Proceedings. 35th Annual Technical Conference, The Society of the Plastics Industry, Reinforced Plastics/Composites Institute, Sect. 24-C, pp. 1-4 (1980)
- 37. Ramakrishna D., Travis S., and Hawley M.C., "Microwave Processing of Glass Fiber/Vinyl Ester-Vinyl Toluene Composites", *Mater Res Soc Symp Proc*, 269, pp. 431-438 (1992)
- 38. Gourdenne A., Maassarani A.H., Monchaux P., Aeussudre S., and Thourel L., "Crosslinking of Thermosetting Resins by Microwave Heating: Quantitative Approach", Polym Prepr Am Chem Soc Div Polym Chem, 20(2), pp. 471-474 (1979)
- 39. Gagliani J., Lee R., and Wilcoxson A.L., "Polyimide Foams by Microwave Irradiation", Polym Prepr Am Chem Soc Div Polym Chem, (1981)
- 40. Gagliani J., Lee R., and Wilcoxson A.L., U.S. Patent 4,305,796 (1981)

- 41. Lewis D., Proceedings. 39th International SAMPE Symposium, pp. 1-12, SAMPE (1994)
- 42. Mashida T., Matsushita S., and Ikegami I., Japanese Patent 50,138,067 (1975)
- 43. H. Jullien, and H. Valot, "Polyurethane Curing by a Pulsed Microwave Field", *Polymer*, 26(4), pp. 506-510 (1985)
- 44. Livi A., Levita G. and Rolla P.A., "Dielectric Behavior at Microwave Frequencies of an Epoxy Resin During Crosslinking", *J Appl Polym Sci*, **50**, pp. 1583-1590 (1993)
- 45. Marand E., Baker K.R., and Graybeal J.D., <u>Radiation Effects on Polymers</u>, "Chapter 23: Dielectric Properties at Microwave Frequencies of Epoxy Undergoing Cure", American Chemical Society, pp. 384-400, 1991
- 46. Finzel M.C., and Hawley M.C., "Dielectric Properties of a Curing Epoxy/Amine System at Microwave Frequencies", *Polym Eng Sci*, 31(16), pp. 1240-1244 (1991)
- 47. Lane J.W., Seferis J.C., and Bachmann M.A., "Dielectric Modeling of the Curing Process", *Polym Eng Sci*, 26(5), pp. 346-353 (1986)
- 48. Delmotte M., Jullien H., and Ollivon M., "Variations of the Dielectric Properties of Epoxy Resins During Microwave Curing", Eur Polym J, 27(4/5), pp. 371-376 (1991)
- 49. Mangion M.B.M., and Johari G.P., "Relaxations of Thermosets. IV. A Dielectric Study of Crosslinking of Diglycidyl Ether of Bisphenol-A by Two Curing Agents", J Polym Sci Polym Phys Ed, 28, pp. 1621-1639 (1990)
- 50. Mangion M.B.M., and Johari G.P., "Relaxations of Thermosets. III. Sub-T<sub>g</sub> Dielectric Relaxations of Bisphenol-A Based Epoxide Cured with Different Crosslinking Agents", *J Polym Sci Polym Phys Ed*, 28, pp. 71-83 (1990)

- 51. Mangion M.B.M., and Johari G.P., "Relaxations in Thermosets. X. Analysis of Dipolar Relaxations in DGEBA-Based Thermosets During Isothermal Cure", J. Polym Sci Polym Phys Ed, 29, pp. 1127-1135 (1991)
- 52. Mijovic J., and Wijaya J., "Comparative Calorimetric Study of Epoxy Cure by Microwave vs. Thermal Energy", Macromolec, 23(15), pp. 3671-3674 (1990)
- 53. Mijovic J., and Wijaya J., "Mechanistic Modeling of Epoxy-Amine Kinetics. 2. Comparison of Kinetics in Thermal and Microwave Fields", *Macromolec*, 25(2), pp. 986-989 (1992)
- 54. Lewis D.A., Ward T.C., Summers J.D., and McGrath J.E., "Cure Kinetics and Mechanical Behavior of Electromagnetically Processed Polyimides", *Preprints*, 29, pp. 174-175 (1988)
- 55. D. A. Lewis, J. C. Hedrick, J. E. McGrath, and T. C. Ward, "The Accelerated Curing of Epoxy Resins Using Microwave Radiation", *Polym Prepr Am Chem Soc Div Polym Chem*, 28(2), pp. 330-331 (1987)
- 56. J. C. Hedrick, D. A. Lewis, T. C. Ward, and J. E. McGrath, "Microwave Processing of Thermoplastic Modified Epoxy Resin Networks", *Proceedings. Society of Plastics Engineers: ANTEC 1991*, pp. 1666-1667 (1991)
- 57. Wei J., Hawley M.C., and DeLong J.D., "Comparison of Microwave and Thermal Cure of Epoxy Resins", *Polym Eng Sci*, 33(17), pp. 1132-1140 (1993)
- 58. Wei J., Hawley M.C., and DeMeuse M.T., "Kinetics Modeling and Time-Temperature-Transformation Diagram of Microwave and Thermal Cure of Epoxy Resins", *Polym Eng Sci*, 35(6), pp. 461-470 (1995)
- 59. Wei J., DeLong J.D., and Hawley M.C., "Thermal and Kinetic Study of Microwave Cured Epoxy Resins", *Proceedings. American Chemical Society*, pp. 239-248 (1990)
- 60. DeLong J.D., Jow J., and Hawley M.C., 2nd Topical Conference on Emerging Technologies in Materials, San Francisco, CA, Nov. 6-9 (1989)

- 61. Beldjoudi N., and Gourdenne A., "Microwave Curing of Epoxy Resins with Diaminodiphenylmethane IV. Average Electric Power and Pulse Length Dependence in Pulsed Irradiation", Eur Polym J, 24(3), pp. 265-270 (1988)
- 62. Jow J., DeLong J. D., and Hawley M.C., "Computer-Controlled Pulsed Microwave Processing of Epoxy", SAMPE Qtly, 20(2), pp. 46-50 (January 1989)
- 63. Lee W.I., and Springer G.S., "Microwave Curing of Composites", *J Compos Mater*, 18, pp. 387-409 (July 1984)
- 64. Wei J., Hawley M.C., Jow J., and DeLong J.D., "Microwave Processing of Crossply Continuous Graphite Fiber/Epoxy Composites", SAMPE J, 27(1), pp. 33-39 (1991)
- 65. Fritz R., and Asmussen J., Jr., "Distribution of Dissipated Power in a Graphite Fiber Reinforced Epoxy Composite Heated in a Microwave Cavity", Ceramic Transactions, American Ceramic Society, 21, pp. 547-556 (1991)
- 66. Wei J., Chang Y., Thomas B.J., and Hawley M.C., "Microwave Heating of Thick-section Graphite Fiber/Epoxy Composites", *Proceedings. International Conference on Composite Materials/VIII*, 1, 10-L, (1991)
- 67. Boey F.Y.C., and Yue C.Y., "Interfacial Strength of a Microwave-Cured Epoxy-Glass Composite", *J Mater Sci Lett*, 10, pp. 1333-1334 (1991)
- 68. Metaxas A.C., and Meredith R.J., ibid., p. 239
- 69. Boey F.Y., and Lee W.L., "Microwave Radiation Curing of a Thermosetting Composite", *J Mater Sci Lett*, 9(10), pp. 1172-1173 (1990)
- 70. Adegbite V., Ph.D. Dissertation, Michigan State University (1995)
- 71. Kashyap S.C., and Wyslouzil W., "Methods for Improving Heating Uniformity of Microwave Ovens", *J Microwave Power*, 12(3), pp. 223-230 (1977)
- 72. Metaxas A.C., and Meredith R.J., ibid., p. 113

- 73. Stover D., "RTM'ing Large Parts", High-Performance Composites, pp. 39-46 (March/April 1995)
- 74. Karbhari V.M., and Slotte S.G., "Effect of Fiber Architecture on Manufacturability and Crush Performance of a Stiffened Plate Type RTM Structure", Composite Structures, 26, pp. 83-93 (1993)
- 75. Valenti M., "Resin Transfer Molding Speeds Composite Making", *Mech Eng*, pp. 46-48 (November 1992)
- 76. Stark E.B., and Breitigam W.V., "Resin Transfer Molding Materials", Engineered Materials Handbook, v.1. Composites, Metals Park, Ohio: ASM International, pp. 168-171, 1987
- 77. Strong B.A., Composites in Manufacturing, Case Studies, 1st ed., Society of Manufacturing Engineers (1991)
- 78. Anon., Reinforced Plastics, pp. 16-19 (February 1991)
- 79. Buckley D.T., U.S. Patent 5,217,654 (1993)
- 80. Buckley D.T., and Horn S.W., U.S. Patent 5,217,656 (1993)
- 81. Buckley D.T., U.S. Patent 5,338,169 (1994)
- 82. Buckley D.T., and Horn S.W., U.S. Patent 5,364,258 (1994)
- 83. Buckley D.T., U.S. Patent 5,382,148 (1995)
- 84. Anon., Reinforced Plastics, pp. 14-19 (June 1991)
- 85. R.F. Harrington, <u>Time-Harmonic Electromagnetic Fields</u>, New York: McGraw-Hill, Inc., pp. 18, 1961
- 86. Metaxas A.C., and Meredith R.J., ibid., p. 30

- 87. Holmberg J.A., "On Flexural and Tensile Strength for Composites Manufactured by RTM", *J Reinf Plast Comp*, v. II, pp. 1302-1320 (1992)
- 88. Outifa L., Jullien H., Moré C., and Delmotte M., "Buildup and Optimization of a Homogeneous Microwave Curing Process for Epoxy-Glass Composites", *Ind. Eng. Chem. Res.*, 34(2), pp. 688-698, 1995
- 89. Akyel C., and Bilgen E., "Microwave and Radio-Frequency Curing of Polymers: Energy Requirements, Cost, and Market Penetration", *Energy*, 14(12), pp. 839-851 (1989)
- 90. R.F. Harrington, ibid., p. 130
- 91. Carnahan B., Luther H.A., and Wilkes J.O., <u>Applied Numerical Methods</u>, Florida: Robert E. Krieger Publishing Company, Inc., p. 463, 1969
- 92. Carnahan B., Luther H.A., and Wilkes J.O., ibid, pp. 441-446

MICHIGAN STATE UNIV. LIBRARIES

31293015725520